

## 5 RESEARCH ACTIVITIES

### 5.1 NUCLEAR PHYSICS

S. Muralithar, N. Madhavan and P. Sugathan

HYRA was used in three thesis experiments, using beams of  $^{19}\text{F}$ ,  $^{30}\text{Si}$  and  $^{48}\text{Ti}$  from Pelletron + SC-LINAC, in order to study entrance channel effects and the role of neutron shell closure in the target through evaporation residue excitation function. The results of three experiments each carried out earlier using HYRA and HIRA were published during the past year. A School on Nuclear Reactions was conducted at IUAC during July 15-20, 2019 which was attended by 48 research scholars and the faculty consisted of several IUAC scientists and experts from other institutes.

Gamma detector arrays INGA and GDA are utilized by users across country and abroad for nuclear structure and reaction research leading to thesis work of scholars and publications in high end journals. Physics studied using gamma spectroscopy tools were: Octupole correlation, nuclear structure at high spin, lifetime measurement for evolution of collectivity, spectroscopy of odd-odd nuclei and reaction dynamics by incomplete fusion. Five users from Guru Ghasidas University, Vishwa Bharathi University, Banaras Hindu University, Delhi University and IUAC performed fusion evaporation experiments using Indian National Gamma Array for studying nuclear structure at high spins. Few 'Incomplete fusion experiments' were done in the General Purpose Scattering Chamber and later recorded the radioactive decay using the offline High purity Ge detector system. A workshop on "INGA experiments: Recent results and future perspectives" was organised on 17-18, September, 2019 at IUAC benefiting numerous research scholars. In the last one year 2 HPGe Clover and 2 Anti-Compton Shield (ACS) BGO detectors were added to the INGA array to increase the efficiency of the array. A plunger device is tested offline and is waiting for in-beam test for measurements of lifetime in sub-nanosecond range with INGA array. A chamber with about 10 CsI detectors for light charge particles is being developed with read out electronics to be used with the INGA array. Preamplifier for Clover Ge detector was developed by in-house scientist/engineers saving foreign exchange and tested to work well. Detectors are periodically serviced (last one year about 10 detectors were serviced). In the last one-year research publications from these facilities in international journals were about 20 and about 40 in international and about 80 in national conferences.

During the LINAC beam schedule for this year, four experiments were performed in the NAND facility in beam hall- II. All four experiments were part of student's thesis experiments studying the dynamics of fission in a heavy mass region by measuring neutron multiplicity and mass distribution of fission fragments. Pelletron plus LINAC accelerators were utilized to accelerate Si and Ti projectiles above the fusion barrier energies and measurements were made on mass gated neutron multiplicities using 50 neutron detectors in the array and pair of multi-wire proportional counters. An exclusive measurement of energy of neutrons emitted from a  $^{241}\text{Am}$ -Be source was also carried out using a sealed 100 mCi neutron source.

The existing Data Acquisition System is being upgraded with a new ingenious VME controller having better throughput than the previous one to address technological obsolescence and there are plans to gradually move to VME and/or DSP for all other applications. The data acquisition software developed for the online acquisition of data using the indigenous VME controller is compatible with ROOT format, the internationally used program for Nuclear Physics and Particle Physics data analysis.

General Purpose Scattering Chamber (GPSC) a versatile facility, extensively used for Nuclear Physics experiments as well as Atomic Physics and Material Science experiments using Pelletron beam was relocated to accommodate the upcoming High Current Injector (HCI) as part of the accelerator augmentation program and was re-installed to the 30° beam line beyond the GDA structure in Beam Hall I. As per the Accelerator Users Committee records there are more than 30 approved beam time proposals (including thesis proposals) yet to be scheduled using this facility in Nuclear Physics.

#### 5.1.1 Lifetime measurement study of octupole deformation in neutron deficient nuclei having $A < 120$

Anand Pandey<sup>1</sup>, Ravi Bhushan<sup>1</sup>, Aman Rohilla<sup>2</sup>, Bharti Rohila<sup>3</sup>, C. Majumder<sup>4</sup>, Subodh<sup>3</sup>, Kaushik Katre<sup>5</sup>, A. Kumar<sup>3</sup>, I. M. Govil<sup>3</sup>, H. P. Sharma<sup>4</sup>, S. Chakraborty<sup>5</sup>, R. P. Singh<sup>5</sup>, S. Muralithar<sup>5</sup>, and S. K. Chamoli<sup>1</sup>

<sup>1</sup>Department of Physics and Astrophysics, University of Delhi, Delhi 110007, India

<sup>2</sup>Institute of Modern Physics, Chinese Academy of Sciences, Lanzhou, China

<sup>3</sup>Department of Physics, Panjab University, Chandigarh 160014, India

<sup>4</sup>Department of Physics, Banaras Hindu University, Varanasi, India

<sup>5</sup>Inter-University Accelerator Centre, Aruna Asaf Ali Marg, New Delhi 110067, India

The nuclei having  $A \sim 120$  ( $50 \leq Z \leq 56$ ) are of considerable interest because of the competing shape driving tendencies of their orbitals occupied by the neutrons and the protons. Because of the presence of both quadrupole and octupole collectivity, the neutron deficient Ba, Cs and Xe nuclei, with mass  $A \sim 120$  amu, have attracted much attention in recent years. For nuclei with  $A < 120$ , due to their closeness to the proton drip line (and therefore difficulty in being populated via fusion evaporation reactions), octupole collectivity has been reported in very few cases e.g.  $^{114,116,117}\text{Xe}$  and  $^{110}\text{Te}$  [1,2]. In these reported cases also, several ambiguities have been observed in the nature of octupole correlations. Like in  $^{110}\text{Te}$ , the measured  $B(E1)$  strengths (the most prominent experimental evidence considered for octupole correlations) are found to be in agreement when compared with those in the neutron-rich barium nuclei. However, when compared with  $^{114,116}\text{Xe}$ , the  $B(E1)$  values in  $^{110}\text{Te}$  are found to be about an order of magnitude larger, thereby making the  $T_z$  scaling of the dipole moment, suggested in [1], questionable. Also, in case of  $^{114}\text{Xe}$ , the  $B(E1)$  value of the  $5^- \rightarrow 6^+$  transition is two orders of magnitude larger than that of  $5^- \rightarrow 4^+$  transition, thus contradicting a simple interpretation based on fixed intrinsic octupole deformation. So, more experiments are needed to systematically investigate whether the octupole phenomenon is common in the  $A \sim 120$  region.

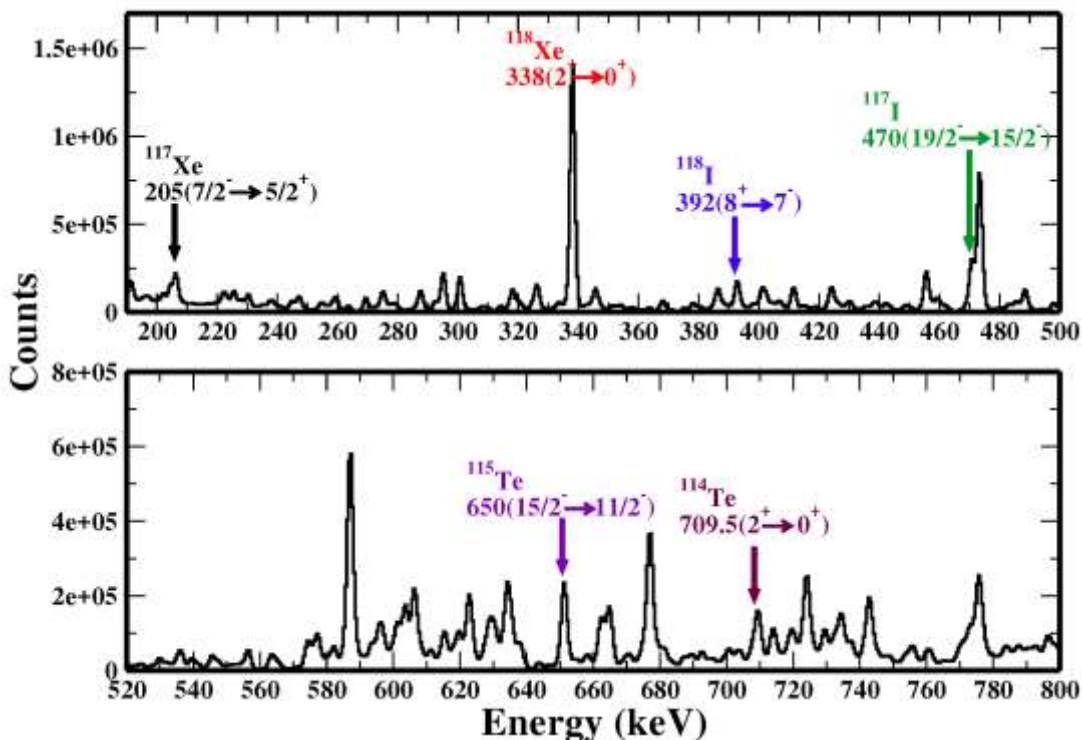


Fig. 5.1.1: Most intense peaks of different nuclei populated in the experiment are clearly marked by different colours.

With this motivation, an experiment was carried out to explore the high spin states in neutron deficient  $^{118}\text{Xe}$  via lifetime measurement using Doppler shift attenuation method (DSAM) technique at IUAC. High spin states in  $^{118}\text{Xe}$  were populated using the  $^{93}\text{Nb}(^{28}\text{Si}, p2n)^{118}\text{Xe}$  fusion evaporation reaction at  $E_{\text{lab}} = 115$  MeV. The target consisted of nicely rolled  $^{93}\text{Nb}$  foil of thickness  $\sim 1.28$  mg/cm $^2$  on an 8 mg/cm $^2$  thick Pb backing. The de-exciting gamma rays were detected with the Indian National Gamma Array (INGA) [3], consisting of 16 Compton-suppressed Clover detectors arranged in five rings at angles  $32^\circ, 57^\circ, 90^\circ, 123^\circ$ , and  $148^\circ$  with respect to the beam direction. Data were collected in  $\gamma\gamma$ -coincidence mode for 9 shifts. To optimize yield of  $^{118}\text{Xe}$ , excitation function was measured at  $E_{\text{lab}} = 112, 115, 116$  and 120 MeV. Fig. 5.1.1 shows part of data with clearly marked gamma peaks from various nuclei populated in the reaction.

#### REFERENCES:

- [1] S. L. Rugari *et al.*, Phys. Rev. C **48**, 2078 (1993).
- [2] E. S. Paul *et al.*, Phys. Rev. C **50**, R534 (1994).
- [3] S. Muralithar *et al.*, Nucl. Instrum. Methods Phys. Res., Sect. A **622**, 281 (2010).

### 5.1.2 Search for octupole collectivity in $^{152}\text{Gd}$

Indu Bala<sup>1</sup>, Saikat Chakraborty<sup>1</sup>, K. Rojeeta Devi<sup>1</sup>, Anuj<sup>2</sup>, K. Katre<sup>1</sup>, Yashraj<sup>1</sup>, Neelam<sup>2</sup>, Subodh<sup>3</sup>, Abhishek Yadav<sup>4</sup>, Suresh Kumar<sup>2</sup>, N. Madhavan<sup>1</sup>, S. C. Pancholi<sup>1</sup> and A. Roy<sup>5</sup>

<sup>1</sup>Inter-University Accelerator Centre, Aruna Asaf Ali Marg, New Delhi 110067, India

<sup>2</sup>Department of Physics and Astrophysics University of Delhi, Delhi 110007, India

<sup>3</sup>Department of Physics, Punjab University, Chandigarh 160014, India

<sup>4</sup>Department of Physics, Jamia Millia Islamia, New Delhi 110025, India

<sup>5</sup>Variable Energy Cyclotron Centre, Kolkata 700064, India

Nuclei along the whole nuclear chart are found to be in different stable shapes, viz. spherical, prolate and oblate, in the ground state. Observation of octupole deformed nuclei, in the ground state, can answer the basic questions of asymmetry in matter and anti-matter in the universe and physics beyond the standard model. Strong octupole correlations leading to pear shapes can arise when nucleons near the Fermi surface occupy states of opposite parity with orbital and total angular momentum differing by  $3\hbar$ . The regions of nuclei with strong octupole correlations correspond to particle numbers near 34 ( $g_{9/2} \leftrightarrow p_{3/2}$  coupling), 56 ( $h_{11/2} \leftrightarrow d_{5/2}$  coupling), 88 ( $i_{13/2} \leftrightarrow f_{7/2}$  coupling), and 134 ( $j_{15/2} \leftrightarrow g_{9/2}$  coupling) [1].

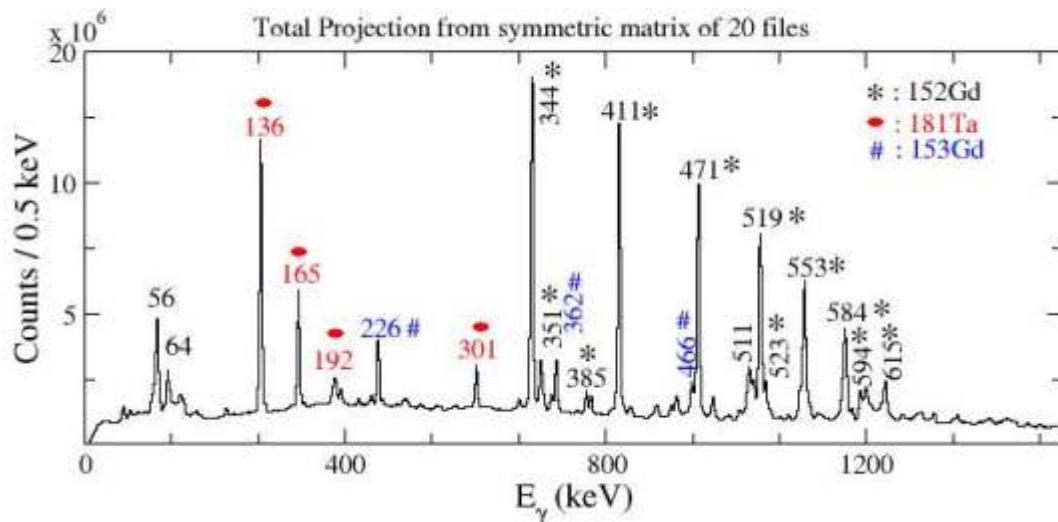


Fig. 5.1.2: Total projection from symmetric  $E_\gamma - E_\gamma$  matrix.

In the present experiment, we aimed to look for octupole correlations in  $^{152}\text{Gd}$ . This nucleus was studied earlier [2]. The observed side band of negative parity was said to be an octupole band based on measurement of  $B(E1)/B(E2)$  via gamma ray intensities. But the claims of octupole band can be confirmed by measuring absolute values of  $B(E1)$ . This can be done by lifetime measurement of nuclear states. Excited  $^{152}\text{Gd}$  was populated by the fusion evaporation reaction  $^{138}\text{Ba}(^{18}\text{O}, 4n)^{152}\text{Gd}$  at  $E_{\text{lab}} = 73$  MeV. The target was prepared by evaporation on a thick Ta backing. Gamma-rays from de-exciting evaporation residues were detected using the Indian National Gamma Array (INGA) [3] at IUAC. INGA consisted of 17 Clover detectors at the time of the experiment. The list mode data were collected for two or higher folds of events using CANDLE software. Fig. shows the total projection of symmetric  $E_\gamma - E_\gamma$  matrix for 20 data files. Further data reduction is in progress.

We acknowledge the staff of the Target Laboratory and the Pelletron group of IUAC for their support. The first author (IB) acknowledges the support and encouragement received from Dr. S. Muralithar and Dr. R. P. Singh.

#### REFERENCES:

- [1] P. A. Butler and W. Nazarewicz, Rev. Mod. Phys. 68,349 (1996).
- [2] S. P. Bvumbi et. al. Phys. Rev. C 87,044333 (2013).
- [3] S. Muralithar et. al. Nucl. Instrum. Methods Phys. Res., Sect. A 622, 281 (2010).

### 5.1.3 Incomplete fusion studies in $^{14}\text{N} + ^{175}\text{Lu}$ system

Ishfaq Majeed<sup>1</sup>, Mohd. Shuaib<sup>1</sup>, M. Shariq Asnain<sup>1</sup>, Mahesh Kumar<sup>2</sup>, Vijay R. Sharma<sup>3</sup>, Abhishek Yadav<sup>4</sup>, Manoj Kumar Sharma<sup>2</sup>, Pushpendra P. Singh<sup>5</sup>, Devendra P. Singh<sup>6</sup>, Unnati Gupta<sup>7</sup>, Rudra Narayan Sahoo<sup>5</sup>, Arshiya Sood<sup>5</sup>, Malika Kaushik<sup>5</sup>, R. Kumar<sup>8</sup>, R. P. Singh<sup>8</sup>, S. Muralithar<sup>8</sup>, B. P. Singh<sup>1</sup>, and R. Prasad<sup>1</sup>

<sup>1</sup>Nuclear Physics Laboratory, Department of Physics, Aligarh Muslim University, Aligarh 202002, India

<sup>2</sup>Department of Physics, Shri Varshney College, Aligarh 202001, India

<sup>3</sup>Deprtamento de Acceleradores, Instituto Nacional de Investigaciones Nucleares Apartado Postal 18-1027, C.P. 11801, Ciudad de Mexico, Mexico

<sup>4</sup>Department of Physics, Jamia Millia Islamia, New Delhi 110025, India

<sup>5</sup>Department of Physics, Indian Institute of Technology, Ropar, Punjab 140001, India

<sup>6</sup>Department of Physics, University of Petroleum and Energy Studies, Dehradun 248007, India

<sup>7</sup>J. C. Bose University of Science and Technology, YMCA, Faridabad, Haryana 121006, India

<sup>8</sup>Nuclear Physics Group, Inter-University Accelerator Centre, Aruna Asaf Ali Marg, New Delhi 110067, India

Heavy ion (HI) reactions involve interaction of large amount of nuclear matter giving rise to a variety of phenomena [1]. Fusion in the HI collisions has got a central importance and has been studied extensively spanning large range of kinematical quantities [2]. In case of complete fusion (CF), a fully equilibrated compound nucleus (CN), with the entrance channel kinetic energy and angular momentum getting distributed among all the accessible degrees of freedom of the composite system, is formed. Here, due to the small driving input angular momentum ( $\ell \leq \ell_{\text{crit}}$ ), the projectile completely fuses with the target nucleus involving entire mass, charge and linear momentum transfer. However, if the angular momentum ( $\ell$ ) of the composite system is not sustainable, the projectile may break-up into fragments. One of the fragments fuses with the target nucleus while the remnant goes on moving in the forward cone as a spectator. This type of process is referred to as break-up fusion (BUF) or incomplete fusion (ICF) [3]. Being a very stable and tightly bound structure,  $\alpha$ -particle is generally favored as an emitted particle in ICF reactions. As such, the residues populated in HI interaction via  $\alpha$ -emission are and remain the candidates for the quantitative studies of ICF. With a view to investigate low energy incomplete fusion reactions, excitation functions (EFs) for several  $xn$ ,  $pxn$ ,  $\alpha xn$ ,  $2\alpha xn$  and  $2\alpha pxn$ -channels, populated in  $^{14}\text{N} + ^{175}\text{Lu}$  system, have been measured at 4 – 7 MeV/amu energies and analyzed in the framework of the theoretical model code PACE4 [4].

The EFs of ten reactions viz.,  $^{175}\text{Lu}(^{14}\text{N}, 3n)^{186}\text{Pt}$ ,  $^{175}\text{Lu}(^{14}\text{N}, 4n)^{185}\text{Pt}^{(\text{g+m})}$ ,  $^{175}\text{Lu}(^{14}\text{N}, 5n)^{184}\text{Pt}$ ,  $^{175}\text{Lu}(^{14}\text{N}, p3n)^{185}\text{Ir}$ ,  $^{175}\text{Lu}(^{14}\text{N}, p4n)^{184}\text{Ir}$ ,  $^{175}\text{Lu}(^{14}\text{N}, \alpha 2n)^{183}\text{Os}$ ,  $^{175}\text{Lu}(^{14}\text{N}, \alpha 3n)^{182}\text{Os}$ ,  $^{175}\text{Lu}(^{14}\text{N}, \alpha p3n)^{181}\text{Re}$ ,  $^{175}\text{Lu}(^{14}\text{N}, 2\alpha 4n)^{177}\text{W}$ , and  $^{175}\text{Lu}(^{14}\text{N}, 2\alpha p2n)^{178m}\text{Ta}$  have been measured. The measured EFs have been compared with the calculations done using the statistical model code PACE4 to separate out the ICF contribution as it takes into account CF only. To reproduce the EFs of  $xn$ -channels using PACE4, different values of the level density parameter K were tested by varying it. The best results for the reproduction of EFs were obtained for K = 8 especially for  $4n$  and  $5n$ -channels. As a typical example, EF for  $^{185}\text{Pt}$  ( $4n$ )-channel is shown in Fig. 1(a).

Further, the experimental EFs of all the  $\alpha$ -emitting channels are found to be enhanced as compared to the theoretical calculations of PACE4, carried out using the same set of parameters that are used for reproducing EFs of  $xn$ -channels. Of all the EFs obtained for the five  $\alpha$ -emitting channels, PACE4 under predicted the cross-sections for three channels  $^{175}\text{Lu}(^{14}\text{N}, \alpha 2n)^{183}\text{Os}$ ,  $^{175}\text{Lu}(^{14}\text{N}, \alpha 3n)^{182}\text{Os}$  and  $^{175}\text{Lu}(^{14}\text{N}, \alpha p3n)^{181}\text{Re}$ , whereas negligible cross-sections were provided by the code for the other two reactions populated by  $2\alpha$ -emission i.e.,  $^{175}\text{Lu}(^{14}\text{N}, 2\alpha 4n)^{177}\text{W}$  and  $^{175}\text{Lu}(^{14}\text{N}, 2\alpha p2n)^{178m}\text{Ta}$ . The population of these two residues may be attributed entirely due to the ICF process. As a typical example, EF for  $^{182}\text{Os}$  ( $\alpha 3n$ )-channel is shown in Fig. 1 (b). The observed enhancement in the experimental EF's as compared to PACE4 predictions is a reminiscent of the fact that ICF process is at play in populating the  $\alpha$ -channels besides the usually considered process of CF. In the same way significant enhancement has been observed for all the  $\alpha$ -emitting channels.

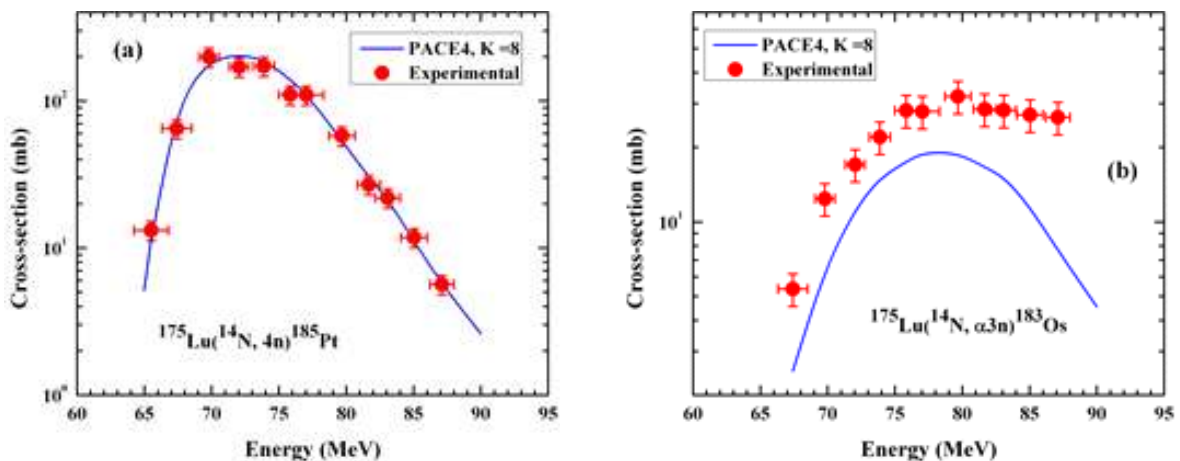


Fig. 5.1.3 (a) Experimental EF of  $^{185}\text{Pt}$  showing very good agreement with theoretical results of PACE4;  
 (b) Enhancement in EF of  $^{183}\text{Os}$  as compared to PACE4.

The relative probability of ICF in fusion dynamics, obtained in terms of incomplete fusion strength function ( $F_{ICF}$ ) has also been deduced. It has been found that the ICF contribution is distributed over the entire range with different magnitudes and increases to  $\approx 12\%$  at the highest energy. Comparative analysis of ICF probability of the present system were performed with other systems, *viz.*  $^{12,13}\text{C}$ ,  $^{19}\text{F} + ^{175}\text{Lu}$  in terms of the procedure suggested by Morgenstern *et al.* [5]. The effect of  $Q\alpha$ -value of the projectile on ICF is found to be in line with the literature [6], indicating the effect of projectile structure on the probability of occurrence of ICF for the present system as well.

#### REFERENCES:

- [1] A. Zucker, Ann. Rev. Nucl. Sci. 10, 27 (1960).
- [2] S. Hofmann, D. Ackermann, S. Antalic, H. G. Burkhard, V. F. Comas, *et al.*, Eur. Phys. J. A **32**, 251 (2007).
- [3] H. C. Britt and A. R. Quinton, Phys. Rev. 124, 877 (1961).
- [4] A. Gavron, Phys. Rev. C 21, 230 (1980).
- [5] H. Morgenstern, W. Bohne, K. Grabisch, D. Kovar, and H. Lehr, Phys. Lett. B 113, 463 (1982).
- [6] A. Yadav, P. Singh, M. Shuaib, V. Sharma, I. Bala, *et al.*, Phys. Rev. C 96, 044614 (2017).

#### 5.1.4 Study of anomalous light particle spectra in heavy-ion induced fusion reactions

Honey Arora<sup>1</sup>, K. Rani<sup>1</sup>, Shruti<sup>1</sup>, M. Kumar<sup>2</sup>, S. Yadav<sup>1</sup>, A. Punia<sup>1</sup>, C. Sharma<sup>1</sup>, D. Arora<sup>2</sup>, S. Singh<sup>1</sup>, A. Kaur<sup>1</sup>, N. Saneesh<sup>2</sup>, Varinderjit Singh<sup>3</sup>, A. Jhingan<sup>2</sup>, K. S. Golda<sup>2</sup>, H. Singh<sup>4</sup>, P. Sugathan<sup>2</sup>, A. Kumar<sup>1</sup>, Gulzar Singh<sup>1</sup>, and B. R. Behera<sup>1</sup>

<sup>1</sup>Department of Physics, Panjab University, Chandigarh 160014, India

<sup>2</sup>Inter-University Accelerator Centre, Aruna Asaf Ali Marg, New Delhi 110067, India

<sup>3</sup>Department of Physics, I. K. Gujral Punjab Technical University, Kapurthala 144603, India

<sup>4</sup>Department of Physics, Kurukshetra University, Kurukshetra 136119, India

The spectra for light charged particles as well as neutrons emitted from various heavy-ion induced fusion reactions are found to be anomalous with respect to the standard statistical model calculations. Various conjectures have been proposed to explain this anomalous behaviour. Fusion hindrance for mass symmetric systems at high excitation energy is one of the conjectures for explaining such anomalous spectra. It is to be noted that the fusion hindrance effect is suggested to show its relevance at higher excitation energy only, but no study has been conducted so far to show whether it is present at near barrier energies. To test this phenomena, same compound nucleus (CN)  $^{80}\text{Sr}$  was populated by two different entrance channels – mass asymmetric channel  $^{16}\text{O} + ^{64}\text{Zn}$  (populated at  $E_{lab} = 45, 59$  and  $89$  MeV) and nearly mass symmetric channel,  $^{32}\text{S} + ^{48}\text{Ti}$  (populated at  $E_{lab} = 85, 94$  and  $125$  MeV) with either matching the excitation energy or the angular momentum of the CN. Data for light particles (p,  $\alpha$  and n) and evaporation residues (ERs) were collected in an experiment using the General Purpose Scattering chamber (GPSC) facility at IUAC.

To demonstrate the above effect, ER-gated neutron and charged particle spectra are to be compared with the predictions of the statistical model. In earlier studies, inclusive neutron and charged particle spectra have been reported but those data might have contaminations from other reaction channels. In the present study, two multi-wire proportional counters were placed at extremely forward angles having active region ranging from  $2^\circ - 10^\circ$ , for gating neutron and charged particle spectra. Four neutron detectors were kept at  $30^\circ, 60^\circ, 90^\circ$  and  $120^\circ$ . CsI detectors, having an angular coverage of  $45^\circ - 115^\circ$ , were used for detection of protons and  $\alpha$ -particle. Light particle spectra (p,  $\alpha$  and n) obtained from these detectors will be gated with the ERs. Preliminary analysis has been performed to obtain neutron and  $\alpha$ -spectra (without gating) at the highest energy for the mass asymmetric system, which are shown in Fig. 5.1.4.

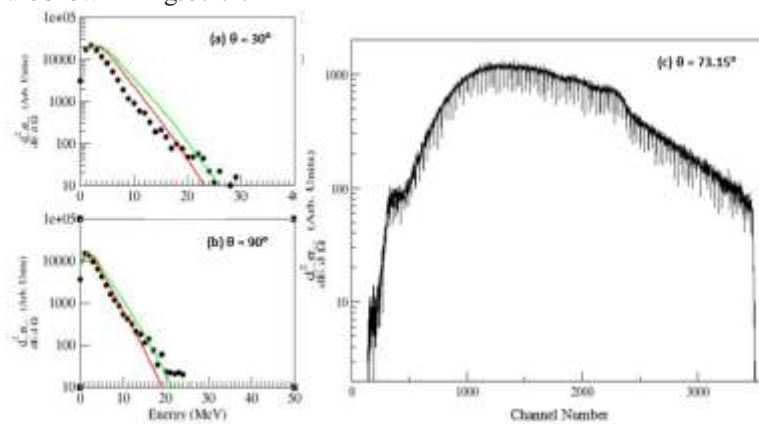


Fig. 5.1.4: Neutron spectrum at (a)  $\theta = 30^\circ$  and (b)  $\theta = 90^\circ$  for  $^{16}\text{O} + ^{64}\text{Zn}$  at  $E_{lab} = 89$  MeV (black dots) fitted with different radius parameters obtained from CASCADE model calculations, where  $R = 1.50$  (red line) and  $R = 1.25$  (green line).

Raw CsI spectrum for  $\alpha$ -particles, for  $^{16}\text{O} + ^{64}\text{Zn}$  at  $E_{lab} = 89$  MeV is shown in panel (c).

### 5.1.5 Fragmentation dynamics and neutron multiplicity measurements for super-heavy nuclei

Shruti<sup>1</sup>, H. Arora<sup>1</sup>, N. Saneesh<sup>2</sup>, D. Arora<sup>3</sup>, Kajol Chakraborty<sup>3</sup>, A. Kaur<sup>4</sup>, Amit<sup>1</sup>, Subodh<sup>1</sup>, Chetan<sup>1</sup>, Raghav<sup>1</sup>, K. S. Golda<sup>2</sup>, A. Jhingan<sup>2</sup>, Mohit Kumar<sup>2</sup>, Hardev Singh<sup>4</sup>, H. J. Wollersheim<sup>5</sup>, J. Gerl<sup>5</sup>, S. Mandal<sup>1</sup>, P. Sugathan<sup>2</sup> and B. R. Behera<sup>1</sup>

<sup>1</sup>Department of Physics, Panjab University, Chandigarh 160014, India

<sup>2</sup>Inter-University Accelerator Centre, Aruna Asif Ali Marg, New Delhi 110067, India

<sup>3</sup>Department of Physics and Astrophysics, University of Delhi, Delhi 110007, India

<sup>4</sup>Department of Physics, Kurukshetra University, Kurukshetra 136119, India

<sup>5</sup>GSI, Darmstadt, Germany

In recent years great success has been achieved in the synthesis of new super-heavy elements (SHE) with both cold (one of the reaction partners is spherical  $^{208}\text{Pb}$  or  $^{209}\text{Bi}$ ) and hot ( $^{48}\text{Ca}$  projectiles on actinide targets) fusion reactions. A good understanding of reaction dynamics is expected to be of great help to optimize the formation of SHE. Recently a series of measurements were made by Thakur *et al.* [1] and Appanannababu *et al.* [2] to understand the fragmentation dynamics of super-heavy systems using a spherical target i.e.  $^{208}\text{Pb}$ . The present experiment is an attempt to study fission dynamics of a super-heavy system

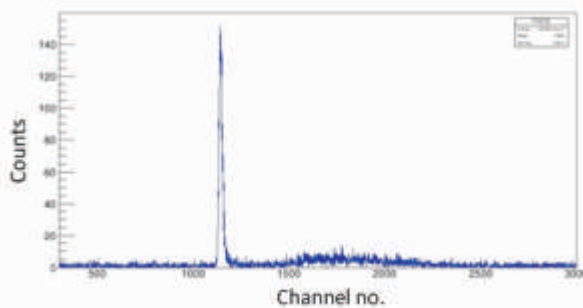


Fig. 5.1.5.1: TOF spectrum from a neutron detector at  $0^\circ$  with respect to the MWPC.

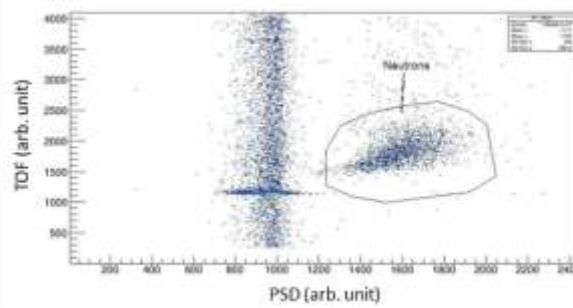


Fig. 5.1.5.2: Pulse shape discrimination (PSD) vs TOF spectrum from the same neutron detector.

#### REFERENCES:

- [1] M. Thakur *et al.*, Eur. Phys. J. A 53, 133 (2017).
- [2] S. Appanannababu *et al.*, Phys. Rev C 94, 044618 (2016).

### 5.1.6 Spectroscopy of $^{63}\text{Zn}$ and $^{66}\text{Ga}$

U. S. Ghosh<sup>1</sup>, S. Rai<sup>1</sup>, B. Mukherjee<sup>1</sup>, A. Biswas<sup>1</sup>, A. K. Mondal<sup>1</sup>, K. Mandal<sup>1</sup>, A. Chakraborty<sup>1</sup>, S. Chakraborty<sup>2</sup>, G. Mukherjee<sup>3</sup>, A. Sharma<sup>4</sup>, I. Bal<sup>5</sup>, S. Muralithar<sup>5</sup>, and R. P. Singh<sup>5</sup>

<sup>1</sup>Department of Physics, Siksha-Bhavana, Visva-Bharati, Santiniketan, West Bengal 731235, India

<sup>2</sup>Department of Physics, Institute of Science, Banaras Hindu University, Varanasi 221005, India

<sup>3</sup>Variable Energy Cyclotron Centre, 1/AF Bidhannagar, Kolkata 700064, India

<sup>4</sup>Department of Physics, Himachal Pradesh University, Shimla 171005, India

<sup>5</sup>Inter-University Accelerator Centre, Aruna Asaf Ali Marg, New Delhi 110067, India

Study of nuclear structures in many Zn and Ga isotopes during the last few decades has revealed many interesting phenomena, which are due to the contributions from single particles as well as collective motions of the nucleons. Many normal and super-deformed bands have been observed in  $^{60,61,62,64}\text{Zn}$  with various shapes [1-7]. Complex nuclear structures have been observed in  $^{63,65,66,67}\text{Ga}$  which are neither exactly due to single particle excitations nor exactly due to collective ones [8-10]. Here, the low spin states are mainly originated from the distribution of nucleons in the 1f and 2p orbitals, whereas the involvement of 1g<sub>9/2</sub> orbital is essential to generate high angular momentum. Presence of holes in 1f<sub>7/2</sub> orbital and particles in 1g<sub>9/2</sub> orbital leads to a transition from spherical to deformed shapes and enhances the possibility of collective rotational excitations. The recent study is to search for phenomena related to single particles and collective motions of the nucleons in some nuclei in A ~ 60, for which lack of detailed study is prevailing. Here, we will report, in brief, on some new results for  $^{63}\text{Zn}$  and  $^{66}\text{Ga}$ .

In the fusion-evaporation reaction, a beam of  $^{18}\text{O}$  at  $E_{\text{lab}} = 72.5$  MeV, was obtained from the 15UD Pelletron accelerator [11] at IUAC. The beam was bombarded onto a  $^{52}\text{Cr}$  (isotopic abundance  $\approx 99\%$ ) target of thickness  $1.0 \text{ mg/cm}^2$  backed by  $8.0 \text{ mg/cm}^2$   $^{197}\text{Au}$ . The emitted  $\gamma$ -rays were detected in coincidence mode with 14 Compton-suppressed HPGe Clover detectors of the Indian National Gamma Array (INGA) [12]. Out of the 14 Clovers, four were kept at an angle of  $123^\circ$  and another four were at  $148^\circ$ , while the remaining six detectors were placed at an angle of  $90^\circ$  with respect to the beam direction. Analysis of the data is performed with the help of the

standard analysis packages *viz.* CANDLE [13], RADWARE [14] and INGASORT [15]. Angular correlation analysis is carried out using the method of directional correlation from oriented states (DCO) [16]. Electric or magnetic nature of  $\gamma$ -ray transitions was determined from the polarization measurement [17, 18], which was analyzed by constructing two asymmetric matrices – one with perpendicular and the other with parallel scattered events (i.e. the events with  $\gamma$ -rays scattered perpendicular or parallel to the emission plane) of 90° detectors in one axis and corresponding  $\gamma$ -rays detected at all angles on another axis.

New level schemes of  $^{63}\text{Zn}$  and  $^{66}\text{Ga}$  have been proposed in the present work, which are based on the coincidence relationship, relative intensity balance, angular correlation and polarization measurements of the emitted  $\gamma$ -rays. Almost all the transitions reported previously are observed in this measurement for these two nuclei. Several new transitions have been observed in these two nuclei which are shown in the gated spectra (Figs. 5.1.6.1, Figs. 5.1.6.2 and Fig. 5.1.6.3). New level schemes are compared with shell model calculations with  $f_{5/2}pg_{9/2}$  model space using jj44bpn and jun45pn interactions. Deformations and shapes of  $^{63}\text{Zn}$  at different rotational frequencies have been predicted by total Routhian surface calculations method. Results for  $^{63}\text{Zn}$  are already published, whereas, those for  $^{66}\text{Ga}$  are communicated.

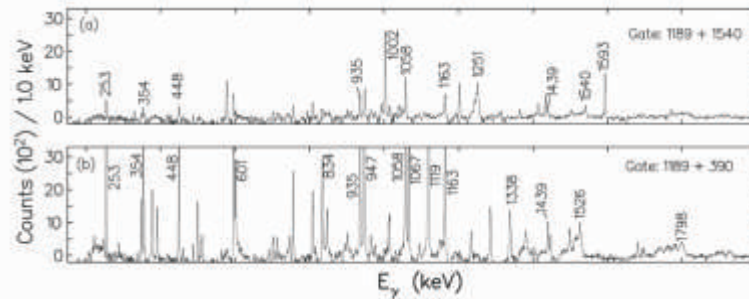


**Fig. 5.1.6.1:** Background subtracted  $\gamma$ - $\gamma$  coincidence spectra for  $^{66}\text{Ga}$  with the sum gate of (a)  $1189 (9^+ \rightarrow 7^+)$  and  $1540 \text{ keV} (10^- \rightarrow 9^+)$ , (b)  $1189 (9^+ \rightarrow 7^+)$  and  $390 \text{ keV} (9^+ \rightarrow 9^-)$ .

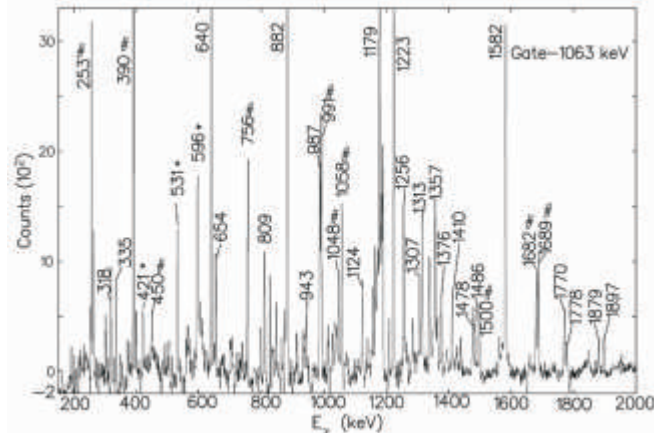


**Fig. 5.1.6.2:** Background subtracted  $\gamma$ - $\gamma$  coincidence spectrum for  $^{63}\text{Zn}$  gated on 1063 keV ( $7/2^+ \rightarrow 3/2^-$ ) transition. Here, y axis represents counts per 1.0 keV. New transitions are marked by asterisks (\*) and few strong peaks are marked with '#' symbols indicating contaminant  $\gamma$ -rays.

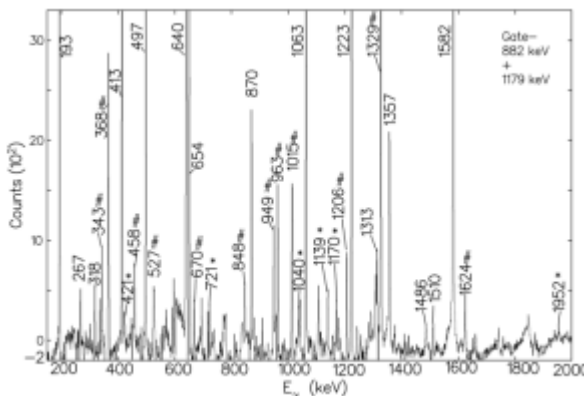


**Fig. 5.1.6.3:** Background subtracted  $\gamma$ - $\gamma$  coincidence spectrum for  $^{63}\text{Zn}$  with the sum gate of 882 keV ( $13/2^+ \rightarrow 9/2^+$ ) and 1179 keV ( $17/2^+ \rightarrow 13/2^+$ )  $\gamma$ -rays. Here, the y axis represents counts per 1.0 keV. New transitions are marked by asterisks (\*) and few strong peaks are marked with '#' symbols indicating contaminant  $\gamma$ -rays.

## REFERENCES:

- [1] C. E. Svensson *et al.*, Phys. Rev. Lett. **82**, 3400 (1999).
- [2] C. -H. Yu *et al.*, Phys. Rev. C **60**, 031305(R) (1999).
- [3] L. -L. Andersson *et al.*, Phys. Rev. C **79**, 024312 (2009).
- [4] C. E. Svensson *et al.*, Phys. Rev. Lett. **79**, 1233 (1997).
- [5] C. E. Svensson *et al.*, Phys. Rev. Lett. **80**, 2558 (1998).
- [6] J. Gellanki *et al.*, Phys. Rev. C **86**, 034304 (2012).
- [7] D. Karlgren *et al.*, Phys. Rev. C **69**, 034330 (2004).
- [8] M. Weiszflog *et al.* Eur. Phys. J. A **11**, 25 (2001).
- [9] S. S. Bhattacharjee *et al.*, Phys. Rev. C **95**, 054330 (2017).
- [10] I. Dankó *et al.*, Phys. Rev. C **59**, 1956 (1999).
- [11] G. K. Mehta *et al.*, Nucl. Instrum. Methods Phys. Res., Sect. A **268**, 334 (1988).
- [12] S. Muralithar *et al.*, Nucl. Instrum. Methods Phys. Res., Sect. A **622**, 281 (2010).
- [13] B. P. Ajith Kumar *et al.*, Proc. DAE-BRNS Symp. Nucl. Phys. **44**, 390 (2001).
- [14] D. C. Radford, Nucl. Instrum. Methods Phys. Res., Sect. A **361**, 297 (1995).
- [15] R. K. Bhowmik *et al.*, Proc. DAE-BRNS Symp. Nucl. Phys. **44**, 422 (2001).
- [16] K. S. Krane *et al.*, Nucl. Data Tables **11**, 351 (1973).
- [17] G. Duchene *et al.*, Nucl. Instrum. Methods Phys. Res., Sect. A **432**, 90 (1999).
- [18] K. Starosta *et al.*, Nucl. Instrum. Methods Phys. Res., Sect. A **423**, 16 (1999).
- [19] U. S. Ghosh *et al.*, Phys. Rev. C **100**, 034314 (2019).

**5.1.7 Structure of positive parity states in  $^{139}\text{Pm}$** 

S. S. Tiwary<sup>1</sup>, H. P. Sharma<sup>1</sup>, S. Chakraborty<sup>1</sup>, C. Majumder<sup>1</sup>, A. K. Gupta<sup>1</sup>, P. Banerjee<sup>2</sup>, S. Ganguly<sup>3</sup>, K. Rojeeta Devi<sup>4</sup>, Neelam<sup>4</sup>, S. Kumar<sup>4</sup>, S. K. Chamoli<sup>4</sup>, A. Sharma<sup>5</sup>, V. V. Jyothi<sup>6</sup>, Mayank<sup>7</sup>, A. Kumar<sup>8</sup>, S. S. Bhattacharjee<sup>9</sup>, Indu Bala<sup>9</sup>, S. Muralithar<sup>9</sup> and R. P. Singh<sup>9</sup>

<sup>1</sup>Department of Physics, Institute of Science, Banaras Hindu University, Varanasi 221005, India

<sup>2</sup>Nuclear Physics Division, Saha Institute of Nuclear Physics, Kolkata 700064, India

<sup>3</sup>Department of Physics, Bethune College, Kolkata 700006, India

<sup>4</sup>Department of Physics and Astrophysics, University of Delhi, New Delhi 110007, India

<sup>5</sup>Department of Physics, Himachal Pradesh University, Shimla 171004, India

<sup>6</sup>Department of Nuclear Physics, Andhra University, Visakhapatnam 530003, India

<sup>7</sup>Amity Institute of Nuclear Science and Technology, Amity University, Noida 201313, India

<sup>8</sup>Department of Physics, Panjab University, Chandigarh 160014, India

<sup>9</sup>Inter-University Accelerator Centre, Aruna Asaf Ali Marg, New Delhi 110067, India

The nuclei, belonging to mass  $\sim$ 140 amu region, offer various scopes for spectroscopic studies, due to the availability of high-j proton and neutron orbitals, with low and high K-values, respectively [1-6]. These nuclei were studied under the framework of various theoretical models. Presence of triaxial deformation was suggested in these nuclei [7]. Investigation for the band structure of promethium nuclei ( $Z = 61$ ) has a special interest, because of the lack of experimental information on positive parity states in previous works [8-10]. The bands associated with positive parity  $\pi g_{7/2}$  and  $\pi d_{5/2}$  configurations were systematically observed in lighter  $^{131-133}\text{Pm}$  isotopes [1,2] but the same has not yet been reported in heavier  $^{135-139}\text{Pm}$  isotopes [3,5-7]. In addition to this, a very interesting sequence of dipole transitions was observed in  $^{139}\text{Pm}$  at very low angular momentum [8-10]. Such a sequence has not been observed in any odd-A  $^{131-137}\text{Pm}$  isotopes [1-3]. The structure of the dipole band needed to be understood but required further experimental data. Therefore, in the present investigation, angular correlation and polarization measurements have been carried out via in-beam  $\gamma$ -ray spectroscopy for the confirmation of spin and parity of the states in  $^{139}\text{Pm}$ .

The experiment has been performed using the 15UD Pelletron accelerator facility of IUAC. The high spin states in  $^{139}\text{Pm}$  have been populated via the fusion-evaporation reaction  $^{127}\text{I}(^{16}\text{O}, 4n)^{139}\text{Pm}$  at  $E_{\text{lab}} = 82$  MeV. Eighteen Compton-suppressed Clover detectors of the Indian National Gamma Array (INGA) have been used to detect the  $\gamma$ -rays. Offline analysis of data has been carried out using INGA-Sort. A number of matrices have been formed by sorting of the gain-matched list mode data in order to carry out the coincidence and angular correlation analysis. In this work, a detailed re-investigation of the low lying levels of  $^{139}\text{Pm}$  has been done via fusion evaporation reaction. RDCO and polarization measurements of several  $\gamma$ -transitions have also been carried out.

Partial level scheme is shown in Fig. 5.1.7.1.

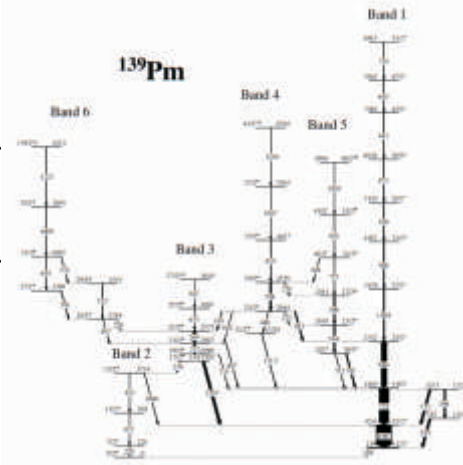


Fig. 5.1.7.1: Partial level scheme of  $^{139}\text{Pm}$ .

The spin and parity of the states have been determined using angular correlation (RDCO) and linear polarization asymmetry ( $\Delta_{\text{asym}}$ ) measurements. A new band, based on single quasi-particle  $\pi g_{7/2}$  configuration, has been established. Additionally, two more band structures, above 1951 and 3389 keV states, have been established to be part of the positive parity bands in  $^{139}\text{Pm}$ . A gated spectrum is shown in Fig. 5.1.7.2. The results have been communicated.

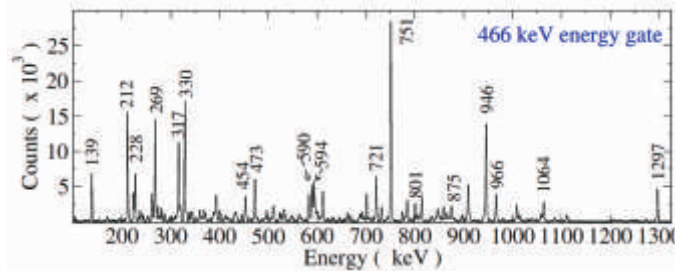


Fig. 5.1.7.2:  $\gamma$ - $\gamma$ -coincidence spectrum gated by 466 keV transition.

#### REFERENCES:

- [1] C. M. Parry *et al.*, Phys. Rev. C 57, 2215 (1998).
- [2] P. Regan *et al.*, Nucl. Phys. A 533, 476 (1991).
- [3] C. W. Beausang *et al.*, Phys. Rev. C 36, 602 (1987).
- [4] D. Sharma *et al.*, Chin. J. Phys. 54, 42 (2016).
- [5] N. Xu, C. W. Beausang *et al.*, Phys. Rev. C 36, 1649 (1987).
- [6] A. Dhal, R. K. Sinha *et al.*, Phys. Rev. C 80, 014320 (2009).
- [7] N. T. Zhang, Zhang Y. H. *et al.*, Phys. Rev. C 84, 057302 (2011).

#### 5.1.8 Signature of octupole correlations in $^{126}\text{Xe}$

S. Chakraborty<sup>1</sup>, H. P. Sharma<sup>1</sup>, S. S. Tiwary<sup>1</sup>, C. Majumder<sup>1</sup>, S. Muralithar<sup>2</sup>, R. P. Singh<sup>2</sup>, S. S. Bhattacharjee<sup>2</sup>, S. Rai<sup>3</sup>, Pragati<sup>4</sup>, Mayank<sup>5</sup>, P. Banerjee<sup>6</sup>, S. Ganguly<sup>7</sup>, S. Kumar<sup>8</sup>, A. Kumar<sup>9</sup>, and R. Palit<sup>10</sup>

<sup>1</sup>Department of Physics, Institute of Science, Banaras Hindu University, Varanasi 221005, India

<sup>2</sup>Nuclear Physics Group, Inter-University Accelerator Centre, Aruna Asaf Ali Marg, New Delhi 110067, India

<sup>3</sup>Department of Physics, Visva-Bharati, Santiniketan 731235, India

<sup>4</sup>Department of Physics, Indian Institute of Technology, Roorkee 247667, India

<sup>5</sup>Amity Institute of Nuclear Science and Technology, Amity University, Noida 201313, India

<sup>6</sup>Nuclear Physics Division, Saha Institute of Nuclear Physics, Kolkata 700064, India

<sup>7</sup>Department of Physics, Bethune College, Kolkata 700006, India

<sup>8</sup>Department of Physics and Astrophysics, University of Delhi, New Delhi 110007, India

<sup>9</sup>Department of Physics, Panjab University, Chandigarh 160014, India

<sup>10</sup>Department of Nuclear and Atomic Physics, Tata Institute of Fundamental Research, Mumbai 400005, India

Existence of alternating-parity rotational bands have been observed in several nuclei with  $N, Z \approx 34, 56, 88, 134\dots$ , due to the breaking of reflection symmetry [1]. Availability of the proton and/or neutron orbitals, differed by  $\Delta j = \Delta l = 3$  and  $\Delta \pi = -1$ , near the Fermi surface are responsible for the emergence of octupole deformation in nuclei. Static octupole deformation are predominantly observed in the Fr, Ra, Ac, Th, U nuclei in 220 amu mass region and Ba, Ce, Nd, Pm, Sm, Eu, Gd nuclei in 145 amu mass region [2, and references therein]. Presence of octupole deformation was also predicted in 110 amu mass region with  $N, Z \approx 56$  [3] and subsequently observed experimentally [4]. In the case of  $^{even}\text{Xe}$  nuclei, octupole correlations have been observed in both proton-rich and neutron-rich isotopes with  $N \approx 56, 88$  [4,5]. Systematic investigation on  $^{even}\text{Xe}$  isotopes predicts the presence of weakly-coupled octupole bands near  $N=72$ , where, the  $d_{5/2}$  and  $h_{11/2}$  octupole driving pair of orbitals are present near both proton and neutron Fermi surfaces [6]. This report presents an experimental investigation on  $^{126}\text{Xe}_{72}$  to search for the octupole correlations.

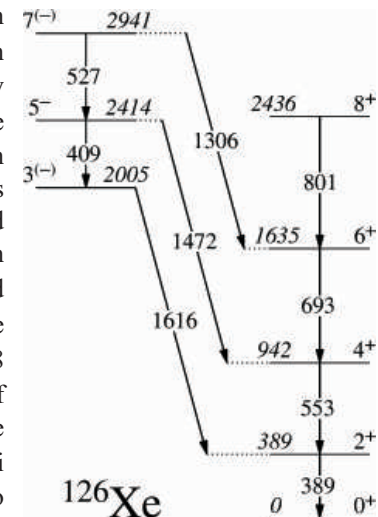


Fig. 5.1.8.1: Partial level scheme of  $^{126}\text{Xe}$ .

Excited states in  $^{126}\text{Xe}$  were populated via the reaction  $^{122}\text{Sn}({}^9\text{Be}, 5\gamma)$  at  $E_{\text{lab}} = 48$  MeV, utilizing the 15UD Pelletron accelerator facility of IUAC. The Indian National Gamma Array with 14 Compton-suppressed Clover detectors was used to collect the  $\gamma$ -rays. Offline analysis of data was carried out using the computer code INGASORT. Details of the experimental set-up and data analysis procedures are available in Ref. [7].

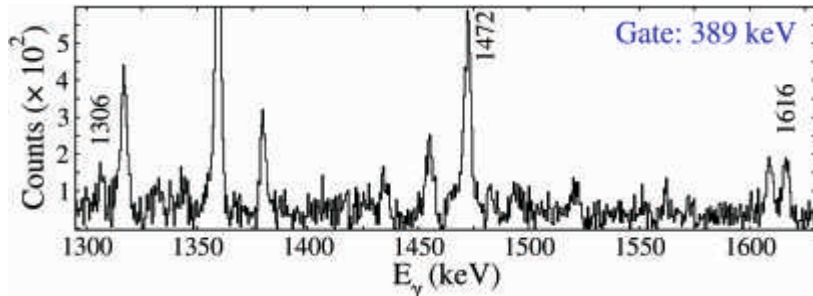


Fig. 5.1.8.2: Coincidence spectrum gated by 389 keV transition.

The levels of present interest in  $^{126}\text{Xe}$  are shown in Fig. 5.1.8.1. The results of angular correlations and linear polarization of the  $\gamma$ -rays of interest decaying from the positive parity ground state band are reported in Ref. [8]. Three states at  $E_x = 2005, 2414$  and  $2941$  keV were known earlier without firm spin and parity information [9]. The negative parity of 2414 keV state has been confirmed in this work from the linear polarization measurement of 1472 keV  $\gamma$ -ray [ $\Delta_{\text{asym}} = +0.07(10)$ ]. Spin of the 2941 keV state has been assigned from the quadrupole nature of 527 keV  $\gamma$ -ray on the basis of  $R_{\text{DCO}}$  [= 1.94 (91)] result, determined from the energy gate of 1472 keV  $E1$   $\gamma$ -transition. A new  $\gamma$ -ray of 1306 keV has been identified to decay from the 2941 keV state to 1635 keV state. States of the negative parity band are found to decay into the positive parity states via  $E1$   $\gamma$ -transitions, as shown in Fig. 5.1.8.2. Existence of these  $3^{(\pm)}$ ,  $5^{(\pm)}$  and  $7^{(\pm)}$  states, decaying into the positive parity ground state band via enhanced  $E1$   $\gamma$ -rays, is the signature of octupole correlations in  $^{126}\text{Xe}$ . For further confirmation, theoretical study is underway.

#### REFERENCES:

- [1] I. Ahmad, P. A. Butler, Annu. Rev. Nucl. Part. Sci. **43**, 71 (1993).
- [2] P. A. Butler, W. Nazarewicz, Rev. Mod. Phys. **68**, 349 (1996).
- [3] J. Skalski, Phys. Lett. B **238**, 6 (1990).
- [4] S. L. Rugari *et al.*, Phys. Rev. C **48**, 2078 (1993).
- [5] Y. Huang *et al.*, Phys. Rev. C **93**, 064321 (2016).
- [6] P. D. Cottle *et al.*, Phys. Lett. B **219**, 27 (1989).
- [7] S. Chakraborty *et al.*, Braz. J. Phys. **47**, 406 (2017).
- [8] S. Chakraborty *et al.*, Nucl. Phys. A **996**, 121687 (2020).
- [9] <https://www.nndc.bnl.gov/>

#### 5.1.9 Spin assignment of a dipole band in $^{104}\text{Ag}$

Kaushik Katre<sup>1</sup>, K. Suryanarayana<sup>2</sup>, A. Tejaswi<sup>2</sup>, M. Kumar Raju<sup>2</sup>, M. Ratna Raju<sup>2</sup>, D. Vijaya Lakshmi<sup>2</sup>, T. Seshi Reddy<sup>2</sup>, J. Matta<sup>3</sup>, A. D. Ayangeakaa<sup>4</sup>, U. Garg<sup>5</sup>, R. Bhattacharjee<sup>4</sup>, S. S. Bhattacharjee<sup>4</sup>, S. Samanta<sup>4</sup>, S. Das<sup>4</sup>, N. Ghosh<sup>4</sup>, R. Raut<sup>4</sup>, S. S. Ghugre<sup>4</sup>, A. K. Sinha<sup>4</sup>, S. Mukhopadhyay<sup>5</sup>, L. Dhanu<sup>5</sup>, B. K. Nayak<sup>5</sup>, D. C. Biswas<sup>5</sup>, A. Y. Deo<sup>6</sup>, S. K. Tandel<sup>6</sup>, N. Kaur<sup>7</sup>, Ashok Kumar<sup>7</sup>, S. Saha<sup>8</sup>, J. Sethi<sup>8</sup>, R. Palit<sup>8</sup>, S. Chattopadhyay<sup>9</sup>, S. Chakraborty<sup>1</sup>, S. Muralithar<sup>1</sup>, P. V. Madhusudhana Rao<sup>2</sup> and R. P. Singh<sup>1</sup>

<sup>1</sup>Nuclear Physics Group, Inter-University Accelerator Centre, Aruna Asaf Ali Marg, New Delhi 110067, India

<sup>2</sup>Department of Nuclear Physics, Andhra University, Visakhapatnam 530003, India

<sup>3</sup>Physics Department, University of Notre Dame, Notre Dame, Indiana 46556, USA

<sup>4</sup>UGC-DAE Consortium for Scientific Research, Kolkata Centre, Kolkata 700098, India

<sup>5</sup>Nuclear Physics Division, Bhabha Atomic Research Centre, Mumbai 400085, India

<sup>6</sup>School of Physical Sciences, UM-DAE Centre for Excellence in Basic Sciences, Mumbai 400098, India

<sup>7</sup>Department of Physics, Panjab University, Chandigarh 160014, India

<sup>8</sup>Department of Nuclear and Atomic Physics, Tata Institute of Fundamental Research, Mumbai 400005, India

<sup>9</sup>High Energy Nuclear and Particle Physics Division, Saha Institute of Nuclear Physics, Kolkata 700064, India

The odd-odd Ag isotopes, having three proton-holes below the  $Z = 50$  shell closure and few neutron-particles above  $N = 50$  shell closure, exhibit small deformation. A dipole band of a sequence of five  $\gamma$ -transitions has been reported above  $I^\pi = 2^+$  state at 7 KeV [1]. The spin and parity of the states are tentatively assigned, except the band-head. As part of this study, we measured the DCO ratio of the  $\gamma$ -rays, so that the spin of these states can be confirmed. The high spin states of  $^{104}\text{Ag}$  were populated using the fusion evaporation reaction  $^{76}\text{Ge}(^{32}\text{S}, p3n\gamma)$  at  $E_{\text{lab}} = 110$  MeV. The beam was delivered by the TIFR-BARC Pelletron facility at Mumbai. The  $\gamma$ -rays were detected by the Indian National Gamma Array (INGA) at TIFR [4], having 18 Clover detectors during this experiment. The detectors were mounted at six different angles with respect to the beam direction. The data were sorted in the  $\gamma$ - $\gamma$  matrix. The matrix is being analyzed using the RADWARE program and all known  $\gamma$ -lines have been conformed in their previous placement. The asymmetric angular correlation matrix is formed in order to

obtain a directional correlation oriented states (DCO) ratio. The directional correlation from oriented states ratio is defined as:

$$R_{DCO} = \frac{I_\gamma(\text{observed at } 140^\circ, \text{ gated on } 90^\circ)}{I_\gamma(\text{observed at } 90^\circ, \text{ gated on } 140^\circ)}$$

$E_\gamma$	$E_{\text{Level}}$	$R_{DCO}$	$J_i^{\pi} \rightarrow J_f^{\pi}$
124	131	$1.22 \pm 0.16$	$2+ \rightarrow 3+$
139	270	$0.91 \pm 0.22$	$3+ \rightarrow 4+$
115	385	$1.37 \pm 0.18$	$4+ \rightarrow 5+$
219	604	$0.87 \pm 0.21$	$5+ \rightarrow 6+$
289	893	$1.16 \pm 0.56$	$6+ \rightarrow 7+$

Table 5.1.9:  $\gamma$ -ray energy, level energy, DCO ratio and their assignment in  $^{104}\text{Ag}$ .

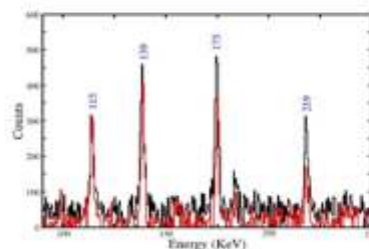


Fig. 5.1.9.1: DCO gated spectra with gate on 124 KeV transition.

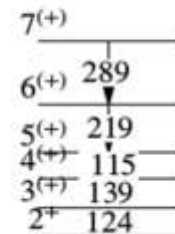


Fig. 5.1.9.2: Band based on  $2^+$  states at 7 keV excitation energy in  $^{104}\text{Ag}$ .

The band at excitation energy 7 keV and band head spin of  $2^+$  might be a mixing of the  $\pi g_{9/2} \otimes \nu d_{5/2}$  and  $\pi g_{9/2} \otimes \nu g_{7/2}$  configurations, as reported in the earlier study [1]. The spin-parity assignment for this band was tentative. We have determined the spin-parity based on DCO measurements. The values of DCO ratios determined from this study are tabulated in Table 5.1.9. Present angular correlation measurement confirms the dipole nature of the  $\gamma$ -rays of this band. Further analysis is in progress.

#### REFERENCES:

- [1] Z. G. Wang *et al.*, Phys. Rev. C **88**, 024306 (2013).
- [2] J. Tr'herne *et al.*, Phys. Rev. C **27**, 166, (1983).
- [3] P. Datta *et al.*, Phys. Rev. C **69**, 044317 (2004).
- [4] R. Palit *et al.*, Nucl. Instrum. Methods Phys. Res., Sect. A **680**, 90 (2012).

#### 5.1.10 Study of shell closure effect through evaporation residue cross-sections measurement of $^{48}\text{Ti} + ^{140,142}\text{Ce}$ systems

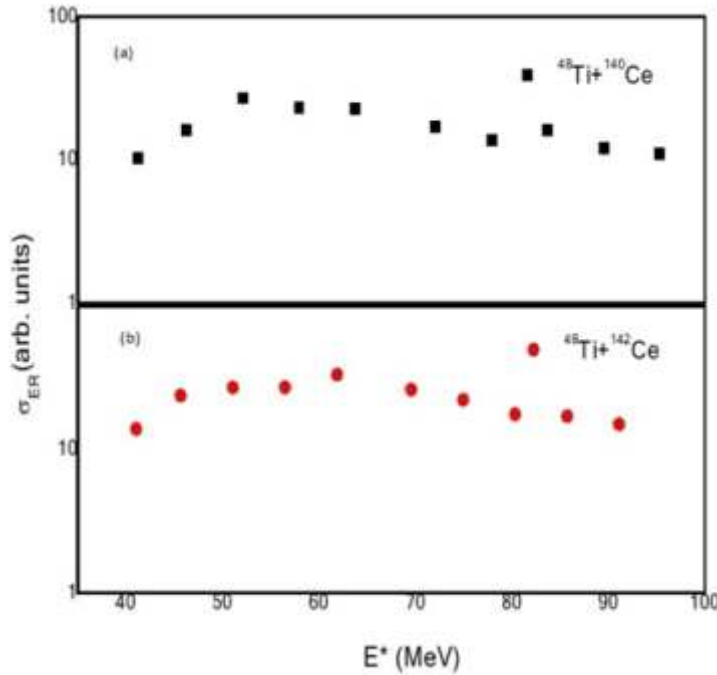
Devinder Pal Kaur<sup>1</sup>, B. R. Behera<sup>1</sup>, N. Madhavan<sup>2</sup>, S. Nath<sup>2</sup>, J. Gehlot<sup>2</sup>, A. Kaur<sup>1</sup>, Raghav<sup>1</sup>, Gonika<sup>2</sup>, R. Biswas<sup>2</sup>, S. Yadav<sup>1</sup>, Amit<sup>1</sup>, A. Parihar<sup>2</sup>, K. Rani<sup>1</sup>, H. Arora<sup>1</sup>, S. Narang<sup>1</sup> and S. Pal<sup>3</sup>

<sup>1</sup>Department of Physics, Panjab University, Chandigarh 160014, India

<sup>2</sup>Inter-University Accelerator Centre, Aruna Asaf Ali Marg, New Delhi 110067, India

<sup>3</sup>CS-6/1, Golf Green, Kolkata 700095, India

Nuclear structure of the colliding nuclei plays a key role in understanding the dynamics of heavy ion induced reactions as it influences the fusion probability. In some of the recent studies, the importance of  $N = 82$  in the heavy ion fusion reaction was proposed. It was reported that shell closure of one of the interacting nuclei can lead to the enhanced ER cross-section and help in the synthesis of heavy nuclei. An experiment has recently been carried out using the HYbrid Recoil mass Analyzer (HYRA) [1] with pulsed  $^{48}\text{Ti}$  beam from 15UD Pelletron + LINAC facility at IUAC. Evaporation residue (ER) cross-sections have been measured at  $E_{\text{lab}}$  in the range of 208 – 273 MeV. Isotopically enriched targets of  $^{140,142}\text{Ce}$  (both of thickness 100  $\mu\text{g}/\text{cm}^2$ ), with a carbon backing of 20  $\mu\text{g}/\text{cm}^2$  and capping of 5  $\mu\text{g}/\text{cm}^2$  have been used. For the purpose of calibration, a target of  $^{122}\text{Sn}$  has also been used in the experiment. Elastically scattered  $^{48}\text{Ti}$  ions have been detected by two silicon detectors placed at  $\pm 26^\circ$  with respect to the beam direction. At all beam energies, helium gas pressure in HYRA has been kept at 0.30 Torr. HYRA magnetic field settings have been calculated using a simulation program [2]. The ERs have been separated from other contaminants using the HYRA and detected by a position sensitive multi-wire proportional counter (MWPC) placed at the focal plane. A time of flight (TOF) spectrum has been generated with timing from the MWPC as the start and the radio-frequency (RF) signal used for beam pulsing as the stop. The logical OR of all the timing signals (from the two monitor detectors and the MWPC) has been used as the master strobe for data acquisition system. The preliminary ER cross-sections ( $\sigma_{ER}$ ) in arbitrary units, measured for both the systems, are shown in Fig. 5.1.10.

Fig. 5.1.10: ER excitation functions for (a)  $^{48}\text{Ti} + ^{140}\text{Ce}$  and (b)  $^{48}\text{Ti} + ^{142}\text{Ce}$ .

## REFERENCES:

- [1] N. Madhavan *et al.*, Pramana – J. Phys. **75**, 317 (2010).  
[2] S. Nath, A Monte Carlo code to model ion transport in dilute gas medium (unpublished).

**5.1.11 High Spin Structure of  $^{129}\text{La}$** 

K. Rojeeta Devi<sup>1</sup>, Suresh Kumar<sup>1</sup>, Naveen Kumar<sup>1</sup>, Neelam<sup>1</sup>, Neeraj Kumar<sup>1</sup>, A. Banerjee<sup>1</sup>, C. V. Ahmad<sup>1</sup>, Anand Pandey<sup>1</sup>, Ravi Bhushan<sup>1</sup>, Unnati Gupta<sup>1</sup>, S. K. Chamoli<sup>1</sup>, S. Verma<sup>1</sup>, Samit Kr. Mandal<sup>1</sup>, R. Garg<sup>2</sup>, Indu Bala<sup>2</sup>, S. Bhattacharya<sup>2</sup>, R. P. Singh<sup>2</sup>, S. Muralithar<sup>2</sup>, Pragati<sup>3</sup>, Ajay Y. Deo<sup>3</sup>, Sutanu Bhattacharyaa<sup>4</sup>, T. Trivedi<sup>4</sup>, Anupriya Sharma<sup>5</sup>, Chandrani Majumder<sup>6</sup>, H. P. Sharma<sup>6</sup>, Vishnu Jyoti<sup>7</sup>

<sup>1</sup>Department of Physics and Astrophysics, University of Delhi, Delhi 110007, India.

<sup>2</sup>Inter University Accelerator Centre, Aruna Asaf Ali Marg, New Delhi 110067, India.

<sup>3</sup>Department of Physics, Indian Institute of Technology, Roorkee, 247667, India.

<sup>4</sup>Department of Pure and Applied Physics, Guru Ghasidas University, Bilaspur, 495009, India.

<sup>5</sup>Department of Physics, Banaras Hindu University, Varanasi 221005, India.

<sup>6</sup>Department of Physics, Himachal Pradesh University, Shimla 171005, India.

<sup>7</sup>Department of Nuclear Physics, Andhra University, Visakhapatnam 530003, India.

The different shapes and structures observed in atomic nuclei are determined by the configuration of the valence nucleons and can be discussed in light of different angular momentum coupling. In mass 130 amu region, the rotational alignment of a pair of  $h_{11/2}$  neutrons along the rotation axis favours oblate shape whereas the alignment of a pair of  $h_{11/2}$  protons gives rise to a prolate shape. Various high spin structure phenomena have been studied in this mass region, such as magnetic and antimagnetic rotation, chiral rotation, superdeformation and identical bands. In recent years, multiple bands and degenerate bands have also been reported in  $^{133}\text{Ce}$  and  $^{133}\text{La}$ . The odd-Z  $^{129}\text{La}$  is expected to show these phenomena and hence it is an interesting candidate for study. Previously,  $^{129}\text{La}$  was studied by using the reaction  $^{51}\text{V}(^{82}\text{Se}, 4n)^{129}\text{La}$ . In the earlier study, two strongly coupled bands, namely, band (1,2) and band (8,9) and many dipole bands were established with mostly tentative spin and parity assignment. However, many discrepancies between the experimentally observed values and the theoretically predicted values were reported. Therefore, the main aim of the present work is to study the high spin structure of  $^{129}\text{La}$  using  $R_{DCO}$  and polarization measurements.

An experiment was performed to populate the excited states of  $^{129}\text{La}$  through the reaction  $^{121}\text{Sb}(^{12}\text{C}, 4n)^{129}\text{La}$ . The beam ( $E_{\text{lab}} = 66$  MeV) was provided by the 15UD Pelletron of IUAC. The target ( $900 \mu\text{g}/\text{cm}^2$ ) had a  $10.0 \text{ mg}/\text{cm}^2$  thick backing of  $^{197}\text{Au}$ . The  $\gamma$ -rays were detected by the Indian National Gamma Array (INGA). It consisted of 18 Compton-suppressed Clover detectors, with four, four, six, two and two detectors placed at  $148^\circ$ ,  $123^\circ$ ,  $90^\circ$ ,  $57^\circ$  and  $32^\circ$  with respect to the beam direction, respectively, at the time of the experiment. The distance between the target and the detectors was 25 cm. List mode data were collected in double and higher folds  $\gamma$ -ray coincidence using the multi-parameter data-acquisition software CANDLE. A total of about  $13 \times 10^7$  events were recorded.

The symmetric and asymmetric matrices were generated by sorting the data with CANDLE and INGASORT programs.

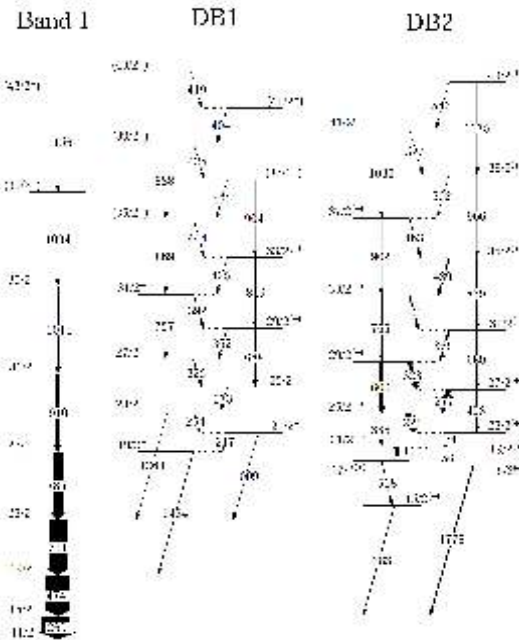


Fig. 5.1.11.1: Partial level scheme of  $^{129}\text{La}$ .

First the band-head energy of the DB2 was established as 2242 keV by observing the  $\gamma$ -ray transitions in the coincidence spectra. The multipolarity of  $\gamma$ -transitions was extracted on the basis of RDCO and polarization measurements. The band-head spin of DB1 was established to have positive parity. Fig. 5.1.11.1 shows partial level scheme established in the present study. Fig. 5.1.11.2 represents the co-incidence spectrum gated by 164 keV in DB2.

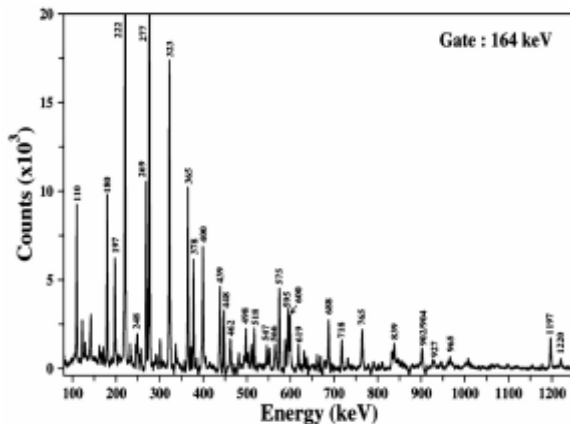


Fig. 5.1.11.2:  $\gamma$ - $\gamma$  coincidence spectrum gated by the 164 keV,  $23/2^{(+)} \rightarrow 21/2^{(+)}$  transition in DB2.

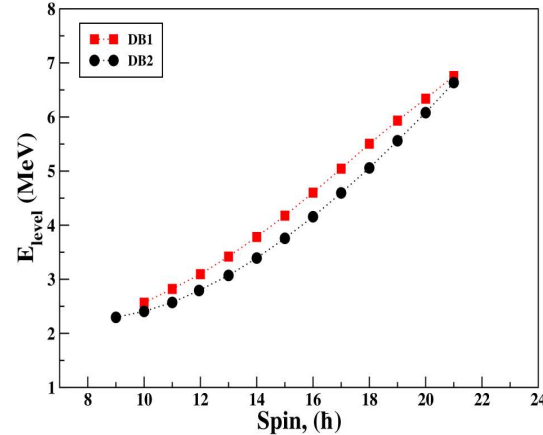


Fig. 5.1.11.3: Spin (h) vs. energy (MeV) plot for DB1 and DB2.

The two dipole bands have an energy separation of 54 keV at spin  $I=19/2^+$  (Fig. 5.1.11.3) and the separation energy increases up to 448 keV at  $I=35/2^+$ . After that the two bands approach in energy with a difference of 119 keV at  $I=43/2^+$ . These bands were further examined by observing the ratio of transition probability,  $B(M1)/B(E2)$ . These ratios for the two dipole bands were found to be very different in behaviour and magnitude. TAC calculations are in progress to understand the structure of these dipole bands.

## REFERENCES:

- [1] S. C. Pancholi, Exotic Nuclear Excitation, (2010).
- [2] J. Meng *et al.*, Mod. Phys. Lett. A **23**, 2560 (2008).
- [3] P.A. Butler, J. Meyer-Ter-Vehn, D. Ward, H. Bertschat, P. Colgbani, R.M. Diamond and F.S. Stephens, Phys. Lett. **56B**, 453 (1975).
- [4] Smith PJ, Unwin D J, Kirwan A, Love D J G, Nelson A H, Nolan P J, Todd D M and Twin P J, J. Phys. G: Nucl. Phys., **11** 1271 (1985).
- [5] Y. He *et al.*, J. Phys. G: Nucl. Part. Phys. **18**, 99-119 (1992).
- [6] I. Sankowska *et al.*, Eup. Phys. J. A **37**, 169-175 (2008).
- [7] S. Frauendorf, J. Meng, Nucl. Phys. **A617**, 131 (1997).
- [8] S. Muralithar *et al.*, Nucl. Instrum. Methods Phys. Res. A **622**, 281 (2010).

### 5.1.12 Study of heavy ion induced fission fragment mass distribution for the decay of the $^{188,190}\text{Hg}$ compound nucleus

Devinder Pal Kaur<sup>1</sup>, B. R. Behera<sup>1</sup>, P. Sugathan<sup>2</sup>, A. Jhingan<sup>2</sup>, K. S. Golda<sup>2</sup>, N. Saneesh<sup>2</sup>, Mohit<sup>2</sup>, A. Kaur<sup>1</sup>, Raghav<sup>1</sup>, S. Yadav<sup>1</sup>, Amit<sup>1</sup>, Kajol<sup>3</sup>, Divya<sup>2</sup>, H. Arora<sup>1</sup> and S. Narang<sup>1</sup>

<sup>1</sup>Department of Physics, Panjab University, Chandigarh 160014, Chandigarh, India

<sup>2</sup>Inter University Accelerator Centre (IUAC), Aruna Asaf Ali Marg, New Delhi 110067, India

<sup>3</sup>Department of Physics and Astrophysics, University of Delhi, Delhi 110007, India

Influence of shell effects on the dynamics of fusion-fission process in the pre-actinide Hg-Pb region is a matter of considerable interest. It is observed that there is a substantial change in the shape of fission fragment mass distribution from asymmetric to symmetric with the increase in the mass number of Hg isotopes from 180 to 196 [1]. To verify these predictions we populated  $^{188,190}\text{Hg}$  at various excitation energies in a recent experiment at IUAC. A pulsed  $^{48}\text{Ti}$  beam, from the 15UD Pelletron + LINAC, was bombarded on the  $^{140,142}\text{Ce}$  targets (both  $100\mu\text{g}/\text{cm}^2$  thick with  $20\mu\text{g}/\text{cm}^2$  carbon backing and  $5\mu\text{g}/\text{cm}^2$  carbon capping). The targets, with carbon backing facing the beam, were placed at the centre of the NAND [2] scattering chamber. Two multi-wire proportional counters (MWPCs) were placed, each at a distance of 25 cm from the center of the target, for detection of fission fragments (FFs). Both the detectors were placed at an angle of  $55^\circ$  with respect to the beam axis. In order to monitor the beam flux, two silicon detectors were mounted in the scattering chamber at an angle of  $\pm 13.5^\circ$  with respect to the beam direction. List mode data were collected using the softwares FREEDOM and NIAS-MARS, developed at IUAC. A two dimensional plot between two anode signals from the two MWPCs, indicating fission-like events, is shown in Fig. 5.1.12.

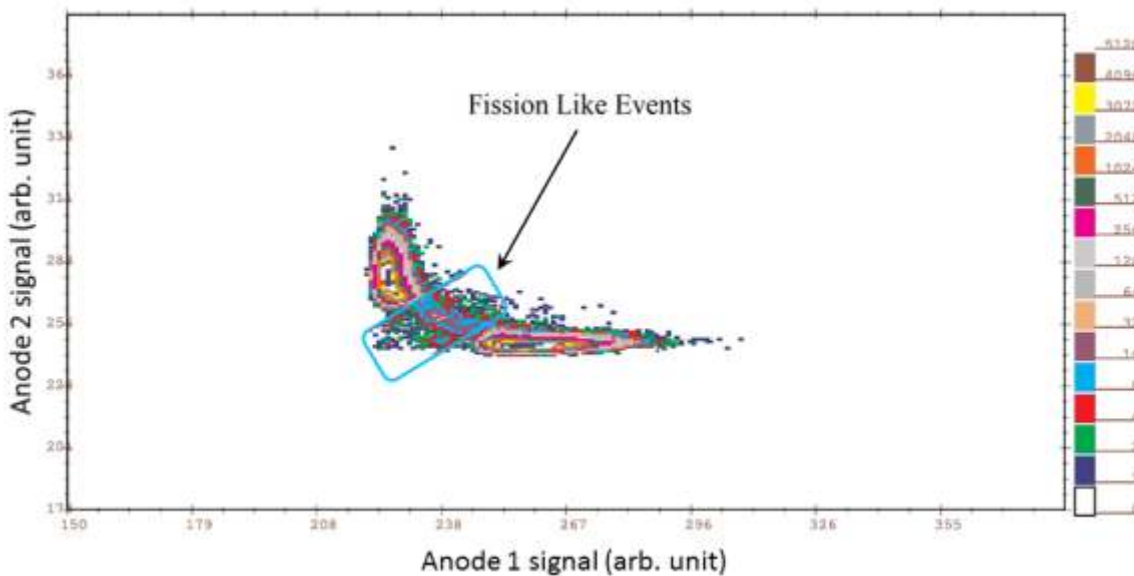


Fig. 5.1.12: Coincidence between the two anode signals from the two MWPCs for the reaction  $^{48}\text{Ti}+^{142}\text{Ce}$  at  $E_{\text{lab}} = 205$  MeV.

#### REFERENCES:

- [1] A. V. Andreev *et al.*, Phys. Rev. C. **86**, 044315 (2012).
- [2] P. Sugathan *et al.*, Pramana – J. Phys. **83**, 807 (2014).

### 5.1.13 Level lifetime measurements of $^{130}\text{La}$ through DSAM: Search for the chiral bands and shape co-existence

Himanshu Kumar Singh<sup>1</sup>, Pragya Das<sup>1</sup>, S. Muralithar<sup>2</sup> and R. P. Singh<sup>2</sup>

<sup>1</sup>Department of physics, Indian Institute of Technology Bombay, Powai, Mumbai 400076, India

<sup>2</sup>Inter-University Accelerator Centre, Aruna Asaf Ali Marg, New Delhi 110067, India

The doubly odd nuclei in mass region  $\sim 130$  amu provide insight on competitive features of single particle and collective behaviour. The above interplay opened up wide range of phenomena at low and high spin states. The opposite shape driving high-j orbitals occupied by odd particles leads to gamma soft core of various shapes and consequently possibility of chiral rotations in triaxial deformed nuclei [1,2]. In the present work, we are trying to establish the chiral bands and other deformed shapes (shape co-existence) in  $^{130}\text{La}$  experimentally. An attempt has been made to find the lifetimes of the high spin states of  $^{130}\text{La}$  by the Doppler shift attenuation method and to gain an insight on their deformations and quadrupole moments.

The experiment was performed using the Indian National Gamma Array (INGA) with eighteen Compton-suppressed HPGe detectors at IUAC in the year 2016. A self-supporting target  $^{116}\text{Cd}$  (thickness  $4.6 \text{ mg/cm}^2$ ) was bombarded by  $^{19}\text{F}$  beam at  $E_{\text{lab}} = 94 \text{ MeV}$ . The choice of beam energy was based on excitation function measurements. The  $^{130}\text{La}$  was formed via the reaction  $^{116}\text{Cd}(^{19}\text{F}, 5n)^{130}\text{La}$ . Three asymmetric matrices at angles  $32^\circ$ ,  $90^\circ$  and  $148^\circ$  vs all detectors were sorted. A symmetric matrix was also created to study the level scheme.

The objective of this work was to identify the existence of chiral bands as well as other deformed bands in  $^{130}\text{La}$ . All three bands were well populated in this experiment and were looked over in distinct energy gates [3]. The positive parity band is considered to be chiral. The partner band is weakly populated and nearly degenerate as compared to the main band. This confirms the initial experimental observation of the chiral band. The interlinking inter-band transitions are also observed with less statistics. The initial fits are done using the Lineshape program as shown in Fig. 5.1.13.1. The measurements of partner bands are still in progress because of low statistics and are tentative.

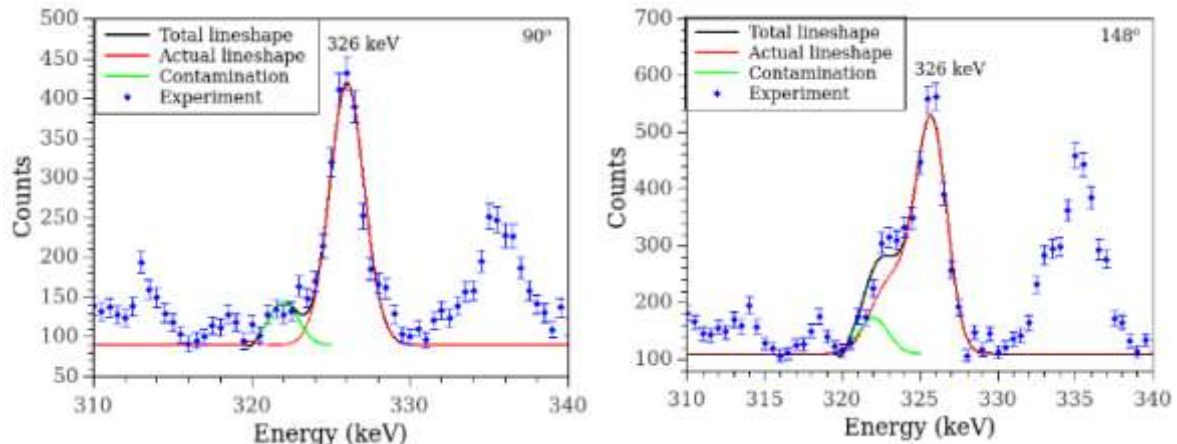


Fig. 5.1.13.1: Lineshape at two different angles.

The negative parity band is built on  $\pi h_{11/2} \otimes \nu g_{7/2}$  particle configuration. To observe the band, a gate was put on the 177 keV transitions. The gated spectrum is shown in Fig. 5.1.13.2. The band consists of strong M1 cross over with weak E2 transitions. The nearly equal spacing of gamma lines suggest a stable deformation or near axial prolate shape ( $\gamma \ll 10^\circ$ ). Currently, we are measuring the level lifetimes of this band.

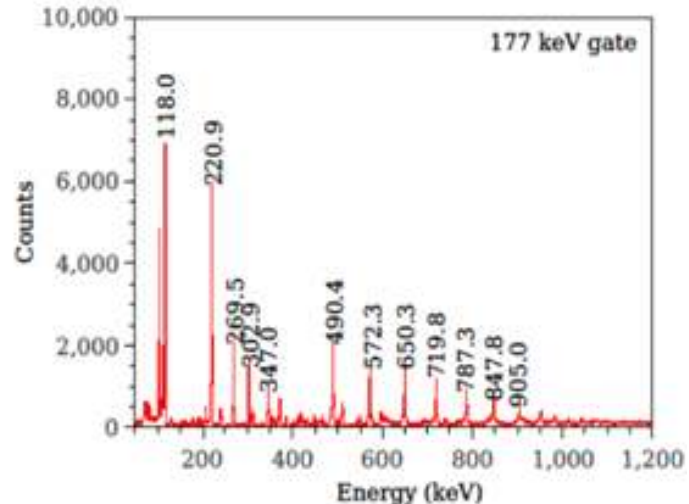


Fig. 5.1.13.2:  $\gamma - \gamma$  coincidence spectrum gated by 177 keV.

The 2016 beam time was a successful experiment. However, the population of chiral partner band is quiet weak to observe the Doppler shifted shape. Moreover, we are able to see all three bands of different deformations. We will look for another band in  $^{130}\text{La}$  of collective oblate (predicted) deformation and establish their particle configuration. The exact linkage of the excited band with low spin states is still unknown. On gating with 242 keV transition, it is clearly observed that the band decays towards the negative parity band side (qualitatively). Study of this band is important to establish the shape co-existence in  $^{130}\text{La}$ .

#### REFERENCES:

- [1] K. Starosta et al., Phys. Rev. Lett. 86, 971 (2001).
- [2] T. Koike et al., Phys. Rev. C 67, 044319 (2003).
- [3] M. J. Godfrey et al., J. Phys. (London) G15, 487 (1989).

## 5.2 MATERIALS SCIENCE

Ambuj Tripathi

The materials science facilities continue to support research programmes of a large number of users from different universities and institutions. This year there were a total of 30 user experiments spread over 102 shifts and were performed without any major beam time loss due to facility break down in materials science beamlines in beamhall I and II. These included 8 BTA runs spread over 25 shifts associated with students' Ph.D. programmes. Though the swift heavy ion (SHI) irradiation and related experiments mostly utilize irradiation chamber in the materials science beamlines in beamhall-I, 2 experiments of 6 shifts requiring low fluence irradiation were performed in GPSC beamline. Besides irradiation facilities, materials science group is also providing many materials synthesis and characterization facilities such as XRD, AFM, SEM, Raman, UV-Vis, I-V, Hall measurement etc and these are heavily utilized by users. This year more than 2100 samples were characterized. Special attention is given to ensure that all experimental facilities are operational at all times. The problems developed earlier in XRD and UV-Vis systems were resolved and at present all facilities are operational. The new FTIR and the electron beam deposition systems have also become operational. The newly installed Transmission Electron Microscope is also being operated as user facility now. The materials science research programmes are being carried out in a wide range of energies varying from tens of keV to hundreds of MeV and the complete list of publications is given in section 6.7. The highlights of the activities are also available in Materials Science group webpage which was updated this year.

This year there were many interesting results in the various areas of research including those on ion beams induced nanostructuring, synthesis of nanocomposites and applications, novel phase formations, etc. Special emphasis is given to in-situ/ on-line measurements and many such experiments were performed this year. The organic-inorganic hybrid heterojunction diode ( $\text{ZnO}:\text{P}3\text{OT}/\text{PS}/\text{p-Si}$ ) parameters such as ideality factor, barrier height, saturation current density, and series resistance is investigated by in-situ current density-voltage (J-V) characteristic measurements during 80 MeV oxygen ( $\text{O}^{6+}$ ) ion irradiation with ion fluence from  $5 \times 10^{11}$  to  $1 \times 10^{14}$  ions/cm<sup>2</sup> and rectifying behavior of pristine hybrid diode is distinctly observed. Swift heavy ions (SHI) irradiation has been used as an effective tool to improve the dispersion of nanofillers in polymer nanocomposites (NCs) and used as an effective tool to tailor and enhance the MW absorption in light-weight  $\text{CoFe}_2\text{O}_4/\text{NG}/\text{PMMA}$  and  $\text{Fe}_3\text{O}_4/\text{NG}/\text{PMMA}$  nanocomposites. The study on fluorite type polycrystalline  $\text{Ce}_{1-x}\text{Zr}_x\text{O}_2$  with  $x=0.2$  (CSZ) via swift heavy ions irradiation is undertaken and though a small swelling and disordering takes place, the material remains crystalline even on irradiation at higher ion fluence. The undoped and  $\text{Tb}^{3+}$  (0.5 mol%) doped  $\text{NaMgF}_3$  were irradiated with carbon ion beam (85 MeV and 50 MeV) at different ion fluences to investigate thermoluminescence (TL) and optically stimulated luminescence (OSL) properties and linear OSL behavior ranging from  $1 \times 10^5 - 5 \times 10^6$  ions/cm<sup>2</sup> for low fluences and up to  $2 \times 10^9$  ions/cm<sup>2</sup> for high fluences was observed. The crystal field analysis of thulium doped aluminum oxide sample is done using IL spectroscopy and it is shown that IL spectrum of undoped sample confirms the presence of  $\text{Cr}^{3+}$  and  $\text{Mn}^{4+}$  impurities in the host samples. Enhanced electrical properties of few layers  $\text{MoS}_2$ -PVA nanocomposite film via homogeneous dispersion and annealing effect induced by 80 MeV Carbon  $^{6+}$  Swift Heavy Ion irradiation is also observed. Defect mediated modification of structural, optical and magnetic properties of  $\text{Xe}^{3+}$  ions irradiated GaN/sapphire films has been studied. Some of the other studies include studies on 120 MeV  $\text{Ag}^{9+}$  ions at the fluence of  $2 \times 10^{12}$  ions/cm<sup>2</sup> irradiated wide-bandgap perovskite materials, zinc stannate ( $\text{ZnSnO}_3$ ) and strontium ( $\text{SrSnO}_3$ ) stannate for optoelectronic applications, and effect of annealing on the magnetic properties of FeCo thin films. Enhanced room temperature ferromagnetism and green photoluminescence with increase in doping in Cu doped ZnO thin film synthesised by neutral beam sputtering was observed. It was shown that synthesised Cu doped ZnO thin films can be used as spin LEDs and switchable spin-laser diodes. Special emphasis is given to in-situ/ on-line measurements and many such experiments were performed this year. In situ current-voltage characteristics of Nb-doped  $\text{TiO}_2/\text{p-Si}$ -based heterojunction diode have been studied under dense electronic excitations of 84 MeV  $\text{Si}^{6+}$  ions. The diode parameters such as ideality factor, barrier height, reverse saturation current and series resistance were found to be a strong function of ion irradiation fluence. Such in situ studies on n-NTO/p-Si heterojunction diode under harsh radiation environment are very appropriate for the better understanding of heterojunction interface properties and make it suitable for use in aerospace industry and nuclear reactors. The defect induced photoluminescence studies on behavior of the Ga doped ZnO (GZO) thin films with varying doping (Ga) concentration and with energetic ion irradiation showed that violet emission might originate from zinc interstitial defects (Zni) and the concentration of Zni increases with increasing doping concentration. The intense energetic ions encountered in space can result in many transient and destructive single event effects (SEE) are studied with low ion fluence ( $\sim 10^6 \text{ cm}^{-2}$ ) test facility at GPSC beam line and three such runs took place this year to evaluate the radiation hardness of many devices designed and fabricated at SCL. Apart from the studies on swift heavy ion irradiation, a large number users have published their work related to effects of low

energy ion implantations and gamma irradiations in various physical properties of materials. The interface formation and magnetic properties due to 3d transition metal ion implantations have been studied. Enhancement of ferromagnetism due to ion implantations has been investigated in FePt. Apart from these studies, work on gas sensing has been reported. Investigations using gamma irradiation have demonstrated the enhancement of water oxidation catalytic performance in graphene oxide, multifunctionality in the same materials etc.

The 5<sup>th</sup> International Conference on Nanostructuring with Ion Beams (ICNIB 2019) was organized by IGCAR Kalpakkam, India, in cooperation with the Inter-University Accelerator Centre (IUAC), New Delhi and Ion Beam Society of India (IBSI). The conference was held at IGCAR Kalpakkam during Nov 6-8, 2019. IUAC has been organizing conferences on the topic of Nanostructuring with Ion Beams (NIB) and the last four conferences in this series were held in Allahabad, Jaipur and Agra and Indore in 2011, 2013 2015 and 2017. The conference was co-chaired by Dr BK Panigrahi (IGCAR) and Dr G Amrendra (IGCAR) and the inaugural address was given by Prof AC Pandey, Director, IUAC. The conference had twenty-eight invited, ten oral talks and 60 poster contributions. The IBSI gave the prizes for best oral presentation and best poster presentation by research scholars. A preconference School on Ion Beams in Materials Science with focus on “Radiation damage in nuclear materials” preceded the conference on Nov 4-5, 2019. The school had 9 lectures, including 3 from abroad.

### 5.2.1 Investigation of hybrid heterojunction diode parameters by *in-situ* J-V measurements during ion irradiation

Jitendra Singh<sup>1</sup>, Subodh K. Gautam<sup>2</sup>, R. G. Singh<sup>3</sup> and Fouran Singh<sup>1</sup>

<sup>1</sup>Materials Science Group, Inter University Accelerator Centre, Aruna Asaf Ali Marg, New Delhi-110067, India.

<sup>2</sup>Laboratory of Solid State Physics (LPS), University of Paris-Sud, 91400 Orsay, France

<sup>3</sup>Department of Physics, Bhagini Nivedita College, Delhi University, New Delhi-110043, India

The organic-inorganic hybrid heterojunction diode (ZnO:P3OT/PS/p-Si) parameters such as ideality factor ( $\eta$ ), barrier height ( $\Phi_B$ ), saturation current density ( $J_s$ ), and series resistance ( $R_s$ ) have been investigated by *in-situ* current density-voltage ( $J$ - $V$ ) characteristic measurements during 80 MeV oxygen ( $O^{6+}$ ) ion irradiation with systematically increasing ion fluence from  $5 \times 10^{11}$  to  $1 \times 10^{14}$  ions/cm<sup>2</sup>. It is distinctly observed that the pristine hybrid diode shows rectifying behaviour, the variation of RR as a function of ion fluence at 2 V bias voltage is shown in Fig. 2 (a). For the fluence  $5 \times 10^{11}$  to  $5 \times 10^{12}$  ions/cm<sup>2</sup> the RR decreases and after that it drastically increases at higher ion fluences and can be attributed to the suppression of leakage current. Further, during irradiation the incident primary  $O^{6+}$  ions are get implanted within the Ag contact because the thickness of Ag contact (135  $\mu$ m) is higher than the ions projectile range (120.6  $\mu$ m). Hence, Ag contact protects hybrid layer from direct exposure of O ions irradiation. The effect of primary O ions are responsible for modifying the hybrid layer properties at outer region only. The implanted O ions produces secondary charge particles through the ballistic collisions are predominately responsible for creation of defect and trap states at the interface and causes to increase in the leakage current at lower ion fluences. However, at higher ion fluences these states are start annealing out due to the fact of self-annealing process. Therefore, an increase in RR is observed at higher ion fluences. The results also show that the  $\eta$ ,  $\Phi_B$  and  $R_s$  values decreases while the  $J_s$  values increases with increasing ion fluences as shown in Fig. 2 (b-d). However, after irradiation, an anomalous behavior in the current density is observed which can be attributed due to the fact that irradiation-induced electrically active defects at the interface at lower ion fluence and their self-annealing process at higher ion fluences. Although, the detailed analysis is in progress.

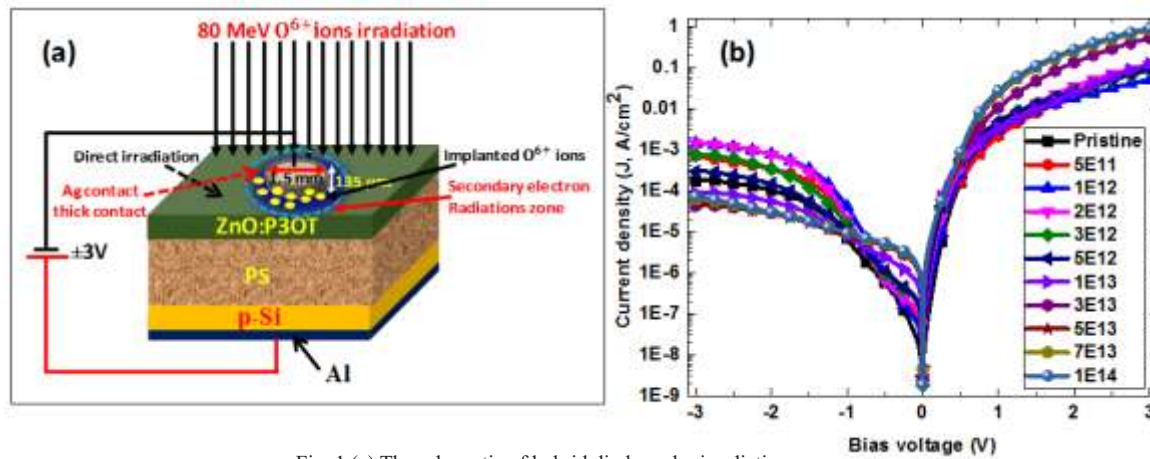


Fig. 1 (a) The schematic of hybrid diode under irradiation  
(b) *In-situ* current density–voltage ( $J$ - $V$ ) characteristics of hybrid diode during ion irradiation.

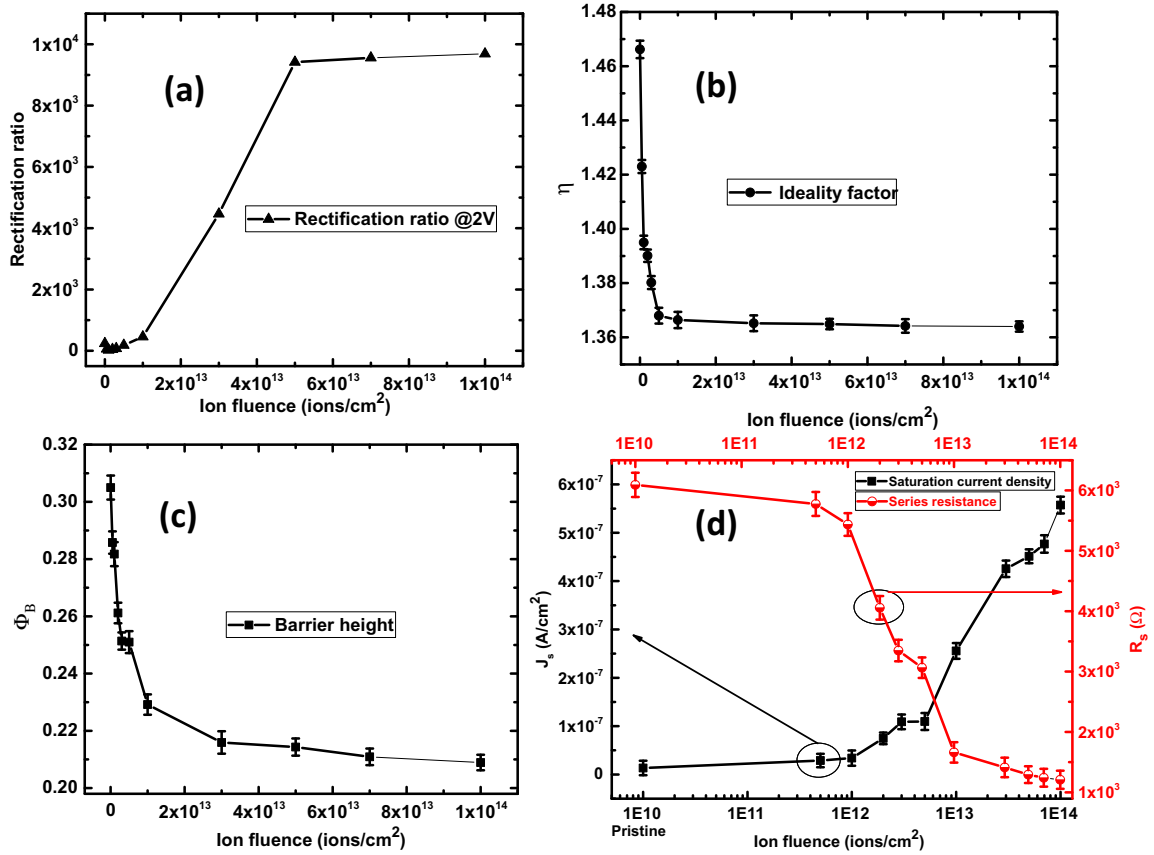


Fig. 2 (a-d) Variation of the various hybrid diode parameters.

### 5.2.2 Swift heavy ions irradiation effects on complex permittivity, permeability, and microwave-absorbing properties of CoFe<sub>2</sub>O<sub>4</sub>/NG/PMMA and Fe<sub>3</sub>O<sub>4</sub>/NG/PMMA nanocomposites

Prachi Yadav<sup>1</sup>, Sunita Rattan<sup>1,\*</sup>, Ambuj Tripathi<sup>2</sup> and Sandeep Kumar<sup>3,4</sup>

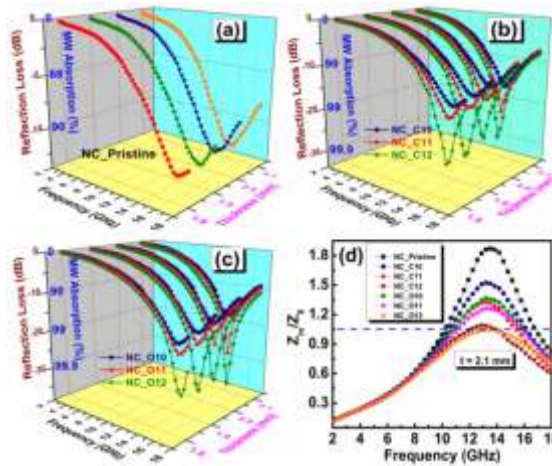
<sup>1</sup>Amity Institute of Applied Sciences, Amity University Uttar Pradesh, Noida, Uttar Pradesh-201303, India

<sup>2</sup>Inter-University Accelerator Centre (IUAC), Aruna Asaf Ali Marg, New Delhi-110067, India

<sup>3</sup>Magnetics and Advanced Ceramics Lab, Department of Physics, Indian Institute of Technology Delhi, Hauz Khas, New Delhi-110016, India

<sup>4</sup>Department of Physics, Bhaskaracharya College of Applied Sciences, University of Delhi, Delhi-110075, India

Swift heavy ions (SHI) irradiation has been used as an effective tool to improve the dispersion of nanofillers and tailor the various properties of polymer nanocomposites (NCs) [1]. The previous reports have shown a significant modification in the material properties (i.e., magnetic, dielectric, electrical, optical, and microstructural etc.) after the SHI irradiation [2]. The high energy (~100 MeV) ions can mostly lose their energy through in-elastic collisions (electronic energy loss ( $S_e$ )) with the atoms of target materials (NCs) leading to a steep rise in the local temperature [3]. As a result, the evolution of short-term (few picoseconds) molten state in NCs can lead to the diffusion of polymer chains directly into the galleries of nanofillers.

Fig. 1. Variations in the calculated reflection loss and %MW absorption against frequency and thickness for (a) pristine, (b) C<sup>6+</sup> (80 MeV) and (c) O<sup>7+</sup> (100 MeV) irradiated CoFe<sub>2</sub>O<sub>4</sub>/NG/PMMA NCs. (d) the frequency dependent relative impedance for all the NCs (pristine and irradiated).

In this report, the combination of  $\text{CoFe}_2\text{O}_4$  (CFO) and  $\text{Fe}_3\text{O}_4$  (FO) nanoparticles and exfoliated nanographites (NGs) has been composited with PMMA polymer using the melt-blending technique.  $\text{CoFe}_2\text{O}_4$  and  $\text{Fe}_3\text{O}_4$  nanoparticles exhibit a relatively higher magnetic loss due its high intrinsic magnetic anisotropy [4]. Further, the exfoliated NG, a derivative of graphite, can be regarded as a promising dielectric MW absorber owing to its low cost, low density, easy processing, large dielectric loss, and high mechanical strength [5]. The coupling of these two nanofillers in the PMMA matrix using the melt-blending technique can furnish excellent MW absorbing properties. Though the melt-blending method is relatively a better technique to attain an improved dispersion of nanofillers, the agglomeration of nanofillers can occur due to the inherent inert nature of NGs and ferromagnetic nature of the CFO and FO nanoparticles [5]. As discussed, the SHI irradiation technique has been used to tailor the properties of polymer NCs for a wide range of applications. However, the effects of SHI irradiation on the MW absorbing properties of polymer NCs have never been investigated (to the best of our knowledge).

In this work, the influence of swift heavy ions (SHI) [ $\text{C}^{6+}$  (80 MeV) and  $\text{O}^{7+}$  (100 MeV)] irradiation on microwave (MW) absorbing properties of  $\text{CoFe}_2\text{O}_4/\text{NG}/\text{PMMA}$  and  $\text{Fe}_3\text{O}_4/\text{NG}/\text{PMMA}$  nanocomposites was investigated in the frequency range of 2–18 GHz. This work is the first attempt to study the comprehensive effects of SHI irradiation on MW absorbing properties of polymer nanocomposites. The scanning electron micrographs of the nanocomposites reveal monotonic improvement in the dispersion of nanofillers with an increase of irradiation dose. With an increase in the fluence of ions, the room temperature saturation magnetization was observed to decrease monotonically, whereas a reverse trend was detected for the coercivity. The SHI irradiated nanocomposites exhibited a relatively stronger MW absorption as well as a higher effective bandwidth of absorption. A minimum reflection loss ( $R_{\text{Lmin}}$ ) of -36.7 dB (99.98% MW absorption) and a broad bandwidth (for  $R_{\text{L}} < -10$  dB) of 7.1 GHz were detected in  $\text{O}^{7+}$  (100 MeV) SHI irradiated nanocomposite at the fluence of  $1 \times 10^{12}$  ions/cm<sup>2</sup>. The results demonstrate that SHI irradiation can be used as an effective tool to tailor and enhance the MW absorption in light-weight  $\text{CoFe}_2\text{O}_4/\text{NG}/\text{PMMA}$  and  $\text{Fe}_3\text{O}_4/\text{NG}/\text{PMMA}$  nanocomposites.

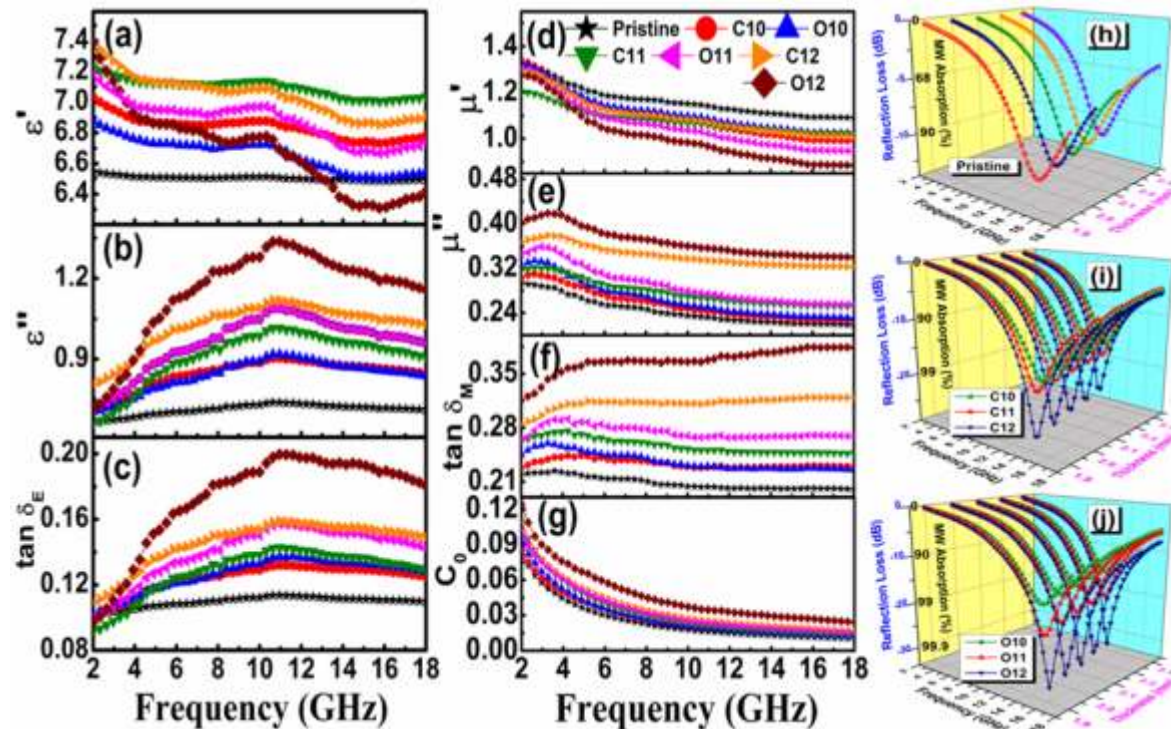


Fig. 2. (a) Real and (b) imaginary complex permittivity, (c) dielectric-loss, (d) real and (e) imaginary complex permeability, (f) magnetic-loss, (g)  $C_o$ -f curve; (h), (i), (j) frequency and thickness dependent reflection loss for all  $\text{Fe}_3\text{O}_4/\text{NG}/\text{PMMA}$  NCs

#### References:

- [1] P. Singhal, S. Rattan, J. Phys. Chem. B, 120 (2016) 3403-3413.
- [2] P. Mazumdar, S. Rattan, M. Mukherjee, RSC Adv., 5 (2015) 69573-69582.
- [3] S. Rattan, P. Singhal, A.L. Verma, Polym. Eng. & Sci., 53 (2013) 2045-2052.
- [4] C. Tyagi, S.A. Khan, I. Sulania, R. Meena, D.K. Avasthi, A. Tripathi, J. Phys. Chem. B, 122 (2018) 9632-9640.
- [5] P. Yadav, S. Rattan, A. Tripathi, S. Kumar, Mater. Res. Express, 6 (2019) 025047-025057.

## 5.2.3 Structural & optical response of 100 MeV Au<sup>+8</sup> irradiated BiFeO<sub>3</sub> thin films

Tarun Patodia<sup>1</sup>, Fouran Singh<sup>2</sup> and Balram Tripathi<sup>1</sup>

<sup>1</sup>Department of Physics, SS Jain Subodh P.G. (Auto.) College, Jaipur-302004

<sup>2</sup>Inter University Accelerator Centre, Aruna Asaf Ali Marg, New Delhi-110067

Ferroelectric materials are interesting due to their spontaneous polarization which is essential for device applications [1-2]. Moreover, they show an intrinsic photovoltaic (PV) response arising from a strong coupling between light, photocurrents, and atomic-scale degrees of freedom that causes a current-driven modulation of the internal field [3]. Photovoltaic properties in both bulk and thin ferroelectric films of BaTiO<sub>3</sub>, LiNbO<sub>3</sub> and Pb(Zr,Ti)O<sub>3</sub> have been studied [4]. However, the pure single phase BiFeO<sub>3</sub> (BFO), due to its superior multiferroic properties and optical bandgap (2.67–2.74eV) in the visible region [5] is highly suitable for PV applications compared to many other wide bandgap ferroelectrics [6]. Recently, Ji et al. [7] reported PV effect in BFO thin films under visible light illumination with a switchable photocurrent with respect to the direction of the ferroelectric polarization. However, photovoltaic properties are sensitive to fabrication process, electronic structure, and interfacial condition. Therefore, precise characterization of BiFeO<sub>3</sub> and investigation of BiFeO<sub>3</sub> based solar cells are of importance. In this present manuscript structural, electronic & optical response of BiFeO<sub>3</sub> thin films deposited on Al<sub>2</sub>O<sub>3</sub> substrate has been studied. BiFeO<sub>3</sub> thin films were grown by utilizing a pulsed laser deposition (PLD) facility. The thin films were grown at ~15 mTorr oxygen pressure and 500° C substrate temperature, and 70 mJ pulse energy at the target with a repetition rate of 10Hz ( $\lambda=248\text{nm}$ ) and of 200-nm thickness on Al<sub>2</sub>O<sub>3</sub> substrate. The films were irradiated at 300 K with 120 MeV Au<sup>+8</sup> ions using 15 UD tandem Pelletron accelerator. Maximum fluence used in the present study was  $5 \times 10^{12} \text{ ions/cm}^2$ . Films fixed to the target ladder were placed inside the high vacuum ( $\sim 10^{-6} \text{ torr}$ ) chamber during irradiation. Irradiation was performed in the direction nearly perpendicular to the sample surface. The ion beam was magnetically scanned over  $1 \times 1 \text{ cm}^2$  area covering the complete sample surface for uniform irradiation. X-ray diffractometer (Bruker D8 advance, PW 1600, CuKa = 1.54026 Å) for structural characterization and Hitachi-4150 spectrophotometer within spectral range 200-800 nm.

Fig. (a) shows a new peak (104) at fluence of  $5 \times 10^{12} \text{ ions cm}^{-2}$ , indicate formation of some impurity phase induced by ion irradiation. A comparison of this peak with those reported in JCPDS file [card no. 71-2494] indicates that the impurity phase may be of Bi<sub>2</sub>Fe<sub>4</sub>O<sub>9</sub>. It has been reported that BiFeO<sub>3</sub> is very unstable at high temperature and it rapidly decomposes into parasitic phases like Bi<sub>2</sub>Fe<sub>4</sub>O<sub>9</sub> or Fe<sub>2</sub>O<sub>3</sub> [8]. The formation of Bi<sub>2</sub>Fe<sub>4</sub>O<sub>9</sub> phase may be due to the effect of increased temperature in the materials medium during the passage of 100 MeV Au ions. Fig. (b) shows optical absorption spectra of the BiFeO<sub>3</sub> thin films. The absorption cut-off wavelengths of the films were approximately 565 nm, in agreement with a previous report [9–10]. The absorption spectrum of the BiFeO<sub>3</sub> film showed a large absorbance in the wavelength from 300 to 500 nm, which is likely associated with lattice distortion in the film. Energy gaps of the BiFeO<sub>3</sub> films were calculated by Tauc formula:

$$(hv\alpha)^n = A(hv - E_g) \dots \dots \dots \quad (1)$$

Here, h, v,  $\alpha$ , A, Eg, and n are the Plank constant, light frequency, absorption coefficient, proportional constant, energy gap, and power index which depends on the nature of the transition, respectively. In the present study n=2 was used for the BiFeO<sub>3</sub> because BiFeO<sub>3</sub> is a direct transition semiconductor [11-12]. The E<sub>g</sub> were estimated by extrapolating the linear part of the Tauc plots to meet  $(hv\alpha)^2 = 0$ , as shown in Fig. (c). The estimated E<sub>g</sub> values matches with previous reports [12]. On the other hand, the estimated E<sub>g</sub> increased from 2.19 eV to 2.65 eV with irradiation fluence indicating that E<sub>g</sub> depended on the structure of the BiFeO<sub>3</sub> and would be a result of lattice distortion in the film. Fig. (d) shows FTIR spectra having peaks at wave numbers, 500 cm<sup>-1</sup> (Fe-O) and stretching vibrations of O-Fe-O at 540 cm<sup>-1</sup>, 1500 cm<sup>-1</sup> (C-H), 1580 cm<sup>-1</sup> (C-C) and the broad band at 3730 cm<sup>-1</sup> (C-H) due to antisymmetric and symmetric stretching. Irradiated thin films showing the identical peaks with high intensity.

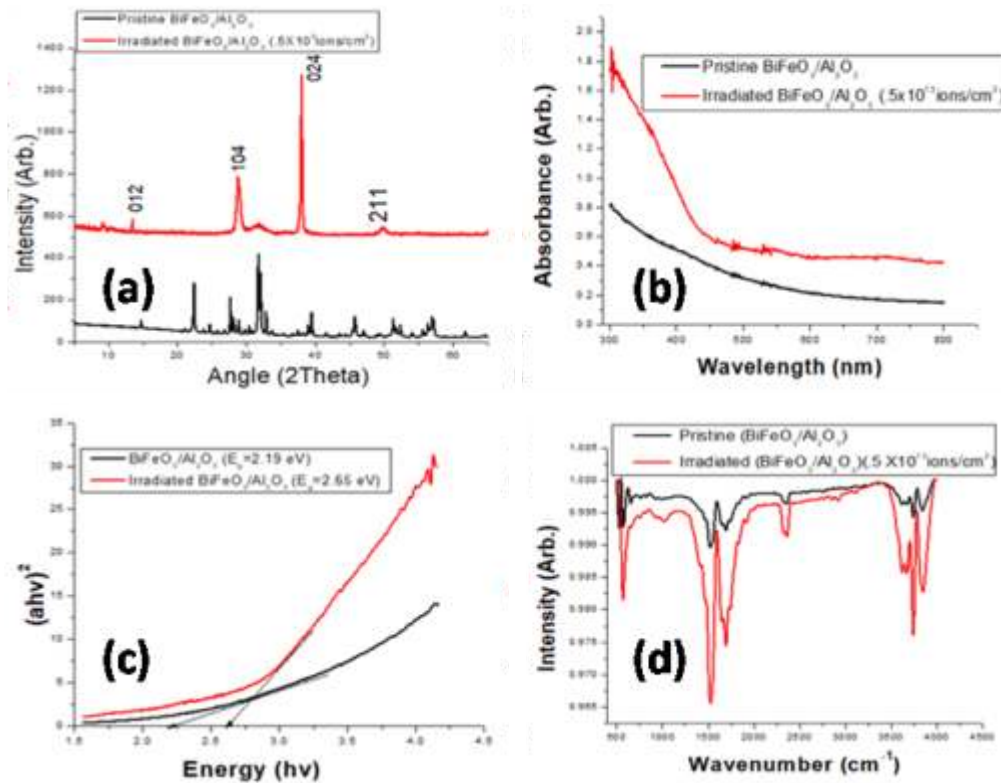


**Figure.** (a) X-ray diffraction pattern of pristine and irradiated  $\text{BiFeO}_3/\text{Al}_2\text{O}_3$  thin films, (b) Optical absorption spectra for  $\text{BiFeO}_3/\text{Al}_2\text{O}_3$  thin films, (c) Tauc plots of  $\text{BiFeO}_3$  thin films, and (d) FT-IR spectra of  $\text{BiFeO}_3$  thin films

Crystal structures and optical properties of  $\text{BiFeO}_3$  thin films prepared from PLD of thickness 200 nm and irradiated with 100 MeV  $\text{Au}^{+8}$  was investigated. Polycrystalline  $\text{BiFeO}_3$  films with a hexagonal system were obtained. The lattice constants, crystallite size, and energy gap of the  $\text{BiFeO}_3$  films have been tuned by the irradiation fluence. The variations in structural parameters and enhancement in optical band gap attributed to the compressive stress relaxation in the  $\text{BiFeO}_3$  films.

Authors are thankful to IUAC New Delhi to providing research facility for execution of the work.

#### References:

- [1] C. H. Ahn, K. M. Rabe, and J.-M. Triscone, Science 303, 488(2004).
- [2] B. I. Sturman and V. M. Fridkin, "The Photovoltaic and Photo-refractive Effects in Non centro symmetric Materials", edited by G. W. Taylor (Gordon and Breach, New York, 1992), Vol. 8.
- [3] D. Daranciang, M. J. Highland, H. Wen, S. M. Young, N. C. Brandt, H. Y. Hwang, M. Vattilana, M. Nicoul, F. Quirin, J. Goodfellow et al., Phys. Rev. Lett. 108, 087601 (2012).
- [4] V. M. Fridkin and B. N. Popov, Sov. Phys. Usp. 21, 981 (1978).
- [5] T. L. Qu, Y. G. Zhao, D. Xie, J. P. Shi, Q. P. Chen, and T. L. Ren, Appl. Phys. Lett. 98, 173507 (2011).
- [6] S. Y. Yang, L. W. Martin, S. J. Byrnes, T. E. Conry, S. R. Basu, D. Paran, L. Reichertz, J. Ihlefeld, C. Adamo, A. Melville et al., Appl. Phys. Lett. 95, 062909 (2009).
- [7] W. Ji, K. Yao, and Y. C. Liang, Adv. Mater. 22, 1763 (2010).
- [8] G. Catalan and J.F. Scott, Adv. Mater. 21 (2009) 2463.
- [9] F. Gao, X. Chen, K. Yin, S. Dong, Z. Ren, F. Yuan, T. Yu, Z. Zou, J.M. Liu, Adv. Mater. 2007, 19, 2889–2892.
- [10] V. Keskin, A. Gupta, G. Szulczewski, Mater. Lett. 2015, 159, 305–308.
- [11] Y. Sun, Z. Liu, J. Zeng, J. Yan, D. Shi, H. Liu, J. Electron. Mater. 2015, 44, 4207–4212.
- [12] X. Xu, Y.H. Lin, P. Li, L. Shu, J. Am. Ceram. Soc. 2011, 94, 2296–2299.

#### 5.2.4 Electronic excitation induced structural modifications in ceria stabilized zirconia ( $\text{Ce}_{1-x}\text{Zr}_x\text{O}_2$ )

Hari Singh<sup>1</sup>, S.K.Sharma<sup>1</sup>, R. C. Meena<sup>1</sup>, P.K. Kulriya<sup>1</sup>

<sup>1</sup>Inter-University Accelerator Centre (IUAC), Aruna Asaf Ali Marg, New Delhi-110067

\*Corresponding author e-mail: pawan@iuac.res.in

Ceria stabilized zirconia (CSZ) is a potential candidate for incineration of actinides in an advanced nuclear reactor. It is envisaged as an inert matrix fuel (IMF) for the fabrication of nuclear fuel for the futuristic advanced

reactors like accelerator-driven subcritical systems [1-3]. Fuel is in reactor is expected to exposed to harsh environment like high temperature, high pressure, severe radiation by the bombardment with neutron, alpha particles, fission fragments ( $\sim 1$  MeV/amu) and recoil nuclei (500 –700 keV) which leads to degradation of structural and mechanical properties of fuel. Moreover, availability of the neutron sources of desired flux and energy become less and rare, so heavy ions, as an alternative radiation sources, have been widely employed to characterize the displacement damages in recent years. Therefore, it is imperative to investigate the radiation induced structural damage as well as performance evaluation on the ceria stabilized zirconia.

This report presents the first-ever study on fluorite type polycrystalline  $\text{Ce}_{1-x}\text{Zr}_x\text{O}_2$  with  $x=0.2$  (CSZ) via swift heavy ions irradiation. Polycrystalline composition of CSZ has been synthesized through a conventional standard solid-state route. In this method, stoichiometry amount of binary oxides  $\text{CeO}_2$  and  $\text{ZrO}_2$  were mixed intimately using mortar and pestle. The physically mixed powder was palletized using a hydraulic press and processed through a single-step heating at a temperature of 1500°C for 10 h in a muffle furnace in the presence of air. The confirmation of single fluorite phase in the as-synthesized pellets was carried out using X-ray diffraction and micro-Raman spectroscopy techniques. Polycrystalline pellets were irradiated with 100 MeV  $\text{I}^{7+}$  ions at fluences ranging from  $1 \times 10^{12}$  to  $5 \times 10^{13}$  ions/cm<sup>2</sup> at room temperature using 15 UD Pelletron accelerators. Figure shows a representative XRD pattern of as-prepared and SHI irradiated  $\text{Ce}_{1-x}\text{Zr}_x\text{O}_2$  composition.

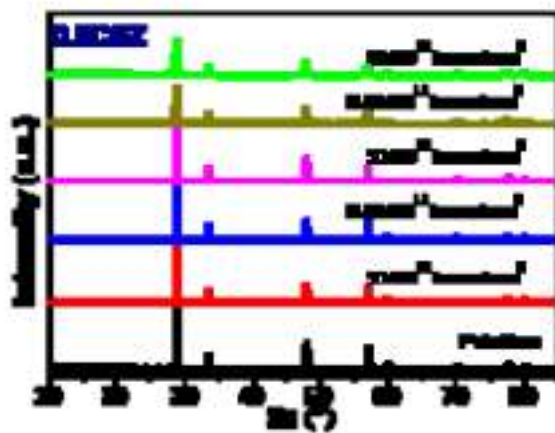


Figure: A representative XRD pattern of as-prepared and SHI irradiated  $\text{Ce}_{1-x}\text{Zr}_x\text{O}_2$  composition.

It shows that XRD peaks appearing at the peak position  $2\theta = 28.81^\circ, 33.12^\circ, 47.40^\circ$  and  $56.52^\circ$  assigned to (111), (200), (220) and (311) planes which correspond to the  $\text{Ce}_{0.8}\text{Zr}_{0.2}\text{O}_2$  phase [JCPDS 28-0271] and confirms formation of single phase solid solution. On SHI irradiation, structure remains intact at lower ion fluence. However, broadening and shift in peak towards lower Bragg's angle was observed on irradiation at high ion fluence ( $\sim 5 \times 10^{13}$  ions.cm<sup>-2</sup>) which confirms grain coarsening and induction of tensile strain due to deposition of huge energy by energetic heavy ions. Further, Raman spectroscopy studies showed modification of the F2g vibrational mode ( $\sim 481.78$  cm<sup>-1</sup>) which indicates band overlapping of dopants and vacancy defects (oxygen vacancies) created during the reduction of ceria from  $\text{Ce}^{4+}$  to  $\text{Ce}^{3+}$ . Our investigation confirms that there are a small swelling and disordering takes place, but the material remains crystalline even on irradiation at such higher ion fluence. Thus, because of its superior radiation resistant response of ceria stabilized zirconia ( $\text{Ce}_{1-x}\text{Zr}_x\text{O}_2$ ), it can be a potential candidate for incineration of actinide in the advance nuclear reactors.

## References:

1. W. Lutze and R. C. Ewing, Radioactiv Waste Forms for the Future, Elsevier, Amsterdam, 1988.
2. F. Lu, J. Zhang, M. Huang, F. Namavar, R. C. Ewing and J. Lian, The Journal of Physical Chemistry C 115 (15), 7193-7201 (2011).
3. Debelle, J. Channagiri, L. Thomé, B. Décamps, A. Boulle, S. Moll, F. Garrido, M. Behar and J. Jagielski, Journal of Applied Physics 115 (18), 183504 (2014).

## 5.2.5 Crystal field analysis of $\text{Al}_2\text{O}_3$ : $\text{Tm}^{3+}$ phosphor using ionoluminescence

S. Satyanarayana Reddy<sup>1,2</sup>, K.R. Nagabhushana<sup>1,2</sup> and Fouran Singh<sup>3</sup>

<sup>1</sup>Physics R & D Centre, PES Institute of Technology, BSK 3<sup>rd</sup> Stage, Bengaluru – 560085, India.

<sup>2</sup>Visvesvaraya Technological University, Belagavi, Karnataka – 590018, India.

<sup>3</sup>Inter University Accelerator Centre, P.O. Box No. 10502, New Delhi – 110 067, India.

The crystal field analysis of microstate splitting in Ionoluminescence (IL) spectrum is most interesting to understand the coordination system of emitter/dopant inside the crystalline structure. The crystal field analysis of thulium doped aluminum oxide sample is done using IL spectroscopy. Since, photoluminescence and diffused reflectance spectrum (DRS) of powder samples do not detect all allowed emission splitting lines corresponds to microstate energy level transitions , the crystal field analysis of the powder samples is rarely available in the literature. Pellets of (5 mm diameter and 1 mm thick) combustion synthesized undoped and  $\text{Tm}^{3+}$  (1 mol%) doped  $\text{Al}_2\text{O}_3$  are irradiated with focused beam of 100 MeV swift  $\text{Si}^{8+}$  ions (beam current = 2 pA) inside a high vacuum material science experimental chamber ( $6 \times 10^{-6}$  Torr) at Inter University Accelerator Centre (IUAC), New Delhi, India. The IL emission is collected at  $45^\circ$  to the incident beam, and the spectrum is recorded using a charged coupled device (CCD) spectrophotometer (Ocean optics spectrometer HR 4000). The IL spectra are recorded in the fluence range  $8.75 \times 10^{12}$  to  $6.75 \times 10^{13}$  ions  $\text{cm}^{-2}$ .

Fig. (a) and (b) shows IL spectra of 100 MeV swift  $\text{Si}^{8+}$  ion irradiated pure and  $\text{Tm}^{3+}$  (1 mol%) doped  $\text{Al}_2\text{O}_3$  for the fluence  $2.63 \times 10^{13}$  ions  $\text{cm}^{-2}$ . Both the spectra exhibit  $\text{Cr}^{3+}$  and  $\text{Mn}^{4+}$  emissions at 695 and 672 nm respectively. The sharp emission at 695 nm corresponds to  $\text{Cr}^{3+}$  impurities emission transition of  $^2\text{E}_g \rightarrow ^4\text{A}_{2g}$  of R lines. The small emission peaks at 678, 683 nm named as N' lines and 708, 716, 729 nm are named as N lines. These N and N' lines indeed belong to the variation of crystal field strength due to  $\text{Cr}^{3+}$  states and  $\text{Cr}^{3+}$  -  $\text{Cr}^{3+}$  pair interaction. The spectra of  $\text{Tm}^{3+}$  (1 mol%) doped  $\text{Al}_2\text{O}_3$  for various fluence ranging from  $8.75 \times 10^{12}$  to  $5.03 \times 10^{13}$  ions  $\text{cm}^{-2}$  exhibits  $\text{Tm}^{3+}$  ion emissions at 359.82, 397.79, 467.46, 528.01, 658.20, 757.00, 764.12 and 808.02 nm along with  $\text{Cr}^{3+}$  and  $\text{Mn}^{4+}$  characteristic emissions. These emission peaks are corresponding to f-electron  $^1\text{D}_2 \rightarrow ^3\text{H}_6$ ,  $^3\text{P}_2 \rightarrow ^3\text{H}_4$ ,  $^1\text{G}_4 \rightarrow ^3\text{H}_6$ ,  $^1\text{D}_2 \rightarrow ^3\text{H}_5$ ,  $^1\text{D}_2 \rightarrow ^3\text{H}_4$ ,  $^1\text{D}_2 \rightarrow ^3\text{F}_3$ ,  $^1\text{D}_2 \rightarrow ^3\text{F}_2$  and  $^3\text{H}_4 \rightarrow ^3\text{H}_6$  transitions of the  $\text{Tm}^{3+}$  ion respectively .

IL emission of  $\text{Tm}^{3+}$  multiple transitions from  $^1\text{D}_2$ ,  $^1\text{G}_4$ ,  $^3\text{H}_4$  to  $^3\text{H}_6$ ,  $^3\text{P}_2$ ,  $^1\text{D}_2$  to  $^3\text{H}_4$  and  $^1\text{D}_2$  to  $^3\text{F}_J$  ( $J = 3, 2$ ) analysis confirms the assignments of microstates. The energy levels of free  $\text{Tm}^{3+}$  ion is calculated using the crystal field theory method using Hamiltonian for a  $4f^2$  configuration. The root mean square (rms) deviation for free  $\text{Tm}^{3+}$  ion is found to be  $0.30 \text{ cm}^{-1}$ . The observed 14 energy levels and lowest energy level is found to be  $^3\text{H}_6$ . Further, the predictive order of  $^1\text{I}_6$ ,  $^3\text{P}_0$ ,  $^3\text{P}_1$ ,  $^3\text{P}_2$  and  $^1\text{S}_0$  energy levels. In-depth understanding the microstates energies of the  $\text{Tm}^{3+}$  (0.04 mol%) ion in  $C_{3v}$  site symmetry of  $\text{Al}_2\text{O}_3$  and  $\text{Tm}^{3+}$  ions (0.96 mol%) in dodecahedra  $C_s$  site symmetry of  $\text{Tm}/\text{YAlO}_3$  lattice are calculated using the crystal field theory method. The crystal field parameters of  $\text{Tm}^{3+}$  ions in  $C_s$  site symmetry in  $\text{TmAlO}_3$  lattice are calculated using Wybourne formalism by fitting the experimental IL peaks. The rms value for the crystal field parameters fitting in  $C_{3v}$  and  $C_s$  site symmetry are found to be 16.41 and  $18.18 \text{ cm}^{-1}$  respectively.

When the lanthanide ion is doped into a crystal, the total degeneracy or number of microstates for a  $4f^n$  electronic configuration is given by equation

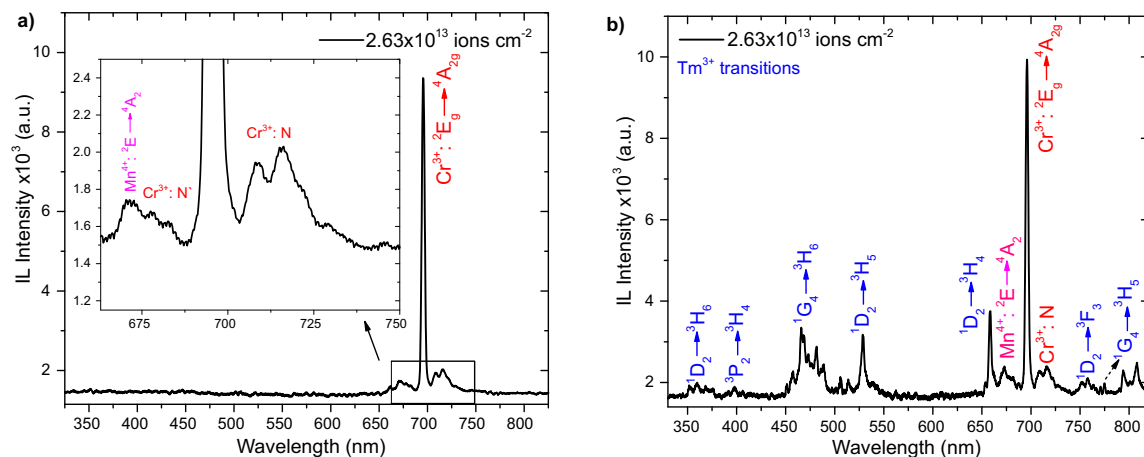


Figure : IL spectra of swift  $\text{Si}^{8+}$  ions irradiated a) undoped and b)  $\text{Tm}^{3+}$  doped  $\text{Al}_2\text{O}_3$  for the fluence  $1.31 \times 10^{13}$  and  $9.63 \times 10^{12}$  ions  $\text{cm}^{-2}$  respectively.

Thus, we can conclude that IL spectrum of undoped sample confirms the presence of  $\text{Cr}^{3+}$  and  $\text{Mn}^{4+}$  impurities in the host samples. IL of  $\text{Tm}^{3+}$  doped samples exhibits multiple splits f-electron transition emissions. Complete f-shell microstates energy structure of free  $\text{Tm}^{3+}$  ion,  $\text{Tm}^{3+}$  ions in  $\text{C}_{3v}$  site of  $\text{Al}_2\text{O}_3$  and  $\text{Tm}^{3+}$  ion in  $\text{C}_s$  site of  $\text{TmAlO}_3$  are found using crystal field theory. The least rms value of crystal field parameters fitting confirms the experimental values are in good argument with theoretical parameters and the  $\text{Tm}^{3+}$  ion is in  $\text{C}_{3v}$  symmetry of host lattice.

## References

- [1] C. Tiseanu, A. Lupei, V. Lupei, Energy levels of  $\text{Tm}^{3+}$  in yttrium aluminium garnet, *J. Phys. Condens. Matter.* 7 (1995) 8477–8486. doi:10.1088/0953-8984/7/44/016.
- [2] A. de Bettencourt-Dias, Lanthanides: Electronic Structure, in: *Encycl. Inorg. Bioinorg. Chem.*, John Wiley & Sons, Ltd, Chichester, UK, 2012: pp. 1–8. doi:10.1002/9781119951438.eibc2009.
- [3] S. Satyanarayana Reddy, K.R. Nagabhushana, F. Singh, Structure and crystal field analysis using ionoluminescence of  $\text{Al}_2\text{O}_3$ ;  $\text{Tm}^{3+}$  phosphor, *J. Lumin.* 214 (2019) 116553. doi:10.1016/j.jlumin.2019.116553.

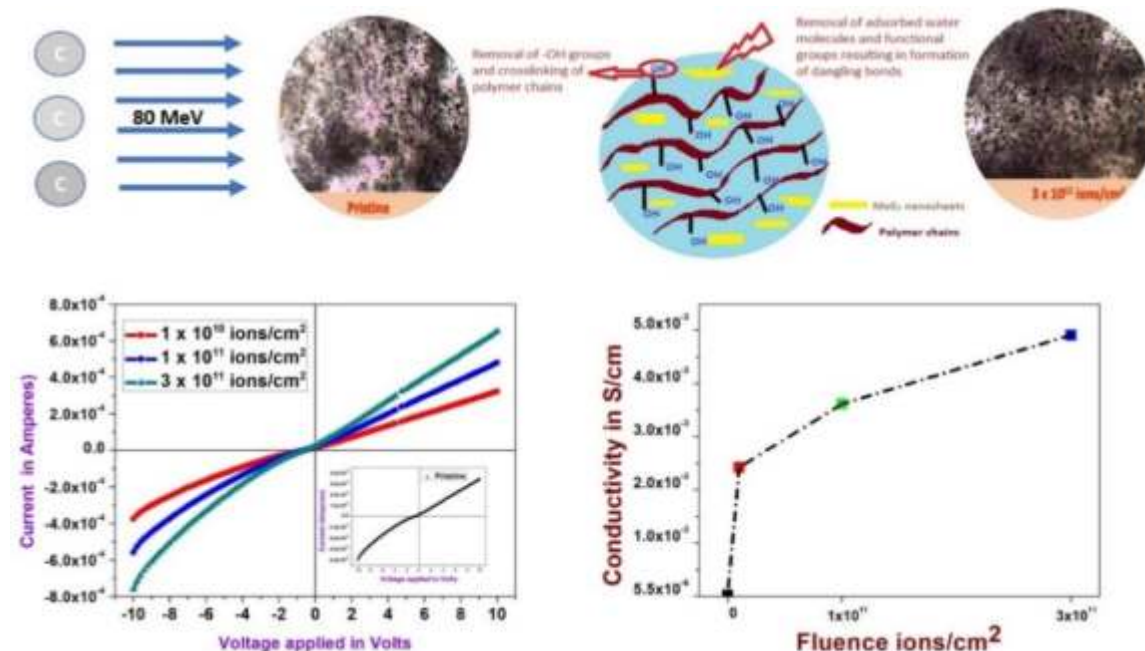
## 5.2.6 Enhanced electrical properties of few layers $\text{MoS}_2$ -PVA nanocomposite film via homogeneous dispersion and annealing effect induced by 80 MeV Carbon $^{6+}$ Swift Heavy Ion irradiation

Amar Ratan<sup>1</sup>, Suhasini Kunchakara<sup>1</sup>, Meenakshi Dutt<sup>1</sup>, Ambuj Tripathi<sup>2</sup> and Vaishali Singh<sup>1\*</sup>

<sup>1</sup> Mesoporous Systems and Nanocomposites Research Laboratory, University School Basic and Applied Sciences, Guru Gobind Singh Indraprastha University, Sector 16-C Dwarka, New Delhi 110078, India

<sup>2</sup> Materials Science Group, Inter-University Accelerator Centre, New Delhi 110067, India

In this work, MoS<sub>2</sub> nanosheets are first synthesized via solvent assisted exfoliation and then incorporated as filler in Polyvinyl alcohol matrix. The free-standing polymer nanocomposite film was irradiated using 80 MeV Carbon swift ion beam at  $1 \times 10^{10}$  ions/cm<sup>2</sup>,  $1 \times 10^{11}$  ions/cm<sup>2</sup> and  $3 \times 10^{11}$  ions/cm<sup>2</sup> to induce structural, spectroscopic and electrical changes due to high deposition of energy. XRD and Raman reveal the annealing effect at low fluence of at  $1 \times 10^{10}$  ions/cm<sup>2</sup>. Upon Swift heavy ion irradiation, a remarkable rise in the conductivity for application in organic electronics, from  $2.58 \times 10^{-5}$  S/cm to  $2.43 \times 10^{-3}$  S/cm at  $1 \times 10^{10}$  ions/cm<sup>2</sup> has been observed. The conductivity continues to rise with increase in ion fluence and attains a value of  $4.92 \times 10^{-3}$  S/cm at  $3 \times 10^{11}$  ions/cm<sup>2</sup>. This is attributed to the formation of conductive tracks and homogeneous dispersion upon SHI irradiation in accordance with Thermal spike model. The details are given in A. Ratan, S. Kunchakara, M. Dutt, A. Tripathi, V. Singh, Mater. Sci. Semicond. Process. 108 (2020) 104877. doi:10.1016/j.mssp.2019.104877



## References:

1. C. Tyagi, S.A. Khan, S. Ojha, D.K. Avasthi, A. Tripathi, Vacuum. 154 (2018) 259–263. doi:10.1016/j.vacuum.2018.05.003.
2. D. Singh, N.L. Singh, A. Qureshi, P. Kulriya, A. Tripathi, D.K. Avasthi, A.N. Gulluoglu, J. Non. Cryst. Solids. 356 (2010) 856–863. doi:10.1016/j.mssp.2019.104877

## 5.2.7 Ionoluminescence Properties of $\text{Ba}_{1-x}\text{MgAl}_{10}\text{O}_{17}:\text{Mn}^{2+}$ nanophosphors

Manvendra Kumar<sup>1</sup> and Fouran Singh<sup>2</sup>

<sup>1</sup>Department of Physics, Shri Vaishnav Vidyapeeth Viswavidyalaya, Indore-452002, India

<sup>2</sup>Inter University Accelerator Centre, Aruna Asaf Ali Marg, New Delhi- 110067 India

$\text{BaMgAl}_{10}\text{O}_{17}$  (BAM) is a vacuum ultraviolet (VUV) phosphor and exhaustively used in plasma display panels (PDPs) and lamps, due to its high luminescence efficiency and good chromaticity [1-2]. It is also used in other displays and light emitting devices, for example, white light-emitting diodes (WLED) and is a possible new generation of Hg-free lamps [3]. Ionoluminescence (IL) properties of chemically synthesized  $\text{Mn}^{2+}$  activated  $\text{Ba}_{(1-x)}\text{Mn}_x\text{MgAl}_{10}\text{O}_{17}$  (BAM) nanophosphors [4] using swift heavy ions (120 MeV  $\text{Ag}^{9+}$ ) is studied [5]. Figure 1 shows IL spectra collected at room temperature for undoped and Mn doped prepared BAM nanophosphors with 1, 5, 10, 20, 25 and 30% Mn ions as shown in figure 1(a). Intense green emission is shown in the IL spectra with a broad band at peak position of 521 nm, which is attributed to  $^4\text{T}_1 \rightarrow ^6\text{A}_1$  transition of  $\text{Mn}^{2+}$  ion. From the spectra, it is confirmed that all the bands are associated with  $\text{Mn}^{2+}$  ion. The IL intensity increases with increase in the doping percentage of Mn ions up to 5% followed by concentration quenching of luminescence as depicted in figure 1(b). Further, the influence of the ion fluence on luminescence properties for each doped nanophosphor were studied in detail. The IL intensity is high for pristine sample and decreases with increase in the fluence. The variation of the integrated IL intensity of the bands with applied ion fluences is shown in Figure 2 (a), where solid line in the figure shows the exponential fit to the decay curve. It is clearly visible that the IL intensity decreases exponentially and saturates at higher ion fluences.

One of the sample,  $\text{Ba}_{0.95}\text{MgAl}_{10}\text{O}_{17}:\text{Mn}_{0.05}$  nanophosphors, was measured at low temperature (LT, 77K) to study the kinetics of the luminescence centers at LT. The fluence dependence of IL intensity deduced from the IL spectra collected at LT is along with the IL intensity deduced from the spectrum collected at RT is shown in Figure 2(b). It is clear that the intensity at LT is lower than the IL intensity observed at RT. The IL intensity decreases with increase in the ion fluence in similar manner as for RT measurement.

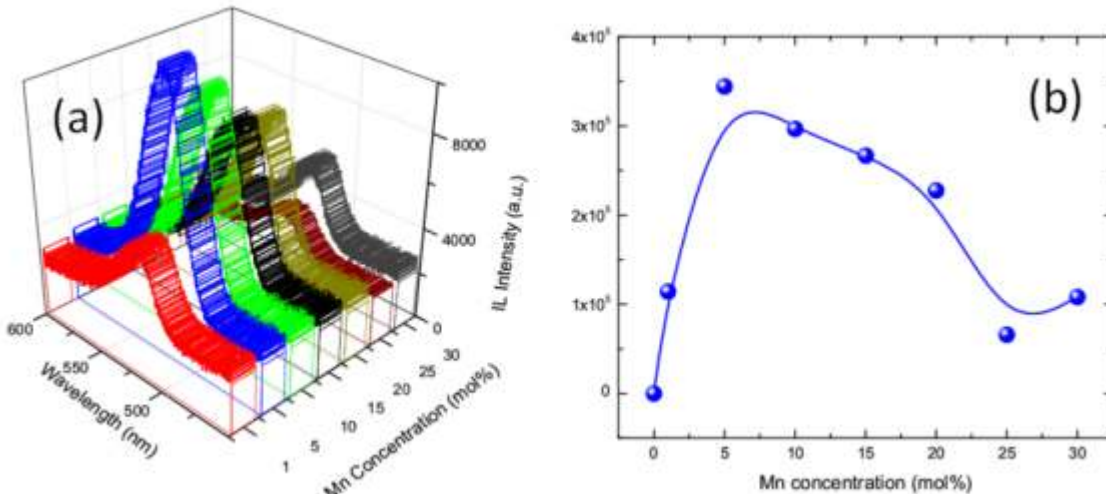


Figure : (a) IL spectra of pristine samples for different  $\text{Mn}^{2+}$  doping concentration.  
 (b) The variation of the integrated IL intensities of the bands with Mn doping percentage.

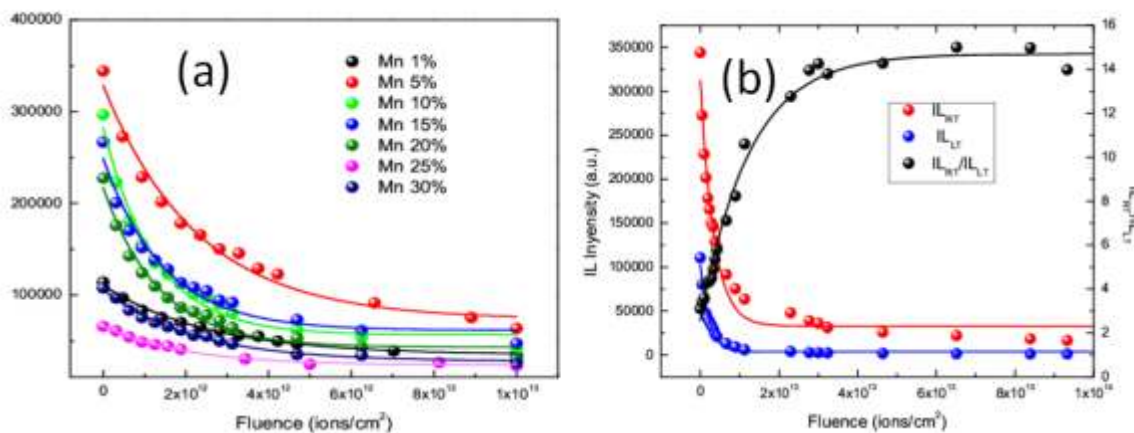


Figure : (a) The variation of IL intensities of the bands with fluence.  
 (b) Variation of IL intensity for  $\text{Ba}_{0.95}\text{MgAl}_{10}\text{O}_{17}:\text{Mn}_{0.05}$  nanophosphors collected at RT and LT and their ratio.

## References

- [1] T. Justel, H. Nikol, C. Ronda, Angew. Chem. Int. Ed. 37 (1998) 3084.
- [2] J. Wang, Y. Yoo, C. Gao, I. Takeuchi, X. Sun, H. Chang, X.D. Xiang, G. Schulte, Science 279 (1998) 1712.
- [3] K.S. Sohn, E.S. Park, C.H. Kim, H.D. Park, J. Electrochem. Soc. 147 (2000) 4368.
- [4] R. S. Yadav, V. K. Shukla, P. Mishra, S. K. Pandey, K. Kumar, V. Baranwal, M. Kumar, A. C. Pandey, J. Alloys Compd. 547 (2013) 1.
- [5] M. Kumar, P. Rajput, P. K. Singh, A. C. Yadav, S. L. Pradhan, V. Baranwal, U. B. Singh, S. N. Jha and F. Singh, J. Alloys Compd. 799 (2019) 556.

## 5.2.8 Effect of Ag ion irradiation on structural properties of pure and Ag-doped Ge<sub>2</sub>Sb<sub>2</sub>Te<sub>5</sub> (GST) thin films

Neetu Kanda<sup>1</sup>, Anup Thakur<sup>2</sup>, Fouran Singh<sup>3</sup> and A.P. Singh<sup>1\*</sup>

<sup>1</sup>\*Department of Physics, Dr. B. R. Ambedkar National Institute of Technology, Jalandhar-144011, India.

<sup>2</sup>Department of Physics, Punjabi University, Patiala, Punjab 147002, India

<sup>3</sup>Inter-University Accelerator Centre, New Delhi, Delhi – 110067

Phase change materials (PCMs) are widely used materials for electronic and optical memory storage. Ge<sub>2</sub>Sb<sub>2</sub>Te<sub>5</sub> (GST) is the most promising material used in data storage and photonic devices [1]. Swift heavy ion irradiation is an important tool to modify material properties. Irradiation using 120 MeV Ag ions also leads to phase change on using a high dose of irradiation [2]. We have irradiated the 3% Ag doped GST thin films with high energy Ag<sup>9+</sup> ions. Defects introduced by electronic energy loss leads to change in their structural properties. Thin films of GST were irradiated with Ag<sup>9+</sup> ions at 120 MeV energy using 15 UD tandem Pelletron accelerator at IUAC, New Delhi at fluences of  $5 \times 10^{11}$ ,  $1 \times 10^{12}$ ,  $5 \times 10^{12}$  and  $1 \times 10^{13}$  ions/cm<sup>2</sup>. Based on different fluence, these films were named as G3Ag0 (pure), G3Ag1e11, G3Ag1e12, G3Ag5e12, G3Ag1e13 respectively. The structural and optical properties of 3% Ag doped GST thin films were investigated using XRD and Raman spectra. These characterizations are carried out at NIT Jalandhar and IUAC, New Delhi respectively.

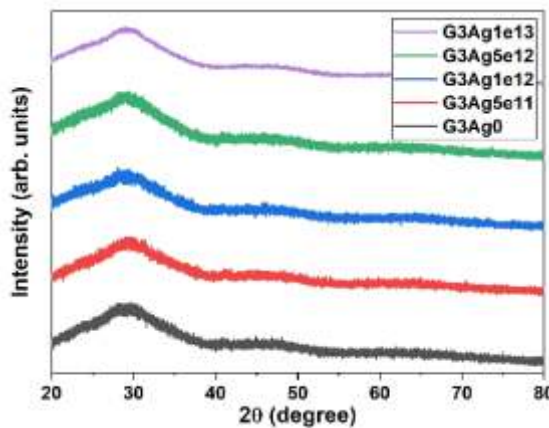


Fig.1 XRD spectra of irradiated thin films.

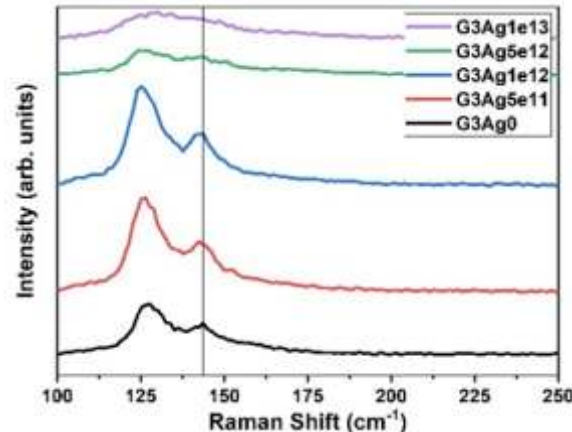


Fig.2 Raman spectra of irradiated thin films.

The XRD spectra in fig.1 show the broad hump which signifies that the phase of the Ag-doped GST thin films remains intact with irradiation. Fig.2 shows the Raman spectra where the first peak corresponds to GeTe<sub>4</sub> tetrahedral vibration and the second peak corresponds to SbTe<sub>3</sub> vibration. It is observed from the spectra that with irradiation these peaks get flattened which indicates the increase of energy density released by the ion inside the Ag-doped GST thin film. During irradiation covalent bonds of the GeTe<sub>4</sub> and SbTe<sub>3</sub> building block may be selectively broken.

## References

- [1] P. Singh, A. P. Singh, N. Kanda, M. Mishra, G. Gupta, and A. Thakur. Applied Physics Letters, 111:261102, 2017.
- [2] N. Kanda, A. Thakur, F. Singh, and A. P. Singh. Nuclear Instruments and Methods in Physics Research Section B: Beam Interactions with Materials and Atoms, 467:40, February 2020.

## 5.2.9 Photoluminescence and thermoluminescence response of swift heavy ion irradiated Dy<sup>3+</sup>, Ho<sup>3+</sup> doped Y<sub>2</sub>O<sub>3</sub> materials for white light emission and dosimetry applications

N.J. Shivaramu<sup>1</sup>, B.N. Lakshminarasappa<sup>1</sup>, K.R. Nagabhushana<sup>2</sup> and Fouran Singh<sup>3</sup>

<sup>1</sup>Department of Physics, Bangalore University, Bangalore, 560056, India

<sup>2</sup>Department of Physics (S & H), PES University, Bangalore 560085, India

<sup>3</sup>Inter University Accelerator Centre, P.O. Box No. 10502, New Delhi 110067, India

The systematic studies based on swift heavy ion (SHI) induced defects in  $Dy^{3+}$  activated  $Y_2O_3$  nanocrystals have been carried out and the results obtained have shown potential applications for use in white light emitting diodes and in high energy dosimetry [1]. The optimum concentration of trivalent  $Dy^{3+}$  in  $Y_2O_3$  was prepared by the solution combustion technique. X-ray diffraction results revealed that the obtained powder form material is a single phase with body center cubic structure. The transmission electron microscopy images indicated that the particles were irregular in shape with an average size of 37 nm. The material upon illumination with ultraviolet light showed the characteristic and predominant greenish yellow emission along with low intensity blue emission. The greenish yellow emission was observed to enhance when it was exposed to 100 MeV swift  $Si^{8+}$  ions and the ratio between yellow and blue emission could be tuned. This was ascribed to the SHI induced electron/hole traps and the energy transfer between the electron/hole recombination centers and activator states in the host. The photometric characterization showed that SHI influences the phosphor material to achieve pure white emission for light emitting diode applications at and beyond a fluence of  $1 \times 10^{11}$  ions  $cm^{-2}$ . Thermoluminescence (TL) glow curves of 100 MeV  $Si^{8+}$  ion irradiated samples showed a prominent glow with peak at 408 K and its intensity was found to increases up to a fluence of  $1 \times 10^{11}$  ions  $cm^{-2}$ . TL studies of holmium (Ho) doped  $Y_2O_3$  irradiated with gamma rays ( $^{60}Co$ ), 100 MeV  $Si^{8+}$  and 150 MeV  $Au^{9+}$  ions revealed that the TL properties of these materials were found to be useful for dosimeter applications [2]. It was concluded that the above energetic radiation produces identical defect centers such as  $F$ ,  $F^+$ ,  $F_2$  color centers in the material.

#### References

- [1] N.J. Shivaramu et al, Journal of Luminescence 209 (2019) 179–187.
- [2] N.J. Shivaramu et al, Journal of Alloys and Compounds 778 (2019) 554–565.

#### 5.2.10 Effects of ion beam irradiation on the structural and optical properties of potassium sodium niobate thin films

Radhe Shyam<sup>a</sup>, Apurba Das<sup>b</sup>, Pamu Dobbidi<sup>b</sup>, Fouran Singh<sup>c</sup>, Pargam Vashishta<sup>d</sup>, Govind Gupta<sup>d</sup> and Srinivasa Rao Nelamarri<sup>a</sup>

<sup>a</sup>Department of Physics, Malaviya National Institute of Technology Jaipur, J.L.N. Marg, Jaipur 302017, India

<sup>b</sup>Department of Physics, Indian Institute of Technology Guwahati, Guwahati 781039, India

<sup>c</sup>Inter-University Accelerator Centre, Aruna Asaf Ali Marg, New Delhi 110067, India

<sup>d</sup>CSIR-National Physical Laboratory, K.S. Krishnan Marg, New Delhi 110012, India

(K, Na)NbO<sub>3</sub> (KNN) is a lead-free ceramic material that has gained considerable interest due to its excellent piezoelectric properties and high Curie temperature ( $T_c$ ). A lot of research has been carried out to exploit its piezoelectric, ferroelectric, and dielectric properties for different applications. However, certain reports on optical properties of KNN thin films have provided substantial evidence on the application of KNN in optical coatings, integrated optical devices, electro-optic modulators, LEDs, and optical storage technology. Swift heavy ion (SHI) irradiation is one of the versatile tools to modify the structural, morphological and optical properties of thin films. KNN films were prepared on Si and quartz substrates in the combined presence of Ar and O<sub>2</sub> gas environment using RF magnetron sputtering at room temperature. Afterward, samples were annealed at 700°C for an hour in air ambience to achieve the crystallinity of KNN films.

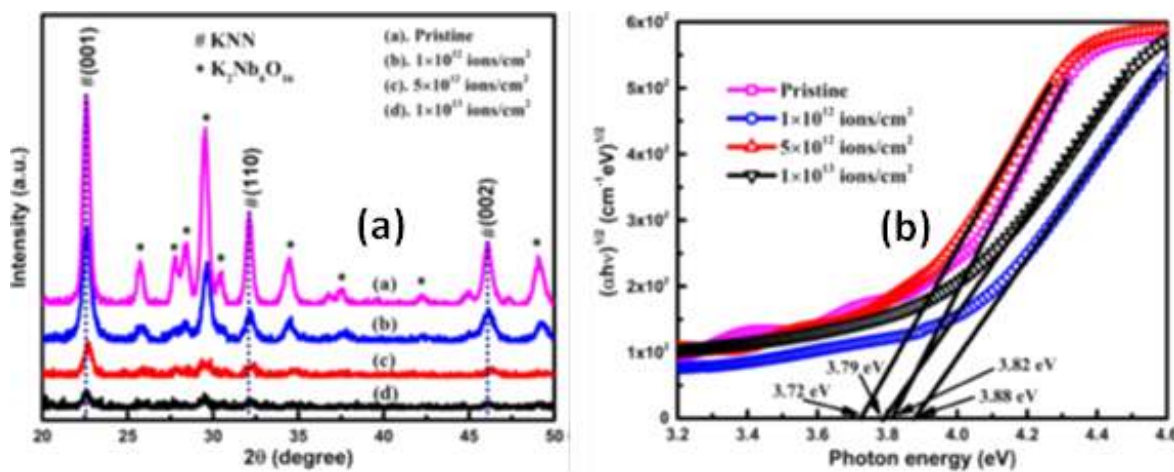


Fig. (a) XRD patterns and (b) Optical band gap of pristine and irradiated KNN thin films

Eventually, the crystalline films were subjected to SHI irradiation at normal incidence on  $1 \times 1$  cm<sup>2</sup> surface area using 100 MeV Ag<sup>7+</sup> ions with fluences ranging from  $1 \times 10^{12}$  to  $1 \times 10^{13}$  ions/cm<sup>2</sup> using Pelletron facility available at Inter-University Accelerator Center (IUAC), New Delhi, India. The pristine and irradiated films were

characterized using various techniques such as X-ray diffraction (XRD), atomic force microscopy (AFM), Raman spectroscopy, and UV–Vis spectroscopy. XRD results reveal that the crystallinity of films decreases drastically upon irradiation as shown in Fig.(a). The intensity of Raman modes decreased with irradiation due to the creation of defects that lead to distortion in NbO<sub>6</sub> octahedron. The surface roughness of films and optical band gap of KNN (shown in Fig.(b) is found to vary non-monotonously with ion fluence. The variation in optical transmittance and energy band gap is due to defect levels generated as a result of SHI irradiation. The monotonous decrease in the refractive index and packing density of films is also observed with ion fluence.

#### References:

- [1] I. Kanno and T. Mishima et al, Sensors Actuators A Phys. **179**, 132 (2012).
- [2] L. Wang, W. Ren, P. Shi, X. Chen, X. Wu, and X. Yao, Appl. Phys. Lett. **97**, 072902 (2010).
- [3] P. Mahesh and D. Pamu, Thin Solid Films **562**, 471 (2014).
- [4] S. Kumar, M. Shandilya, S. Thakur, and N. Thakur, J. Sol-Gel Sci. Technol. **88**, 646 (2018).
- [5] R. Shyam and S. R. Nelamarri et al, Appl. Phys. A **126**, 1 (2020).

#### 5.2.11 Depth and width analysis of crater for SHI ions irradiated SnO<sub>2</sub> and TiO<sub>2</sub> nanocomposite thin films

Vikas Kumar<sup>1</sup>, Vishnu Chauhan<sup>1</sup>, Jagjeevan Ram<sup>1</sup>, I. Sulania<sup>2</sup>, Fouran Singh<sup>2</sup> and Rajesh Kumar<sup>1\*</sup>

<sup>1</sup>USBAS, Guru Gobind Singh Indraprastha University, New Delhi–110078, India.

<sup>2</sup>Inter University Accelerator Centre, Aruna Asaf Ali Road, New Delhi–110067, India

\*E-mail: kumarrpi@gmail.com

The study of the surface morphology of nanocomposite thin films has been carried out by using AFM and the same has been discussed here in brief in this report. ***SnO<sub>2</sub>-TiO<sub>2</sub> nanocomposite thin films were grown on silicon and ITO substrates using RF magnetron sputtering technique. These thin films were irradiated by 120 MeV Au<sup>9+</sup> SHI beam with varying fluences to induced modifications in thin films by dense electronic excitation [1].*** AFM micrographs were taken in the tapping mode at different place of the samples. AFM micrograph reveals crater like formation on the surface of thin film irradiated at a higher fluence. The cross-sectional outline of one crater has been demonstrated in Fig. 1. The size and behavior of grains were calculated by grain mapping of 2 μm×2 μm areas in scanned micrographs for a large number of grains. The average grain size of virgin and irradiated samples was determined by Gaussian distribution. The grain size of the virgin sample was observed in between 72 nm to 78 nm. The size of craters was around 550nm.

In this case, the following equation can be used to determine the increases in local lattice temperature through ion interaction with matter [2].

$$W_b = \varepsilon k (T^4 - T_0^4) \quad (1)$$

Where  $\varepsilon=0.18$  [2] is the effective emittance of the film, T is the substrate temperature and  $T_0=300$  K is the surrounding target chamber temperature,  $W_b$  is the input power density of the beam,  $k=5.67 \times 10^{-12} \text{ Wcm}^{-2} \text{ K}^{-4}$  is the Stephan-Boltzmann constant. The modification in the material by SHI beam can be explained by the various models, like Lattice Instability Model (LIM) [3], Thermal Spike Model (TSM) [4] and Coulomb Explosion Model (CEM) [5].

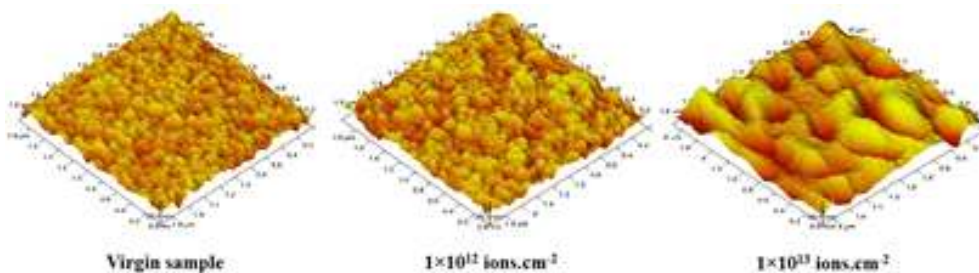


Fig. 1. Depth and width analysis of crater for 120 MeV Au<sup>9+</sup> ions irradiated SnO<sub>2</sub>-TiO<sub>2</sub> nanocomposite thin films for a fluence of 2E13 ions.cm<sup>-2</sup> [Ref. 1].

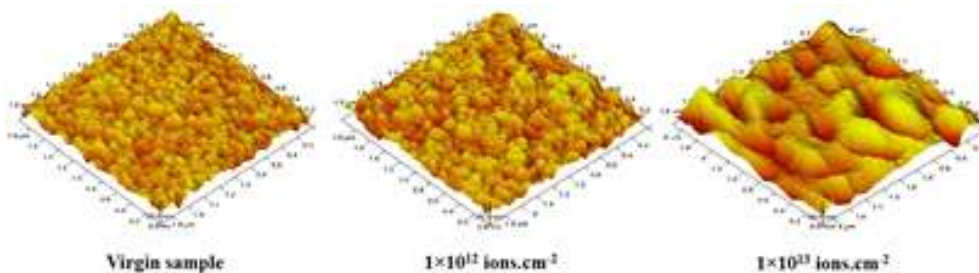


Fig. 2. AFM Micrographs for virgin and irradiated thin films with varying ion fluence [Ref. 1].

Fig. 2 clearly shows the agglomeration of grains in three dimensional micrographs of ion irradiated  $\text{SnO}_2\text{-TiO}_2$  nanostructured thin films.

#### References:

- [1] Vikas Kumar, R. Gupta, V. Chauhan, J. Ram, P. Singh, M. Prasad, R. Mehra, Rajesh Kumar, Applied Nano Science, 9 (2019)1265–1280.
- [2] Abhirami K, Matheswaran P, Gokul B, Sathyamoorthy R, Kanjilal D, Asokan K, Vacuum 90 (2013)39-43.
- [3] Innocenti M, Cattarin S, Loglio F, Cecconi T, Seravalli G, Foresti M, Electrochim. Acta 49 (2004)1327-1337.
- [4] Stampfli P, Nucl. Instrum. Methods Phys. Res., Sect. B 107 (1996)138-145.
- [5] Toulemonde M, Dufour C, Paumier E, Phys. Rev. B 46 (1992)14362.
- [6] Yavlinskii YN, Nucl. Instrum. Methods Phys. Res., Sect. B 245: (2006)114-116.

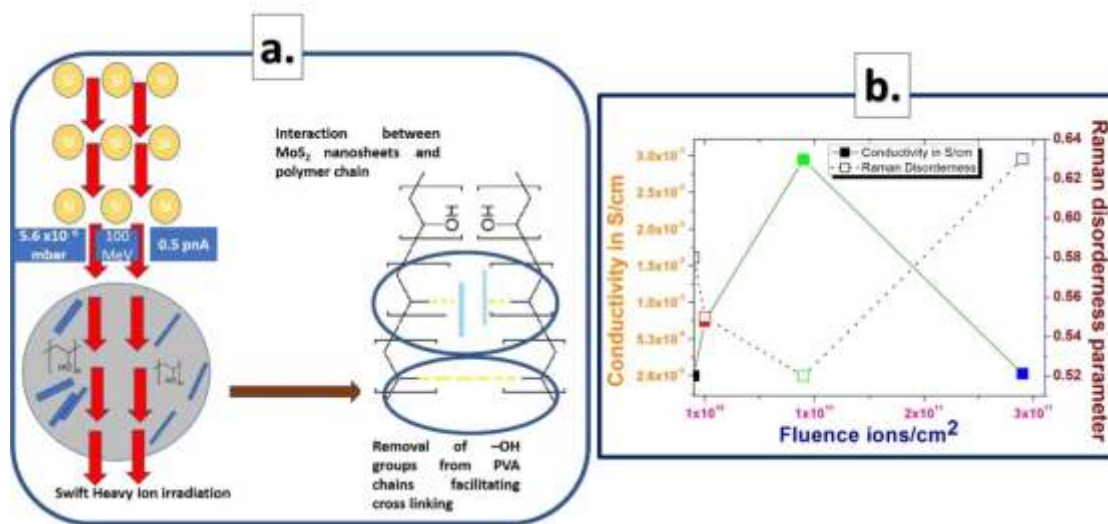
#### 5.2.12 100 MeV Silicon<sup>9+</sup> swift heavy ion irradiation - Strategic defect annealing approach to enhance the electrical conductivity of few-layered MoS<sub>2</sub>sheets - PVA nanocomposite film

Amar Ratan<sup>1</sup>, Suhasini Kunchakara<sup>1</sup>, Meenakshi Dutt<sup>1</sup>, Ambuj Tripathi<sup>2</sup> and Vaishali Singh<sup>1</sup>

<sup>1</sup> Mesoporous Systems and Nanocomposites Research Laboratory, University School Basic and Applied Sciences, Guru Gobind Singh Indraprastha University, Sector 16-C Dwarka, New Delhi 110078, India

<sup>2</sup> Materials Science Group, Inter-University Accelerator Centre, New Delhi 110067, India

In this study, we report a strategic route to enhance the electrical conductivity of solvent exfoliated MoS<sub>2</sub> nanosheets dispersed in Poly-vinyl alcohol (PVA) matrix as a free-standing thin film. 100 MeV Silicon<sup>9+</sup> swift ion beam is used to anneal the defects and decrease the degree of disorderness of MoS<sub>2</sub> while in the polymer matrix. Homogeneous dispersion and strong interfacial interaction between the nano-sheets and PVA matrix increases the charge carrier mobility, which in turn results in a dynamic increase of conductivity by 2 orders of magnitude i.e. from  $2.5 \times 10^{-5}$  S/cm (pristine) to  $2.9 \times 10^{-3}$  S/cm (irradiated) at a fluence of  $1 \times 10^{11}$  ions/cm<sup>2</sup>. For details, see: A. Ratan, S. Kunchakara, M. Dutt, A. Tripathi, V. Singh, Vacuum. 169 (2019) 108939. doi:10.1016/j.vacuum.2019.108939.



#### References:

- [1] Z.D. Xiang, F.R. Jones, Compos. Sci. Technol. 57 (1997) 451–461. doi:10.1016/S0266-3538(96)00168-6.
- [2] N.L. Singh, S. Shah, A. Qureshi, A. Tripathi, F. Singh, D.K. Avasthi, P.M. Raole, Bull. Mater. Sci. 34 (2011) 81–88

#### 5.2.13 The correlation between optical and elastic properties of swift heavy ion irradiated samples of chemically synthesized group II-VI semiconductor nanocrystals

Debojyoti Nath, Simi Debnath, Pijush Ch. Dey, Fouran Singh and Ratan Das

A few Gr. II-VI semiconductor nanocrystals such as Cadmium selenide (CdSe) and Cadmium sulfide (CdS) nanocrystals have been prepared by chemical method and subsequently characterized using SEM, TEM and XRD. XRD study confirms the crystalline nature of both the prepared samples with cubic zinc blende lattice geometry, whereas SEM, TEM analysis indicates the spherical morphology of the prepared nanoparticles.

Further, SHI irradiation experiment on the prepared CdSe and CdS nanocrystals has been performed at IUAC, New Delhi with 120 MeV Ni<sup>10+</sup> and Ag<sup>7+</sup> heavy ions with different ion fluences such as  $1 \times 10^{11}$ ,  $1 \times 10^{12}$  and  $3 \times 10^{13}$  ions/cm<sup>2</sup> for both the ion sample. The effect of SHI irradiation on the structural properties has been studied using

X-Ray diffraction and Raman spectra. From both the XRD and Raman spectra, a cubic to hexagonal phase transformation has been observed in these two samples but it has also been observed that amount of hexagonal fraction is directly related to the specification of the heavy ion. Further, the evolution as well as the mechanism of the cubic to hexagonal phase has been studied using ion impact model. Many elastic parameters have been obtained from the Williamson-Hall plot method, SSP method and Halder -Wagner Method. Again, SHI induced phase transformation also has been confirmed from the Rietveld refinement of the experimental XRD pattern. The output crystal structure information of the Rietveld refinement has been employed in the Quantum espresso code as an input parameter to study the change in the elastic constants due to the SHI irradiation by first principles. Now, using those elastic constant values, microstructural modifications of SHI irradiated samples has been obtained using Variance methods. Finally, Raman spectral analysis has been performed for the determination of tensile stress as induced by SHI irradiation on the prepared samples. These results are published or discussed in series of recent publications [1-4].

#### List of Publications

- [1] D. Nath, F. Singh, and Ratan Das, Materials Chemistry and Physics, 239 (2020) 122021.
- [2] D. Nath & Ratan Das, Applied Surface Science, 509 (2020) 144708.
- [3] D. Nath, S. Debnath, P. C. Dey, F. Singh, and Ratan Das, J. Alloys and Compounds, 824 (2020) 153968.
- [4] D. Nath, F. Singh, Ratan Das, Mats. Science in Semicond. Processing, 114 (2020) 105079.

#### 5.2.14 Effect of the grain sizes on the swift heavy ion induced deformation in $\text{Nd}_2\text{Zr}_2\text{O}_7$

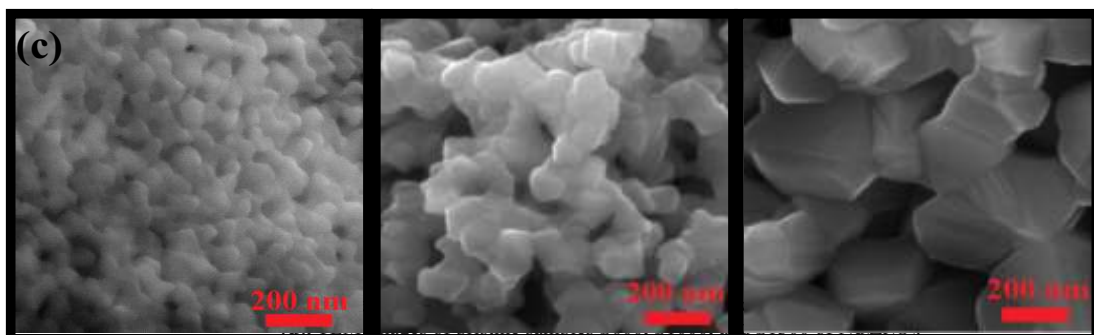
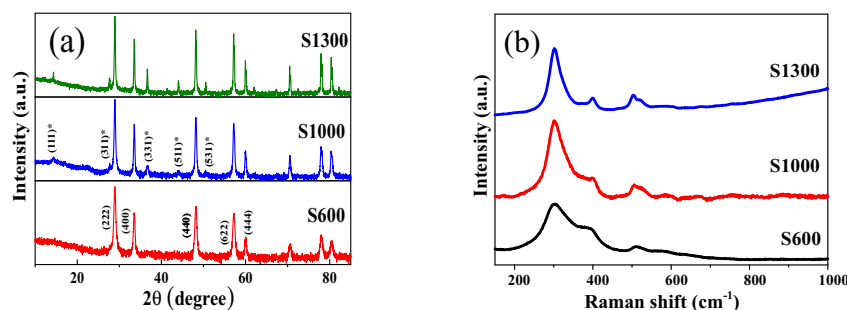
Sharma S. K.<sup>a</sup>, Hussain Abid<sup>a</sup>, Grover Vinita<sup>b</sup>, Tyagi A. K.<sup>b</sup>, Kulriya P. K.<sup>a</sup>

<sup>a</sup> Material Science Group, Inter-University Accelerator Centre, New Delhi 110067, India

<sup>b</sup> Chemistry Division, Bhabha Atomic Research Centre, Mumbai 400085, India

Email Id: sharmasaurabh030@gmail.com

The pyrochlore ceramic materials are the most significant oxides not only for the immobilization of highly radioactive nuclear waste but also for the fabrication of mixed oxide fuel for the advance nuclear reactors [1-4]. Some studies claim that nano-crystalline ceramic is more radiation-resistant **due to high defect and particle sink density**. **Theoretical simulation studies** performed on nano-crystalline pyrochlore by *Bai et. al.*, showed greater radiation tolerance of nano-crystalline than bulk pyrochlore because of the presence of a large number of grain boundaries which act as a sink for an accumulation of the defects [3]. To experimentally validation of the above hypothesis, we have synthesized nanocrystalline powder of  $\text{Nd}_2\text{Zr}_2\text{O}_7$  pyrochlore composition through the auto-combustion process at BARC, Mumbai. Sample of desired grain size was prepared by the sintering the cylindrical pellets of as-synthesized nanocrystalline powder at 600°C for 2 h, 1000°C for 10 h, and 1300°C for 36 h, which are marked as S600, S1000, and S1300, respectively using furnaces available at IUAC. Experimentally measured densities of these samples are 74 %, 81%, and 86%, respectively. The structural and microstructural properties of the pristine samples were characterized using XRD, micro-Raman spectroscopy, SEM, and TEM investigations. Figure 1 shows the (a) XRD pattern, (b) Raman spectra, (c) FE-SEM images, and (d) TEM images of the S600, S1000, S1300 pristine samples.



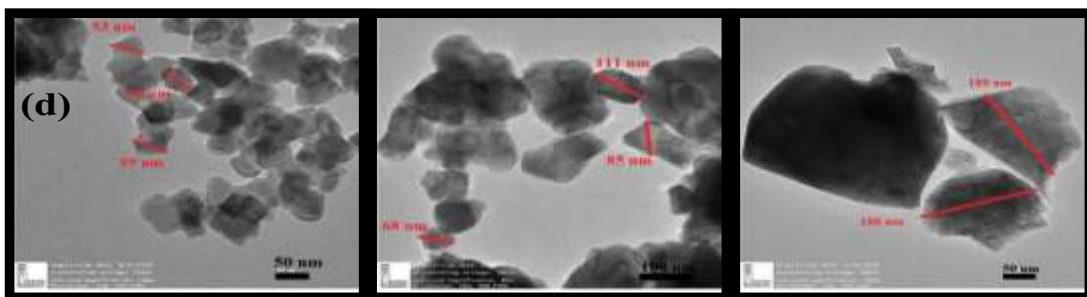


**Figure 1.** A representative of (a). XRD pattern, (b). Raman spectra, (c). FE-SEM images, and (d). TEM images of pristine samples S600, S1000, and S1300 of Nd<sub>x</sub>Zr<sub>2-x</sub>O<sub>7</sub>.

Pellets, as well as powder of pyrochlore dispersed on TEM grids, has been irradiated at room temperature with 100 MeV iodine beam at the ion fluence ranging from  $3 \times 10^{11}$  to  $5 \times 10^{13}$  ions.cm $^{-2}$ . The damage fraction calculated using direct impact model from the XRD data showed that samples with smaller grain size exhibit higher radiation stability. Thus, improved radiation stability of nano-structured Nd<sub>2</sub>Zr<sub>2</sub>O<sub>7</sub> confirmed that it can be a most promising inert matrix fuel (IMF) for the fabrication for mixed oxide fuel (MOX fuel) for the closed fuel cycle.

### References:

1. Subramanian *et al.*, Oxides pyrochlores – A Review, Prog. Solid State Chem. 15 (1983) 55.
  2. Sickafus *et al.*, Radiation Tolerance of Complex Oxides, Science 289 (2000) 748.
  3. Bai *et al.*, Efficient annealing of radiation damage near grain boundaries via interstitial emission, Science (80), 327(2010)1631.
  4. Sharma *et al.*, V. Grover, A.K. Tyagi, D.K. Avasthi, U.B. Singh, P.K. Kulriya, Probing the temperature effects in the radiation stability of  $\text{Nd}_2\text{Zr}_2\text{O}_7$  pyrochlore under swift ion irradiation, Materialia 6 (2019)

## **5.2.15 Surface Modification of Titania Nanotube Arrays using Low Energy Ion Beam in Nitrogen Environment for Photocatalytic and Sensing Applications (BTR No. 62503)**

Shikha Wadhwa<sup>a\*</sup>, Devraj Singh<sup>b</sup>, Ambuj Tripathi<sup>c</sup> and Devrani Devi<sup>c</sup>

<sup>a</sup>Amity Institute of Nanotechnology, Amity University Uttar Pradesh, Sector-125, Noida-201313

<sup>b</sup> Amity Institute of Applied Sciences, Amity University Uttar Pradesh, Sector-125, Noida-201313

<sup>c</sup> Inter-University Accelerator Centre (IUAC), Aruna Asaf Ali Marg, New Delhi 110067, India

An enzyme based electrochemical sensor using ion-beam modified Titania nanotube (TiNT) electrode surface has been developed. The TiNT electrode surface was modified with Nitrogen (N<sup>+</sup>) and gold (Au<sup>-</sup>) ions and 80 keV accelerating voltage using ECR and SNICS facilities at IUAC, Delhi. The electrode was characterised using SEM, XPS and Electrochemical Impedance Spectroscopy (EIS). The modified electrode surface was treated with chemical linker molecules necessary for efficient binding of tyrosinase enzyme. Excellent sensor performances were observed with Au-TiNT and N-TiNT with as low as nanometer range detection limit and response time of ~ 1 minute. Low energy ion beam modified TiNT electrodes can hence be employed for highly sensitive and real-time detection of Tyrosine.

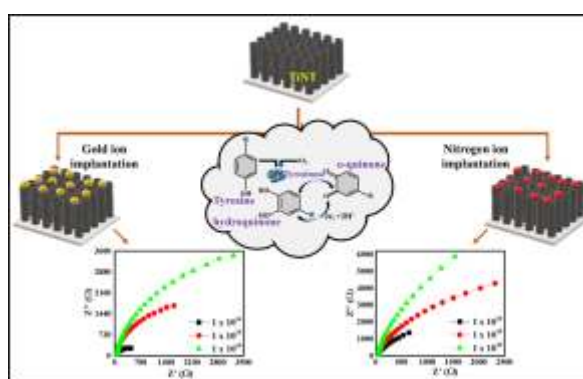


Fig.1: Enzymatic electrochemical detection of L-Tyrosine using Au-TiTNT and N-TiTNT electrodes

### References:

- [1] S. Roy, A. John, S. Nagabooshanam, A. Mishra, S. Wadhwa, A. Mathur, J. Narang, J. Singh, N. Dilawar, J. Davis, *Appl. Surf. Sci.* 488 (2019) 261–268.
  - [2] I. M. Apetrei, C. Apetrei, *Materials* 12 (2019) 1009.
  - [3] X. Hou, F. Liu, K. Yao, H. Ma, J. Deng, D. Li, B. Liao, *Mat. Lett.* 124 (2014) 101–4.

### 5.2.16 Effect of Fe Ion Implantation on the Thermoelectric Properties of CoSb<sub>3</sub> Thin Films

Anha Masarrat<sup>1,2</sup>, Anuradha Bhogra<sup>1</sup>, Ramcharan Meena<sup>1</sup> T. Som<sup>3</sup>, Ashish Kumar<sup>1</sup>, A. Niazi<sup>2</sup> and K. Asokan<sup>1</sup>

<sup>1</sup>Inter-University Accelerator Centre, Aruna Asaf Ali Marg, New Delhi, 110067, India

<sup>2</sup>Department of Physics, JMI, New Delhi

<sup>3</sup>Institute of Physics, Bhubaneswar, 751005, India.

Among different skutterudites, CoSb<sub>3</sub> shows the best thermoelectric properties as it owns excellent electronic properties. CoSb<sub>3</sub> is a low band gap skutterudite compound semiconductor with high S and high carrier mobility<sup>1</sup>. It has a cubic structure with the formula of MX<sub>3</sub> where M is metal ions like Co, Rh, and Ir and X any metalloid like As and Sb. Of all the eight sub cubes in a cubic unit cell, two cubes are voids that can accommodate guest atoms that rattle inside. Ion implantation by Fe, Ni or light ions like B or C ions are expected to occupy the Co or Sb sites whereas metals like Th, Ur, La, Eu or Ce ions are expected to occupy voids and rattle inside these voids which help in enhancing the thermoelectric properties [1-3]. Present study focuses on the morphological, structural, electrical and thermoelectric properties of the Fe ion implanted CoSb<sub>3</sub> thin films deposited by PLD. Further, X-ray absorption spectroscopy has been used to understand the local electronic structures of these Fe implanted CoSb<sub>3</sub> samples.

Bulk CoSb<sub>3</sub> target was prepared by solid state reaction method. The films were deposited on Si (100) substrates using the PLD system from M/S Excel Instruments, Mumbai. The deposited films were then implanted with 120 keV Fe ions using the Negative Ion Implanter facility of IUAC New Delhi with three different fluencies: 1×10<sup>15</sup>, 2.5×10<sup>15</sup> and 5×10<sup>15</sup> ions/cm<sup>2</sup>. All these films were then annealed using rapid thermal annealing (RTA) technique. The RTA was done for 2 min at 873K under Ar gas. For convenience hereafter, the pristine film will referred pristine as P; rapid annealed film as PA, the films 1×10<sup>15</sup>, 2.5×10<sup>15</sup> and 5×10<sup>15</sup> as I<sub>1E15</sub>, I<sub>2.5E15</sub>, I<sub>5E15</sub>, respectively and implanted but rapid annealed samples as I<sub>1E15</sub>A, I<sub>2.5E15</sub>A, I<sub>5E15</sub>A.

Fig 1(a) shows the GIXRD pattern of P, PA, I<sub>1E15</sub>, I<sub>1E15</sub>A, I<sub>2.5E15</sub>, I<sub>2.5E15</sub>A, I<sub>5E15</sub>, and I<sub>5E15</sub>A. Due to ion implantation, the films become amorphized which regain its crystallinity after RTA process under Ar atmosphere. The pristine, as-deposited films, are polycrystalline and single phase in nature and indexing of the peaks are done based on the simple cubic structure of CoSb<sub>3</sub>(JCPDS19-0336). Due to ion implantation, the films become amorphized which regain its crystallinity after RTA process under Ar atmosphere. The bond lengths as obtained from the Rietveld refinement data is Co-Sb (2.531 Å), Sb-Sb short pair (2.855 Å) and Sb-Sb long pair (3.43 Å). It is comparable with values given in literature for unfilled CoSb<sub>3</sub>.

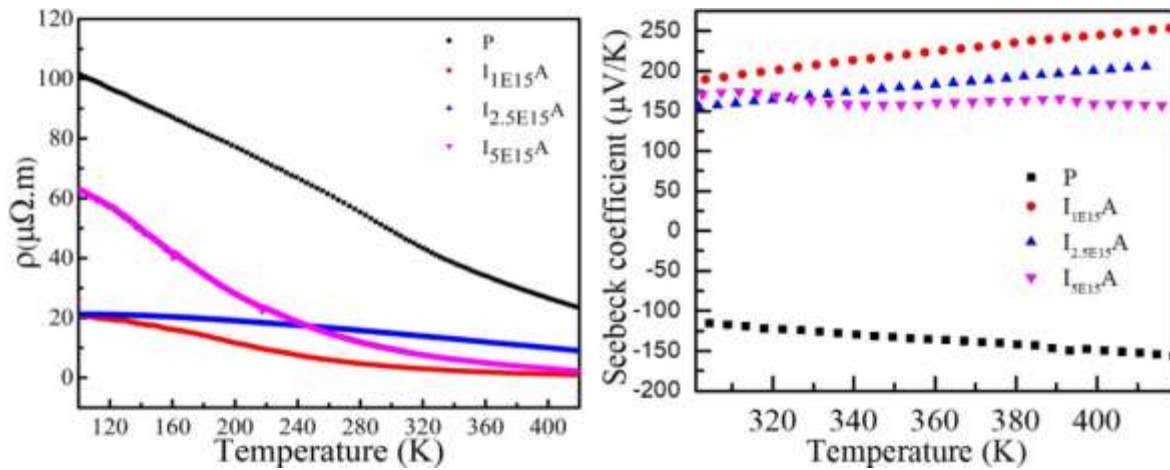


Figure . (a) Resistivity of PA, I<sub>1E15</sub>A, I<sub>2.5E15</sub>A, and I<sub>5E15</sub>A. (b) Seebeck coefficient of PA, I<sub>1E15</sub>A, I<sub>2.5E15</sub>A, and I<sub>5E15</sub>A

Fig 2(b) shows the variation of S with temperature for P, I<sub>1E15</sub>A, I<sub>2.5E15</sub>A, and I<sub>5E15</sub>A samples from 300 K to 420 K. The S of P sample is negative indicating n-type conduction. However, for the Fe implanted system, the S is positive showing a p-type conduction behaviour. The P film gives S as -120  $\mu\text{V/K}$  at room temperature which increases up to -157  $\mu\text{V/K}$  at 420 K. For the Fe implanted sample, the S decreases with increasing Fe fluence.

The S for I<sub>1E15</sub>A, I<sub>2.5E15</sub>A, and I<sub>5E15</sub>A at 400 K are 245, 200 and 158  $\mu\text{V/K}$  respectively. The decrease in S with increasing fluence may be also due to the generation of large number of defect created during implantation process. As Fe ion enters the material, they create defect in the system. The defect can be present in the form of the implanted ions itself or the creation of interstitial or vacancy pairs. The power factor (P.F =  $S^2 / \mu$ ) for Fe ion implanted samples is found to be greater than the pristine sample. A highest value of P.F = 700  $\mu\text{W/mK}^2$  is

obtained at 420 K for  $I_{\text{Fe}}\text{A}$  sample. The large increase in P.F can be attributed to the increase in the carrier concentration, high S and low  $\mu$  of the Fe ion implanted samples. The electrical resistivity decreases substantially after Fe doping indicating that the Fe ions are electrically active and act as electron acceptor which is further well confirmed with the changing of sign of S from negative to positive after Fe ion implantation. Yang et al reported that hole concentration increases by Fe doping at a rate of  $\sim 0.03$  holes per Fe ion and concluded that Fe substitute in a low spin  $d^5$  configuration in the  $\text{CoSb}_3$  lattice in a trivalent state. Similarly, from the XAS results it can be concluded that Fe implanted is in 3+ state. For the implanted samples, the decrease in resistivity is due to the addition of p-type charge carriers. It is observed that the S decreases with the increase in Fe ion fluence. The lowest fluence ( $I_{\text{Fe}}\text{A}$ ) has the highest S in the complete temperature range. Due to the doping of Fe ions, the hole carrier concentration increases which shift the Fermi level towards the valence band and hence the S is positive.

Polycrystalline  $\text{CoSb}_3$  thin films with the skutterudite structure were deposited by PLD on Si (100) substrate and investigated for their structural, optical, and morphological properties due to Fe ion implantation after RTA. The sign of S changed from negative to positive with Fe doping giving the highest value of  $S=245 \text{ } \square \text{ V/K}$  for  $I_{\text{Fe}}\text{A}$  at 400 K and highest value of P.F ( $700 \text{ } \mu\text{W/mK}^2$ ). The Fe substitution on Co site leads to the creation of vacancies which gives rise to high concentration of holes. The high Seebeck Coefficient and reduced electrical resistivity of the Fe implanted sample leads to high power factor. Fe L edge XANES spectra show that Fe occupies the Co site in trivalent state. By optimising the parameter of implantation,  $\text{CoSb}_3$  might lead to advanced thermoelectric applications.

#### References

- [1] M. V. Daniel, M. Lindorf and M. Albrecht, *J. Appl. Phys.*, 2016, **120**, 125306–1.
- [2] J. Peng, J. Yang, X. Song, Y. Chen, S. Bao and T. Zhang, *Front. Mater. Sci. China*, 2007, **1**, 177–180.
- [3] P. Wei, W. Zhao, D. Tang, W. Zhu, X. Nie and Q. Zhang, *J Mater.*, 2016, **2**, 280–289.
- [4] J. Yang, G. P. Meissner, D. T. Morelli and C. Uher, *Phys. Rev. B*, 2000, **63**, 1–11.

#### 5.2.17 Electrical and Thermoelectric Properties of N ion implanted $\text{SrTiO}_3$ Thin Films

Anuradha Bhogra<sup>1</sup>, Anha Masarat<sup>1</sup>, Ramcharan Meena<sup>1</sup>, Dilruba Hasina<sup>2</sup>, T. Som<sup>2</sup>, Ashish Kumar<sup>1</sup> and Asokan Kandasami<sup>1</sup>

<sup>1</sup>Inter-University Accelerator Centre, Aruna Asaf Ali Marg, New Delhi, 110067, India

<sup>2</sup>Institute of Physics, Bhubaneswar, 751005, India.

Increasing demand for the clean energy resources led to an alternative approach of environment friendly high performance thermoelectric devices to reuse the waste heat via solid state refrigeration and power generation [1,2]. **This study focuses on the effect of low energy N ion implantation on the crystal and electronic structures, electrical and thermoelectric properties of STO.** All the films were deposited by pulsed laser deposition on Si substrate using STO target and implanted with 60 keV N ions with fluence;  $1 \times 10^{16}$  and  $5 \times 10^{16}$  ions/cm<sup>2</sup>. For simplicity, hereafter, annealed films of pristine,  $1 \times 10^{16}$  ions/cm<sup>2</sup> and  $5 \times 10^{16}$  ions/cm<sup>2</sup> referred as STO, STO-N116, and STO-N516, respectively.

Figure 1(a) shows the XRD spectra of pristine and N implanted STO films. Implantation of 60 keV N+ ions resulted in amorphization in the top layers of STO film as probed by XRD and hence these films were subjected to vacuum annealing of 2 hrs. After annealing, a crystalline phase evolves and gets more pronounced at higher fluence. Figure 1(b) shows the experimental RBS spectra of STO-P, STO-N116 and STO-N516 along with the simulated spectrum of STO-P using XRUMP Software. The average thickness was estimated to be 280 nm which is close to the measured value.

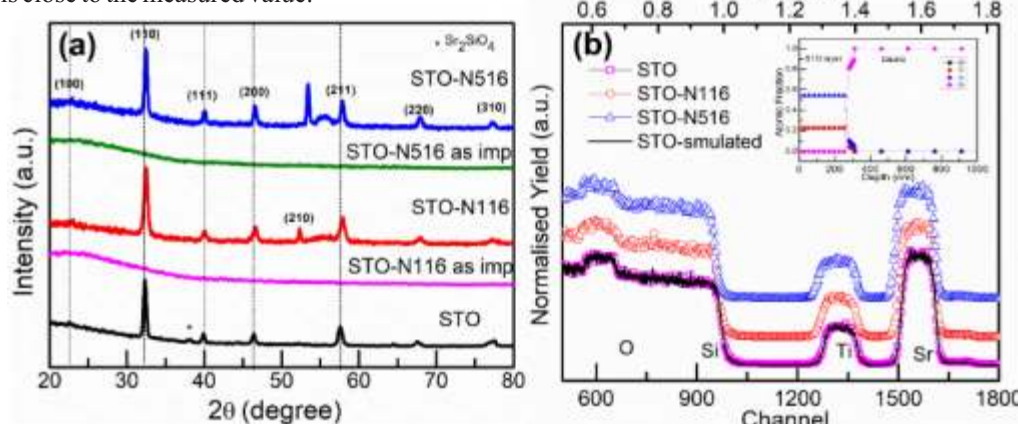


Figure 1. (a) X-ray diffraction patterns of STO thin films: STO, STO-N116 and STO-N516.

(b) RBS spectra of STO films: STO, STO-N116 and STO-N516.

The O K edge spectra of pristine and implanted films are shown in Fig. 2(a). The peak intensity in O K-edge is related to the number of unoccupied 2p orbitals and also reflects the hybridization with Ti 3d and Ti 4sp orbitals [3,4]. The intensity ratio of  $t_{2g}$  to  $e_g$  changes with the ion implantation. For high N fluence, the  $t_{2g}/e_g$  ratio decreases as compared to the STO and STO-N516.

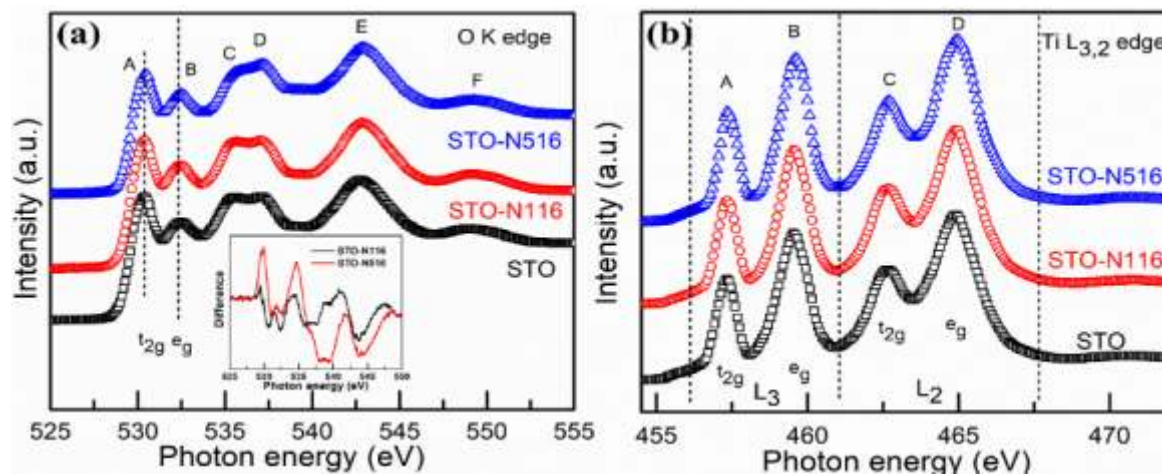


Figure 2. The X-ray absorption spectra of STO, STO-N116 and STO-N516 samples at (a) O K-edge and (b) Ti L-edge of STO, STO-N116 and STO-N516 samples.

The Ti L-edge spectra of N implanted STO samples are shown in Fig. 2(b). It is observed that there is noticeable broadening in the overall spectra of Ti L-edges which is attributed either to the nitrogen occupancy or defects introduced during N ion implantation. To understand the electrical and thermoelectric properties, the temperature dependent resistivity and Seebeck co-efficient were measured. Figure 3 shows the resistivity of pristine and implanted films in the temperature range of 80-400 K. It is evident that the resistivity decreases with temperature indicating a typical semiconducting behaviour in all samples [5]. For the film STO-N116, the resistivity increases as compared to the STO for the entire temperature range.

The Seebeck coefficient is measured in the temperature range of 300-400 K and displayed in Fig. 4(a). The sign of S is negative throughout the measured temperature range revealing n-type behaviour for all the samples and S increases with temperature. Figure 4(b) shows the variation of power factor of N implanted thin films as a function of temperature. A significant increase in power factor in the order of  $15 \mu\text{Wm}^{-1}\text{K}^{-2}$  at 400 K is observed for STO-N516.

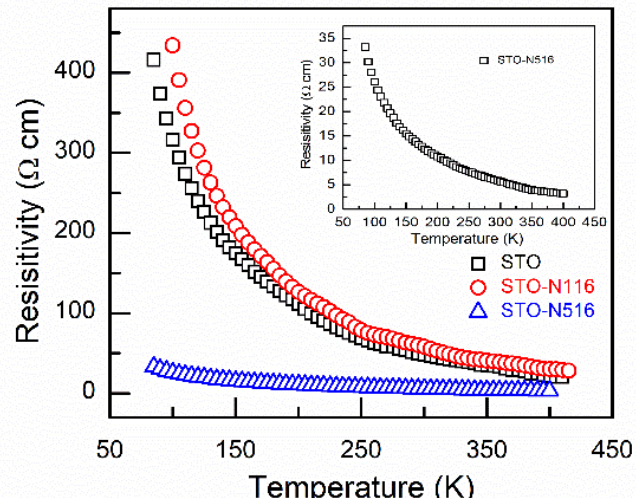


Figure 3. Temperature dependence of resistivity of pristine and N implanted STO thin films. All the films show semiconducting behaviour with temperature. Inset shows the resistivity of STO-N516 with temperature.

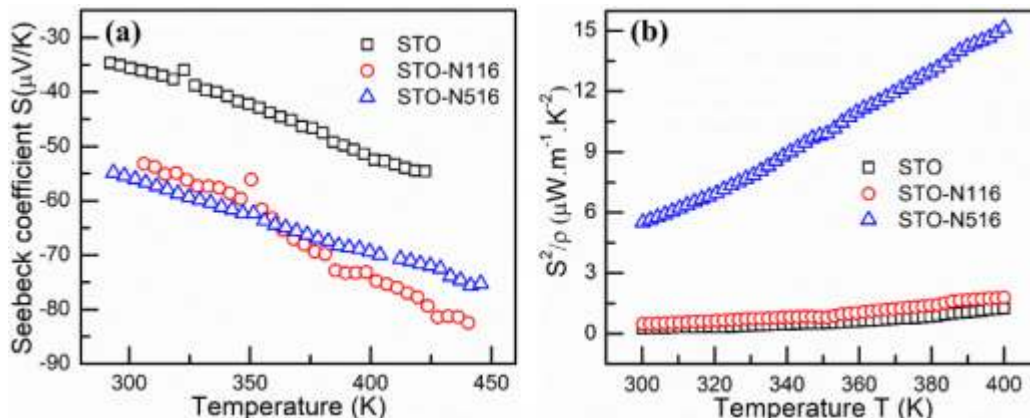


Figure 4. (a) Temperature dependence of the S of all the films, (b) Power factor as a function of temperature in range 300-400 K. The maximum power factor of  $15 \mu\text{Wm}^{-1}\text{K}^{-2}$  at 400 K for STO-N516.

In summary, ion implantation studies on PLD deposited STO thin films were carried out to understand the electrical transport and scattering mechanisms. The XRD confirms the cubic perovskite phase of pristine and implanted films. The X-ray absorption spectra show that N implantation affects the local symmetry of TiO<sub>6</sub> octahedron by generating defects mainly oxygen vacancies. There is an enhancement in electrical conductivity and thermopower at high implantation dose. The electrical transport properties of N ion implanted STO films reveal different conduction mechanisms: the band conduction in the high temperature regime, nearest neighbour and variable range hopping in the low temperature regime attributed to the presence of defect induced localized states in the band gap. The increased power factor ( $15 \mu\text{Wm}^{-1}\text{K}^{-2}$ ) for higher fluence film depicts the significance of ion implantation technique which provides a new tool for defect engineering in the applications of thermoelectric devices.

#### References:

- [1] Alam, H. & Ramakrishna, S. A review on the enhancement of figure of merit from bulk to nano-thermoelectric materials. *Nano Energy*, 2, (2013)190–212,
- [2] Kumar, A. et al. Enhancement of thermopower in GaN by ion irradiation and possible mechanisms. *Applied Physics Letters* 111, (2017) 222102.
- [3] Soriano, L., Abbate, M., Fernández, A., González-Elipe, A. R. & Sanz, J. M. Chemical Analysis of Ternary Ti Oxides using Soft X-ray Absorption Spectroscopy. *Surface and Interface Analysis* 25, (1997) 804–808,
- [4] Asokan, K. et al. Electronic structures of Ba<sub>1-x</sub>CaxTiO<sub>3</sub> studied by x-ray absorption spectroscopy and theoretical calculation. *Journal of Physics: Condensed Matter* 13, (2001) 11087–11095.
- [5] Kang, S. D., Dylla, M. & Snyder, G. J. Thermopower-conductivity relation for distinguishing transport mechanisms: Polaron hopping in CeO<sub>2</sub> and band conduction in SrTiO<sub>3</sub>. *Physical Review* B97, (2018) 235201.

#### 5.2.18 Structural and Optical Properties of Ni Implanted NiO Thin Films

Razia Nongjai, Ksh Devarani Devi and K. Asokan

*Materials Science Division, Inter University Accelerator Centre (IUAC), Aruna Asaf Ali Marg, New Delhi 110067, India*

NiO thin films were deposited on quartz substrate by the electron evaporation method at room temperature from high purity (Alfa Aesar 99.99 %) polycrystalline NiO target. The thickness of the thin film was about 100 nm as measured by quartz crystal thickness monitor equipped with the evaporator. Then, Ni ions were implanted on these films with 100 MeV Ni ions at fluences  $1 \times 10^{14}$  (1E14),  $1 \times 10^{15}$  (1E15) and  $1 \times 10^{16}$  (1E16) ions/cm<sup>2</sup> using low energy negative ion implanter facility (MC-SNICS) at IUAC, New Delhi. The structural properties of the pristine and Ni ion implanted films were characterized by X-ray diffractometer (Bruker D8Advanced) with Cu – K<sub>α</sub> ( $\lambda=1.54 \text{ \AA}$ ) and optical properties by UV-vis spectrometer (JASCO 670). From the XRD spectrum, it is observed that the pristine film exhibits crystallographic texture along [111] as indicated by high relative intensity ratio of (111) diffraction peak compared to (200) (JCPDS File No. 78-0643). The intensity ratio (111)/(200) is 106% which is much larger than corresponding value of 67% for polycrystalline target. The implantation of Ni ions reduces the crystallinity upto fluence of 1E15 and a stress is induced in the samples as seen from the shifting of the peak position to higher angles. However, the crystallinity improves at the fluence 1E16 and become relax isotropic structure. The transmittance as well as band gap decreases with implantation with and further decreases increasing fluences. Lower band gap values of the implanted samples can be attributed to due to the increased defects introduced by the energetic ion implantations [1-3].

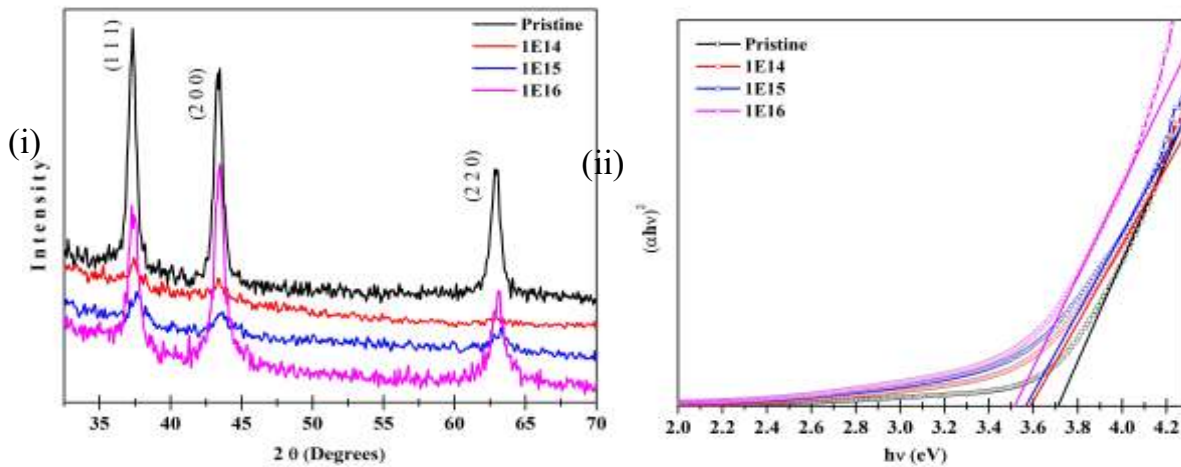


Figure: (i) XRD pattern of NiO pristine and implanted thin films. (ii) Variation of  $(\alpha h\nu)^2$  versus  $h\nu$  of NiO pristine and implanted thin films.

#### References:

- [1] N. Wang, C.Q. Liu, C.Q. Liu B. Wen, H.L. Wang, S.M. Liu, W.W. Jiang, W.Y. Ding and W.P. Chai, *Thin Solid Films* **616**, 587–593 (2016).
- [2] Y. Huang, Q. Zhang, J. Xi and Z. Ji, *Applied Surface Science* **258**, 7435–7439 (2012).
- [3] T. Dutta, P. Gupta, A. Gupta, and J. Narayan *J. Appl. Phys.* **108**, 083715 (2010).

## 5.2.19 Impact of Low Energy Fe-ion Implantation on the Physical Properties of Topological Insulator $Sb_2Te_3$ Thin Films

Jyoti Yadav<sup>a</sup>, Rini Singh<sup>b</sup>, Anoop M D<sup>a</sup>, Nisha Yadav<sup>a</sup>, D. Devi<sup>c</sup>, N.S. Rao<sup>a</sup>, F. Singh<sup>c</sup>, K. Awasthi<sup>a</sup> and Manoj Kumar<sup>a</sup>

<sup>a</sup>Department of Physics, Malaviya National Institute of Technology Jaipur, Rajasthan, 302017, India

<sup>b</sup>Graduate School of Engineering, Hiroshima University, Higashi-Hiroshima, 739-8527, Japan

<sup>c</sup>Inter-University Accelerator Centre (IUAC), New Delhi - 110067, India

$Sb_2Te_3$  is a narrow band gap, p-type ternary tetradymite compound having topological insulator behavior. Thin films of topological insulator  $Sb_2Te_3$  have significant research interests because of their potential applications in spintronics and quantum information processing. Since the magnetic dopants can alter the topological surface states it is therefore of great importance to tune the physical properties of topological materials. The present studies summarize the influence on the physical properties of  $Sb_2Te_3$  thin films by 100KeV  $Fe^{+}$  ion implantation. Thin films synthesized by e-beam evaporation were implanted at 3 different Fluences ( $1 \times 10^{13}$ ,  $1 \times 10^{14}$ ,  $5 \times 10^{14}$  ions/cm<sup>2</sup>) of  $Fe^{+}$  ion at IUAC, New Delhi using 15 UD Pelletron Accelerator. The energy of the ion beam is set to be 100 KeV and current of the beam was 10  $\mu$ A.

The x-ray diffraction (XRD) studies were performed on pristine and implanted films to understand the structural changes because of ion implantation. The higher order planes corresponding to (001) observed in XRD spectra clearly demonstrate oriented growth of the films (Figure 1). The peaks in the diffraction pattern of the  $Sb_2Te_3$  thin films were matched with JCPDS reference code 01-071-0393 which corresponds to rhombohedral crystal structure with R-3m space group (166). The parameters of the  $Sb_2Te_3$  pristine and implanted thin films are refined with Sb atoms distributed randomly over (00z) position and two types of Tellurium atoms at positions 3a (000) and 6c (00z) respectively. The atomic coordinate z is refined for both Sb and Te atoms simultaneously along with the peak shape parameters (u, v, w). Considering the values of the atomic radii of antimony and iron ( $R_{Sb} = 0.140$  nm,  $R_{Fe} = 0.117$  nm), the observed slight decrease in the lattice volume V with implantation of Fe ions, can be explained by the formation of a substitutional defects. However, at low implantation dose, creation of substitutional defects may not be a significant. There might be a greater number of Fe ions intercalated with interstitial sites rather substitutional sites. Slight increase in the value of lattice parameter 'c' is indicative to the generation of strain during implantation as the implanted Fe ions occupy the Sb lattice or interstitial voids. However, the lattice parameter  $a=b$  does not vary significantly. Interestingly, intensity of the peak corresponding to (015) plane at  $2\Theta = 27.8^\circ$  increased significantly for fluence  $1 \times 10^{14}$  ions/cm<sup>2</sup> while a monotonic increase with fluence was observed for (114) plane. An overall increase in the intensity of selected peaks may be attributed to the creation of both substitution defects and interstitial defects during implantation.

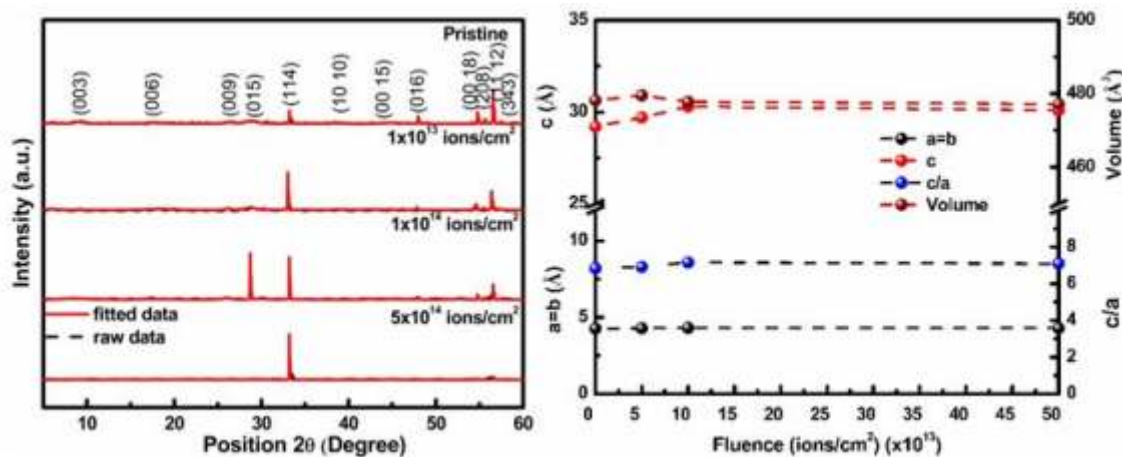
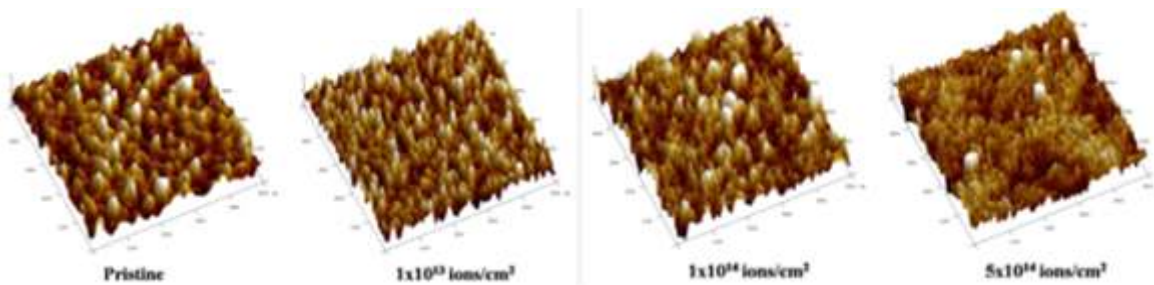


Figure 1: The X-ray Diffraction pattern of pristine and implanted  $Sb_2Te_3$  Thin films (left) and the variation of lattice parameters (right)

The AFM images in the Fig. 2 show the 3-D surface profile (scan area 500 nm × 500 nm) of pristine and Fe ion implanted  $Sb_2Te_3$  thin films. The surface roughness increases under ion implantation from 0.8 nm to 1 nm for pristine and ion fluence of  $1 \times 10^{14}$  ions/cm<sup>2</sup> respectively. However, at the highest fluence of  $5 \times 10^{14}$  ions/cm<sup>2</sup> the surface roughness decreased to 0.5 nm. The decrease in roughness of ion implanted  $Sb_2Te_3$  thin films can be attributed to the formation of smaller sized nano-crystallites, grain growth and better filling of pores upon implantation due to increase of local annealing effect. The appearance of the nanocrystalline structures also signifies the improvement in crystallinity of thin films as indicated by XRD results.



**Figure 2:** AFM images of the pristine and implanted  $\text{Sb}_2\text{Te}_3$  thin films showing the surface reconstruction after ion implantation

The electronic transport properties of the thin films were studied in the temperature range from 300 K to 4 K at High Pressure Physics Lab, MNIT Jaipur using a closed cycle cryostat. An overall increase in resistivity was observed with increasing Fe dose up to  $1 \times 10^{14}$  ions/cm $^2$  (left panel in Figure 3). The increase in resistivity may be associated with a decrease in the mobility of the free current carriers. Another possible reason for increase in resistivity could be due to the acceptor defects created by Fe implantation. Interestingly, with increasing the fluence an upturn in resistivity develops at low temperature except for the highest fluence. Furthermore, the temperature dependence of resistivity weakens consistently with increase in the fluence and becomes almost independent for the highest fluence. It can therefore be concluded that heating of the films stimulated the out diffusion of Fe atoms from substitutional sites towards surface or deep into the bulk decreasing the resistivity value. A clear transition from *p*-type to *n*-type majority carriers was observed with increasing the fluence (right panel in Figure 3) in Hall effect studies. The variation of Hall coefficient with implantation suggests that the Fermi level moves towards the conduction band under implantation. With increase the Fe ion dose, tuning of Fermi level from valence band towards the centre of the band gap is observed. It is worth to highlight that for the intermittent fluences the Fermi level pins at the middle of the band gap. This observation strongly supports the idea of utilizing the ion implantation for fine tuning the electronic structure of topological insulators.

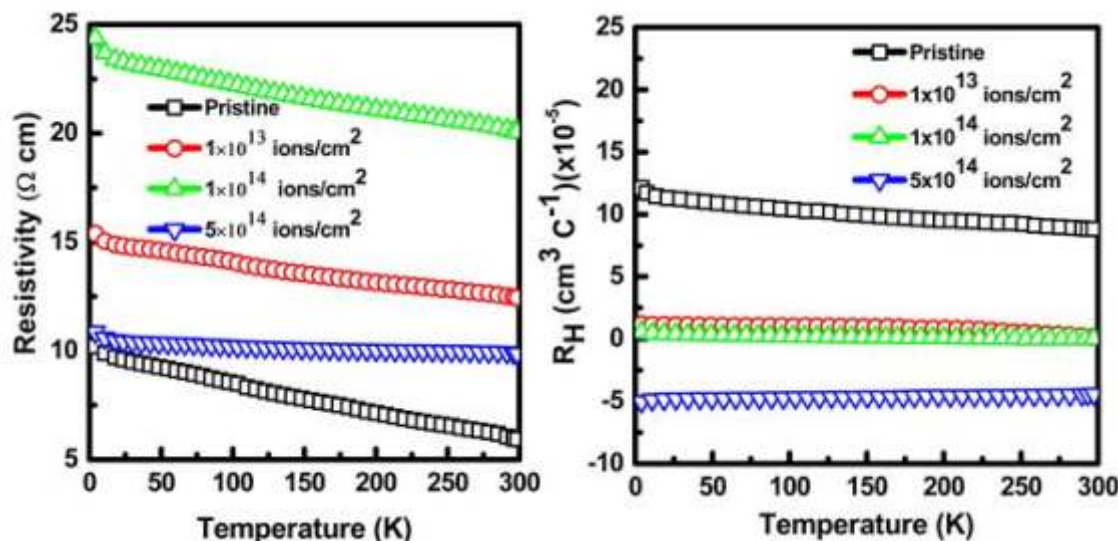


**Figure 3:** The *p*-*T* plot of the pristine and implanted  $\text{Sb}_2\text{Te}_3$  thin films (left) and the variation of Hall coefficient with temperature at different implantation doses (right).

Polycrystalline thin films of topological insulator compound  $\text{Sb}_2\text{Te}_3$  were successfully synthesized by e-beam evaporation. XRD studies confirmed the formation of a rhombohedral crystal structure with R-3m (166) space group. Our results demonstrate significant increase in the structural deformation and lattice strain with the fluence of Fe ion implantation. Present work demonstrates the highly controllable tuning of Fermi level with Fe ion implantation and transition of charge carriers from dominating *p*-type to *n*-type with implantation.

#### References:

- [1] H.Li et al. American Society of Mechanical Engineers, 5A (2016) 83–86.
- [2] Z.Zhou et al. Journal of Applied Physics, 99 (2006) 043901.
- [3] M.Lang et al. Nano Letters, 13 (2013) 48–53.
- [4] A.Y.Kuntsevich et al. Physical Review B, 94 (2016)

### 5.2.20 Fabrication of plasmonic dye-sensitized solar cells using ion-implanted photoanodes

N. Kaur<sup>1</sup>, V. Bhullar, O. Prakash<sup>1</sup>, A. Mahajan<sup>1\*</sup>, D. P. Singh<sup>1</sup>, F. Singh<sup>2</sup>, D. K. Kshetri<sup>2</sup> and S. Chopra<sup>2</sup>

<sup>1</sup>Department of Physics, Guru Nanak Dev University, Amritsar-143005, India

<sup>2</sup>Inter University Accelerator Center, New Delhi-110067, India

In past few years, a unique characteristic property of metal nanoparticles i.e. localized surface plasmon resonance (LSPR), have been explored in third generation dye sensitized solar cells (DSSCs); to efficiently improve their power conversion efficiency *via* extending the absorption wavelength range of dye into the visible region of solar spectrum as well as reducing the recombination reactions occurring at photoanode/electrolyte interface [1-3]. However, metal nanoparticles exhibited instability issues with iodine based electrolytes; that further negatively affects the long term stability of DSSCs [4]. Further, the core-shell structures have been investigated, which although improves the stability of DSSCs up to a certain extent, suffers from optimal utilization of LSPR for light harvesting [5]. Ion implantation has been opted out as an alternative to resolve the corrosion issue of metal nanoparticles with electrolyte as well optimal utilization of LSPR of Mnps [6-7]. On the basis of the literature survey [8-10] and our preliminary investigations on DSSC, thorough proposal has been planned with the objectives of: 1) Implantation of metal nanoparticles (Ag, Au, Cu and Al) possessing surface plasmon resonance (SPR) peaks for enhancing effective absorption cross-section of dye in TiO<sub>2</sub> matrix using low energy beam (few keV), 2) Implantation of bimetallic nanostructures in TiO<sub>2</sub> matrix to further enhance and broaden the SPR, and 3) Fabrication and characterization of highly efficient and stable DSSCs using ion beam engineered photoanodes.

In order to complete the proposed work, TiO<sub>2</sub> photoanodes were implanted using low energy ion beam facility at IUAC, for the fabrication of DSSCs. TiO<sub>2</sub> matrix was prepared by the initial deposition of a compact layer of TiO<sub>2</sub>, prepared from titanium iso-propoxide solution, on pre-cleaned FTO substrates which was then kept for annealing at 450°C for 30 min. Further, TiO<sub>2</sub> paste was doctor bladed with thickness 3 μm on TiO<sub>2</sub> compact layer deposited FTO and subsequently annealed for 30 min. at 450°C. Ag, Au and bimetallic Mnps were implanted onto TiO<sub>2</sub> matrix with energy 80 and 120 keV. Ag and Au penetrate up to 17 and 22 nm depth in TiO<sub>2</sub> matrix and were estimated from the stopping and range of ions in matter (SRIM) software. The fluence range of Ag and Au Mnps was kept from 10<sup>12</sup> to 10<sup>16</sup> ions/cm<sup>2</sup>. The implanted samples were characterized structural and optical properties using FESEM, XRD, XPS, UV-Vis, PL, and Raman and kelvin probe spectroscopic techniques. The DSSCs were fabricated using implanted photoanodes and it was observed that Au, Ag, and bimetallic implanted photoanodes based DSSCs showed an enhancement of 44.7%, 65.3 and 87.9% in PCE in comparison to unimplanted reference DSSCs [11-12].

#### References:

- [1] H.Y. Jung, I.S. Yeo, T.U. Kim, H.C. Ki, H.B. Gu, *Applied Surface Science* 432 (2018) 266.
- [2] M. Hossain, J. Park, D. Yoo, Y.K. Baek, Y. Kim, S. Hyung Kim, D. Lee, *Current Applied Physics* 16 (2016) 397.
- [3] Tanvi, A. Mahajan, R. K. Bedi, S. Kumar, V. Saxena, A. Singh and D. K. Aswal, *RSC Advances*, 6 (2016) 48064.
- [4] D.H. Song, H.S. Kim, J.S. Suh, B.H. Jun, W.Y. Rho, *Nanomaterials* 7 (2017) 136.
- [5] D. Eli, A. Anderson Kassimu, S. Bolarinwa, *Journal of the Nigerian Association of Mathematical Physics* 43 (2018) 311.
- [6] J. Luo, J. Zhou, H. Guo, W. Yang, B. Liao, W. Shi, Y. Chen, *RSC Adv.* 4 (2014) 56318.
- [7] Y. K. Mishra, F. Singh, D. K. Avasthi, J. C. Pivin, D. Malinovska and E. Pippl, *Applied Physics Letters*, 91 (2007) 063103.
- [8] H.W. Chen, C.Y. Hong, C.W. Kung, C.Y. Mou, K. C. W. Wu and K.C. Ho, *Journal of Power Sources*, 288 (2015) 221.
- [9] D.N. Joshi, . Ilaiyaraaja, C. Sudakar, R.A. Prasath, *Solar Energy Materials and Solar Cells* 185 (2018) 104.
- [10] Xu, Q., Liu, F., Liu, Y., Cui, K., Feng, X., Zhang, W., Huang, Y. *Scientific Reports* 3 (2013) 2112.
- [11] Kaur, N., Mahajan, A., Bhullar, V., Singh, D.P., Saxena, V., Debnath, A.K., Aswal, D.K., Devi, D., Singh, F., Chopra, S. *RSC Advances* 9 (2019) 20375.
- [12] Kaur, N., Mahajan, A., Bhullar, V., Singh, D.P., Saxena, V., Debnath, A.K., Aswal, D.K., Devi, D., Singh, F., Chopra, S. *Chemical Physics Letters*, (2019) 137070.

### 5.2.21 Optical properties of Cobalt implanted Indium Phosphide and Gallium Phosphide

R. L Dubey<sup>a,b\*</sup>, S. K. Dubey<sup>b</sup>, D. Bhattacharya<sup>c</sup>, T. V. Chandrasekhar Rao<sup>c</sup>, Ksh. Devarani Devi<sup>d</sup> and Indra Sulania<sup>d</sup>

<sup>a</sup>Department of Physics, St. Xaviers college-Autonomous, Mumbai-400 001, India.

<sup>b</sup>Department of Physics, University of Mumbai, Mumbai-400 032, India.

<sup>c</sup>Solid State physics Division, BARC, Mumbai-400 094, India.

<sup>d</sup>India. Inter University Accelerator Centre (IUAC), Aruna Asaf Ali Marg, New Delhi 110067, India.

Semiconductors from III-V group when doped with small concentration of magnetic transition metal ions show ferromagnetism with rather high Curie temperatures. These materials, called Dilute Magnetic Semiconductors (DMS), are perceived to be futuristic device materials for spintronics applications. Typically, the magnetic

element substitutes randomly on some of the lattice sites and in most cases the magnetic element is Mn, although there are a few other examples like Fe, Ni, Co etc. Because the equilibrium solubility of transition metals is orders of magnitude lower than the concentrations required for ferromagnetism in III-V semiconductors, single-phase DMS's are difficult to produce.

Ion implantation is a versatile technique that has been used in the fabrication of a number of semiconductor devices. Negative ion implantation is one of the promising techniques to solve the charging problem in Integrated circuit/device. The incoming negative charge of implanted negative ions is easily balanced by the outgoing negative charge as a part of secondary electron [1].

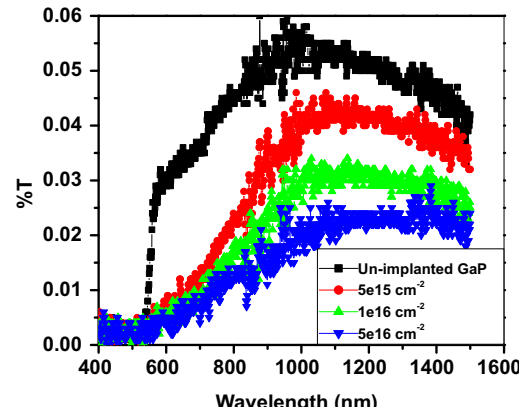
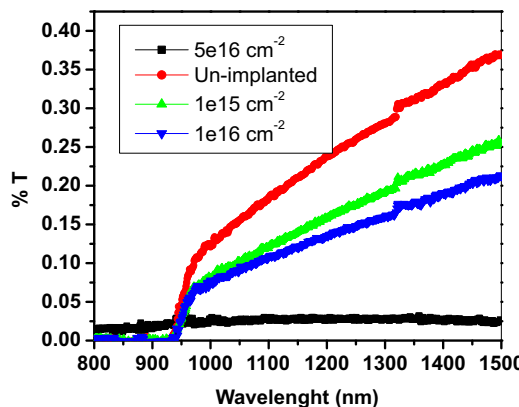


Figure.1: Transmittance spectra of 70 keV Co implanted InP

Figure.2: Transmittance spectra of 70 keV Co implanted GaP

In the present scheme, Single crystal InP and GaP samples were implanted with 70 keV Co negative ions for ion fluences  $5 \times 10^{15}$ ,  $1 \times 10^{16}$  and  $5 \times 10^{16} \text{ cm}^{-2}$  using low energy negative ion facility at Inter University Accelerator Centre, IUAC, New Delhi. Ultraviolet-visible-near infrared (UV-VIS-NIR) transmittance spectra of unimplanted sample and all the implanted samples of Indium Phosphide and Gallium Phosphide were recorded in the spectral region 200 nm to 1500 nm using a Shimadzu UV-3600 UV-VIS-NIR Spectrophotometer at university of Mumbai. Figure 1 shows the transmittance spectra of 70keV Co negative ion implanted InP. It can be clearly seen from the graph that the absorption is increasing with increasing ion fluences. The absorption edge is also found to shift towards the higher wavelength. Which indicates the presence of implantation induced defects in InP after implantation. The similar results have also been found in the 70 keV Co negative ion implanted GaP as shown in the figure.2. However the percentage transmission is very less as compared to the InP samples.

**The following studies are under progress and the results are being under analysis: X-ray diffraction (XRD), Magnetic property measurements** such as temperature variation of magnetization under different fields, Curie's temperature, remnant magnetization, Magneto-resistance etc.

In our previous run, we have implanted GaAs and SiO<sub>2</sub> with 100 keV silicon negative ions for different ion fluences varying from  $1 \times 10^{15}$  to  $2 \times 10^{17} \text{ cm}^{-2}$ . All the implanted samples has been characterised by various characterization techniques such as X-Ray Diffraction, Raman spectroscopy, Atomic force microscopy, Scanning electron microscopy and the results have been published elsewhere [2-7].

The authors are thankful to low energy negative ion implantation group at IUAC, New Delhi for their help during the ion implantation experiment.

#### References:

- [1] Junzo Ishikawa, H. Tsuji et.al –*Nuclear Instruments and Methods in Physics Research B* 96 (1995) 7-12.
- [2] Ajay Yadav, S. K. Dubey, V. Bambole, R. L. Dubey, I. Sulania and D. Kanjilal, *Radiation Effects and Defects in Solids*, 174 (2019) No.7-8, 636-646.
- [3] A. R. Yadav, S. K. Dubey, R. L. Dubey, N. Subramanyam and I. Sulania, *International Journal of Nanoscience* Vol. 18, No. 6 (2019) 1950019:1-7.
- [4] Ajay Yadavbau01bau005, Seshmani Dubeybau015bau010, Radhekrishna Dubey, bau020bau015Nagaraju Subramanyam, bau025bau020Indra Sulaniabau025, *Material Today: Proceedings*, vol. 23, Part 2 (2020), 309-316.
- [5] S. B Vishwakarma, S.K. Dubey, R. L. Dubey, A. Yadav, Vidya Jadhav, V. Bambole, I. Sulania and D. Kanjilal, *AIP conference Proceedings* 1942 (2018), 050110.
- [6] S.B. Vishwakarma, S.K. Dubey, R. L. Dubey, *Journal of Emerging Technologies and Innovative Research*, vol. 6, issue 6 (2019) 148-154.
- [7] Suraj B.Vishwakarma, Sheshmani K. Dubey, R. L. Dubey, V. Bambole, I. Sulania, D. Kanjilal, *Material Today: Proceedings*, vol. 23, Part 2 (2020), 345-351.

## 5.2.22 Impact of low energy ions beam irradiation on $TiO_2/TiO_2$ -Graphene Thin Films.

Sharma Sunita and Gaur Deepika

Department of Applied Sciences, The NorthCap University, Gurugram-122017, Haryana  
Inter University Accelerator Centre (IUAC), Aruna Asaf Ali Marg, New Delhi 110067, India

**$TiO_2/TiO_2$ -Graphene nanocomposites thin films have been irradiated with 700 keV  $Ar^{2+}$  and 300 keV  $He^{1+}$  ions.** The unexposed (pristine) and ions beam irradiation exposed thin films were characterized using XRD, FE-SEM, UV-Vis spectroscopy and solar simulator to determine the interaction mechanism between the low energy ions beam and thin films. FESEM images show the size of  $TiO_2$  nanoparticles after irradiation became smaller than before irradiation but TGr based thin films does not exhibit major change after exposure of ion irradiation. XRD manifested the formation of the  $TiO_2/TGr$  and no change in phase was observed after irradiation and affirmed its structural stability under exposed environment. The figure of merit of the low energy ions beam irradiated TGr thin films was amplified by a factor of 10 as obtained from the electrical conductivity measurement [1].

### References:

- [1] Koh, Seok-Keun, Sung-Chul Park, Sung-Ryong Kim, Won-Kook Choi, Hyung-Jin Jung, and Kook D. Pae.

"Surface modification of polytetrafluoroethylene by  $Ar^+$  irradiation for improved adhesion to other materials." *Journal of applied polymer science* 64, no. 10 (1997): 1913-1921.

## 5.2.23 AFM Investigations of Ripple Pattern Formation on Si and Ge using 100KeV Ar Ion Beam: A Comparative Study

<sup>a</sup>Indra Sulania, <sup>b</sup>Harpreet Sondhi, <sup>c</sup>Tanuj Kumar, <sup>d</sup>Sunil Ojha, <sup>e</sup>G R Umapathy, <sup>f</sup>Ambuj Mishra, <sup>g</sup>Ambuj Tripathi, <sup>h</sup>Richa Krishna and <sup>i</sup>D K Avasthi

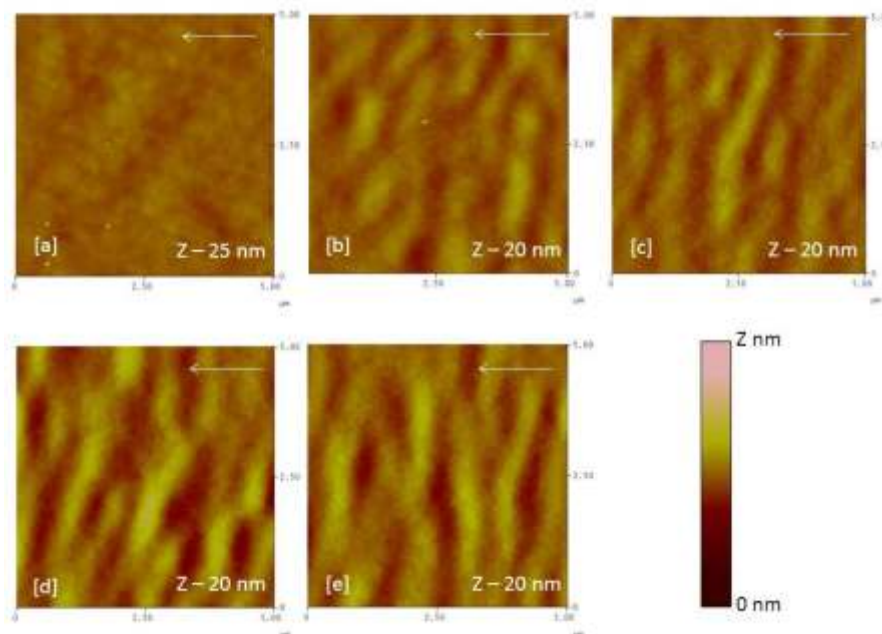
<sup>a</sup>Inter University Accelerator Centre, Aruna Asaf Ali Marg, New Delhi 110067, India

<sup>b</sup>Amity Institute of Nanotechnology, Amity University, Noida 201303, India

<sup>c</sup>Katholieke University, Faculty of Engineering Science, Leuven 3000, Belgium

<sup>d</sup>Central University of Jammu, TAB, Sainik Colony, Jammu 180011, India

Modifications of surface topography at nanoscale can be achieved using low and medium energy ion beams irradiation. In the present work, a comprehensive study of self-organized ripple pattern formation on Si(100) and Ge(100) using 100keV  $Ar^+$  ion beam is discussed. The irradiation has been carried out in the ion fluence range of  $\sim 3 \times 10^{17}$  to  $9 \times 10^{17}$  ions/cm<sup>2</sup> incident at  $\sim 60^\circ$  with respect to surface normal. The investigation focuses on the morphological studies of the pattern formed using Atomic Force Microscope (AFM). The results reveal the formation of ripple pattern on both the surfaces which are going perpendicular to the direction of the beam. The wavelength of patterns is found to increase from 400 to 710 nm for Si and becomes uniform with ion fluence.



AFM images of Si surfaces irradiated with Ar<sup>+</sup> ion beam: (a) Pristine (b)  $3 \times 10^{17}$  ions/cm<sup>2</sup>, (c)  $5 \times 10^{17}$  ions/cm<sup>2</sup> (d)  $7 \times 10^{17}$  ions/cm<sup>2</sup>, (e)  $9 \times 10^{17}$  ions/cm<sup>2</sup>.

The AFM image shows the surface of the Si substrate before erosion (a). The rms roughness  $Rq$  is approx. 0.5 nm. After 60° incidence irradiation, figure (b-e) shows some correlated surface structures with a surface roughness of  $Rq = 1.0$  nm as calculated. Although, the earlier reports suggested that Ge (not shown here) is resistant to structural changes for Ar<sup>+</sup> ion irradiation, but in present case, ripple pattern at fewer spots are observed which are not too regular in shape.

#### **5.2.24 Defect mediated modification of structural, optical and magnetic properties of Xe<sup>3+</sup> ions irradiated GaN/sapphire films**

Singh Preetam<sup>1</sup>, Ghosh Santanu<sup>1,\*</sup>, Singh Arvind<sup>1</sup>, Kumar Sunil<sup>1</sup>, Ojha Sunil<sup>2</sup> and Srivastava Pankaj<sup>1</sup>

<sup>1</sup>Department of Physics, Indian Institute of Technology Delhi, New Delhi-110016, India

<sup>2</sup>Inter University Accelerator Centre, Aruna Asaf Ali Marg, New Delhi, 110067, India

Several ion-irradiation studies revealed that GaN exhibits a range of intriguing behavior involving extreme property changes under ion beam irradiation. Its electronic transport, optical and magnetic properties can be tuned by modifying the nature and position of energy levels corresponding to point and/or extended defects. For example, ferromagnetic properties in GaN is attributed to Ga vacancies. Optical properties of GaN can also be tuned by defects and defect complexes. Ion-generated point defects ( $V_{Ga}$ ,  $V_N$ ,  $Ga_i$  and  $N_i$ ), which survive after quenching of collision cascades, may migrate through the lattice and experience annihilation and/or cluster formation. It has been shown that the dynamic annealing process (i.e. defects interaction processes) in GaN is extremely efficient even during heavy ion bombardment. Firstly, it was reported by Tan et. al. that GaN exhibit a very efficient dynamic annealing during bombardment with 90 keV Si ions at liquid nitrogen temperature. Further studies of damage processes in GaN have confirmed the presence of a very efficient dynamic annealing in GaN under wide range of implantation conditions.

Procured GaN films (~5 μm) have been irradiated at two different fluences  $1 \times 10^{16}$  and  $5 \times 10^{16}$  ions-cm<sup>-2</sup> and the as deposited and irradiated films will be abbreviated as S1, S2 and S3 respectively. Room temperature (RT) PL spectra of the S1, S2 and S3 films are shown in Figure below. The results for the S1 film in Figure (a) shows two distinct peaks, the narrow one centered at ~3.4 eV is attributed to the free excitonic emission or near band edge (NBE) emission of the electron from the conduction band to valence band of GaN and the second and much broader YL peak centered between 2.2 and 2.3 eV is a point of debate for quite some time. It is a typical signature of GaN films. Most of the reports attribute it to  $V_{Ga}$ -related defects or carbon related defects. Earlier, some theoretical calculations predicted that the YL was favored by VGa defects or  $V_{Ga}O_N$  related complexes. Recent calculations suggest that it is caused by an isolated carbon defect ( $C_N$ ) or  $C_NO_N$  complex. Si impurities along with  $V_{Ga}$ -related defects can also be one of the reasons of YL. Armitage et. al. have reported that YL in C-doped GaN is due to C when carbon concentration is quite high in comparison to  $V_{Ga}$  ( $[C] = 2 \times 10^{18}$  cm<sup>-3</sup> and  $[V_{Ga}] < 1 \times 10^{16}$  cm<sup>-3</sup>) and in undoped GaN, it is due to  $V_{Ga}$  when  $[C] = 6 \times 10^{16}$  cm<sup>-3</sup> and  $VGa > 1 \times 10^{17}$  cm<sup>-3</sup>. So, it is difficult to ascertain the origin of YL that it is due to the VGa-related point defects or defect complexes with unintentional impurities (like C and O). In the present case, YL can be assigned to  $V_{Ga}$  or the unintentional impurity complexes with point defects of GaN as large Ga and N related point defects are formed after irradiation. In the present case, we have considered a band model (to explain our PL result) similar to that proposed by Toshio Ogino et. al. shown in Figure (d). The Ga deficiency or  $V_{Ga}$  in the S1 film acts like an acceptor-like defect and a compensating center. The 2-/3-, 1-/2- and 0/1- transition levels of VGa are estimated to be 1.1, 0.64 and 0.25 eV respectively. Slightly higher related values of 1.5, 1.0 and 0.5 eV are reported elsewhere. The 3- state of the  $V_{Ga}$  is most probable having the minimum vacancy formation energy and the YL (~2.2-2.3 eV) is due to the transition of an electron from the conduction band to 3-/2- level of  $V_{Ga}$  as depicted in Figure (d). Figure (b) shows the PL spectrum of the S2 film. Along with the broad YL peak, one more peak centered at ~3.06 eV can also be seen. The excitonic peak at ~3.27 eV is slightly red-shifted as compared to that in the S1 film. The broad peak is deconvoluted into three different peaks centered at ~2.09, 2.3 and 2.65 eV. The peak at 2.3 eV is due to the transition of electrons from the conduction band to  $V_{Ga}$  level. Ion irradiation of GaN facilitates the formation of nitrogen vacancy ( $V_N$ ) along with Gallium vacancy ( $V_{Ga}$ ). The creation of N deficiencies, i.e.,  $V_N$  is more probable than the  $V_{Ga}$  due to higher formation energy for the latter.  $V_N$  acts as a donor level just below the conduction band and it was shown that the n-type conductivity in GaN is accredited to  $V_N$ . In this framework, an electron from the resonance state 0/1-, located at ~2.7 eV above the valence band, would auto ionize to the bottom of the conduction band giving rise to n-type conductivity. So, the emission peak at ~2.65 eV can be assigned to the transition of electron from the 0/1- level to the valence band and the peak at ~2.09 eV is attributed to the donor-acceptor pair (DAP) recombination

as indicated in Figure (d). The peak at 3.06 eV can be associated with basal plane stacking faults or the recombination of excitons bound to prismatic stacking faults and the peak at 3.27 eV can be assigned to the transition of electron from continuum level (large no. of defect states just below the conduction band, behaving like a continuum level, -have been created due to the ion beam irradiation) to the valence band maxima. The PL spectrum of the S3 film (shown in Figure (c)) is similar to that of the S2 film with the maximum energy peak slightly shifted to 3.4 eV with comparatively lower intensity in comparison to the S1 film.

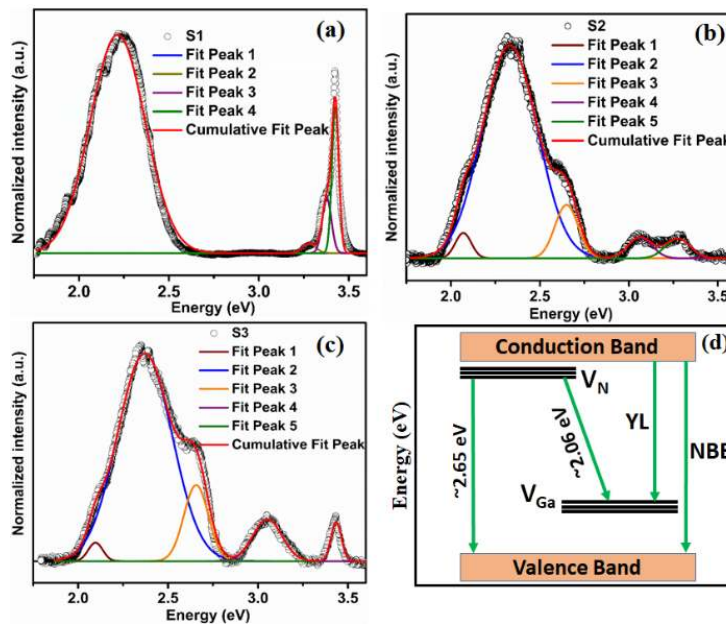


**Figure:** Room temperature PL spectra of (a) S1, (b) S2 and (c) S3 films and (d) the schematic of the band structure showing different transitions.

#### Reference:

1. B. Roul, M. K. Rajpalke, T. N. Bhat, M. Kumar, A. T. Kalghatgi, S. B. Krupanidhi, N. Kumar, and A. Sundaresan, Appl. Phys. Lett. **99**, 162512 (2011).

### 5.2.25 Phase transformation and photoluminescence study of low energy keV Kr<sup>5+</sup> ions irradiated ZrO<sub>2</sub> thin films

Vishnu Chauhan<sup>1</sup>, F. Singh<sup>2</sup> and Rajesh Kumar<sup>1\*</sup>

<sup>1</sup>University School of Basic and Applied Sciences  
Guru Gobind Singh Indraprastha University, New Delhi–110078, India.

<sup>2</sup>Inter University Accelerator Centre, Aruna Asaf Ali Road, New Delhi–110067, India  
\*E-mail: kumarrpi@gmail.com

Here, X-ray diffraction (XRD) and Photoluminescence (PL) analysis were done to understand the influence of low energy ion beam irradiation on structural changes in RF deposited zirconium oxide thin films. ZrO<sub>2</sub> thin films were irradiated by 800 keV Kr<sup>5+</sup> with varying fluences at IUAC, New Delhi, India. Fig.1. depicts the XRD patterns of ZrO<sub>2</sub> thin films of pristine and irradiated samples at fluence 1E16 ions.cm<sup>-2</sup> and 1E17 ions.cm<sup>-2</sup>. The peaks obtained at peak position (38.4°), (43.7°) (44.6°) and (65.1°) confirm the presence of monoclinic phase [1]. Further, the peaks obtained at position (30.26°) and (50.8°) confirm the presence of tetragonal phase (JCPDs #50-1089) [2]. The peak observed at (29.4°) also affirms the tetragonal phase. Careful observations of XRD pattern shows that the peaks at peak position of (36°), (39.26°), (47.3°), (48.3°) and (57.3°) also corresponds to presence of monoclinic phase (JCPDs #70-2491). At lower angle, the decrease in the peak intensity with the fluence may be due to the generations of defects and dislocations or splitting of grains with the ion fluence [3]. It is worth mentioning that the new peaks were formed at (59.9°) and (35°) corresponds to the tetragonal phase. The enhancement in new peaks intensity presents the clear proof of the small fraction of the material has transformed from monoclinic to tetragonal phase [4]. Crystallite size (D) of the both the phase i.e. monoclinic (38.4°) and tetragonal (30.26°) of ZrO<sub>2</sub> pristine and irradiated samples were calculated using the Debye - Scherrer formula [2].

$$D = \frac{k\lambda}{\beta \cos \theta} \quad (1)$$

The crystallite size for monoclinic phase was found to be 29.90 nm, 35.01 nm and 36.73 nm for pristine and irradiated sample at 1E16 and 1E17 ions.cm<sup>-2</sup> respectively. Further, the crystallite size of tetragonal phase was found to be 25.85 nm, 18.34 nm and 27.02 nm for pristine and irradiated samples. The increase in crystalline size can be attributed to increase in the density of defects which leads to an increase in density of nucleation center.

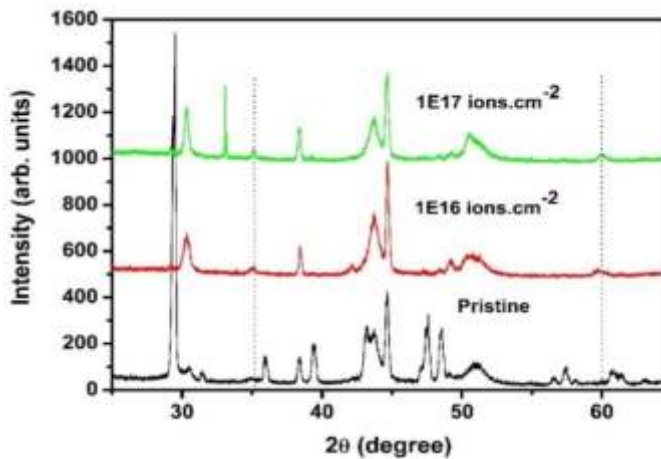


Fig. 1. XRD spectra of pristine and  $\text{Kr}^{5+}$  ion irradiated  $\text{ZrO}_2$  thin films [Ref.1]

Fig. 2. Shows the photoluminescence emission spectra of pristine and irradiated sample at  $1\text{E}16$  and  $1\text{E}17 \text{ ions.cm}^{-2}$  deposited on glass substrate. Two broad emission bands were determined at 350 nm and 430 nm in range of 320-550 nm when excited with wavelength of 290 nm. The determined peaks attributed to ultra-violet (UV) emission and formation of Zr vacancies due to free-exciton recombination respectively. At lower fluence  $1\text{E}16 \text{ ions.cm}^{-2}$ , the increase in peak intensity (at 350 nm) as compared to pristine sample can be ascribed to increase in defects concentration cause by Kr ion irradiation. While at higher fluence  $1\text{E}17 \text{ ions.cm}^{-2}$ , the decrease in intensity might be cause of annihilation of primary defects and formation of new defects [5]. Further, two shoulder peaks obtained at 335 nm and 383 nm are in good agreement with the  $\text{ZrO}_2$  nanoparticles [6].

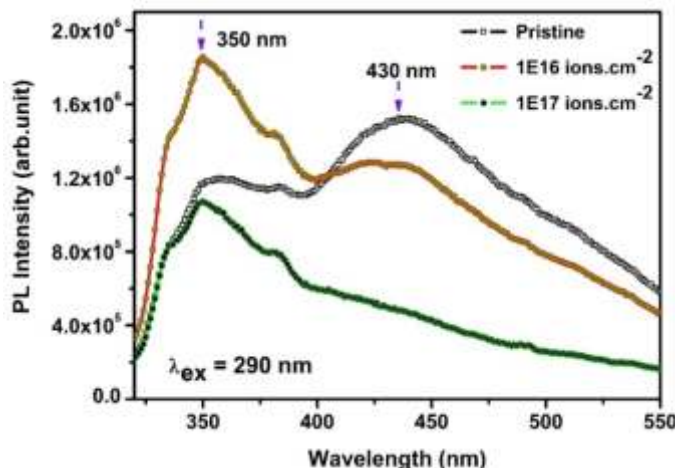


Fig. 2. (a) PL emission spectra of pristine and irradiated thin films at different fluence [Ref. 1].

#### References

- [1] V. Chauhan, R. Kumar, Phase transformation and modifications in high-k  $\text{ZrO}_2$  nanocrystalline thin films by low energy  $\text{Kr}^{5+}$  ion beam irradiation, Mater. Chem. Phys. 240 (2020) 122127.
- [2] K. Prabakar, A. Park, N. Cho, W.I. Lee, C.K. Hwangbo, J.G. Lee, et al. RF-Magnetron sputter deposited  $\text{ZrO}_2$  dielectrics for metal-insulator-semiconductor capacitors. Vacuum 82 (2008) 1367–70.
- [3] Y.S. Chaudhary, S.A. Khan, R. Shrivastav, A study on 170 MeV  $\text{Au}^{13+}$  irradiation induced modifications in structural and photoelectrochemical behavior of nanostructured CuO thin films, 225 (2004) 291–6.
- [4] P. Balasaritha, S. Amirthapandian, P. Magudapathy, R.M. Sarguna, S.K. Srivastava, Ion beam induced phase transformation and krypton bubble formation in monoclinic zirconium oxide, J. Nucl. Mater. 508 (2018) 385–394.
- [5] K. R. Nagabhushana, B.N. Lakshminarasappa, D. Revannasiddaiah, Singh F. Luminescence studies on swift heavy ion irradiated nanocrystalline aluminum oxide. J. Lumin 131 (2011) 764–767.
- [6] A. Emeline, G. V. Kataeva et al. Spectroscopic and Photoluminescence Studies of a Wide Band Gap Insulating Material: Powdered and Colloidal  $\text{ZrO}_2$  Sols. Langmuir 14 (1998) 5011–5022.

### 5.2.26 Electrical and optical properties of Zinc- and Strontium-Stannate thin films

Yogesh Kumar<sup>1</sup>, Ravi Kumar<sup>2</sup>, K Asokan<sup>3</sup> and A P Singh<sup>1</sup>

<sup>1</sup>Department of Physics, Dr. B. R. Ambedkar National Institute of Technology, Jalandhar-144011.

<sup>2</sup>Centre for Material Science and Engineering, National Institute of Technology, Hamirpur-177005.

<sup>3</sup>Inter-University Accelerator Centre, New Delhi-110067.

Perovskite-structured materials are the most technologically important materials in this era because of their large range of physical properties [1]. In the present study, we proposed two wide-bandgap perovskite materials, zinc stannate ( $ZnSnO_3$ ) and strontium ( $SrSnO_3$ ) stannate, for optoelectronic applications. Swift heavy ion (SHI) irradiation have been used to modify the structural and other physical properties of the materials [2]. These thin films were irradiated with 120 MeV  $Ag^{9+}$  ions at the fluence of  $2 \times 10^{12}$  ions/cm<sup>2</sup> using a 15UD tandem pelletron accelerator. The temperature-dependent resistivity for pristine and irradiated thin films was studied in the range from 100 K to 300 K using Keithley make electrometer model 6517B based system with two probe method at IUAC. The Rutherford backscattering spectrometry (RBS) was used to calculate thin film thickness using 5SDH-2 MV Tandem accelerators at Pelletron Accelerator for RBS-AMS System (PARAS) at IUAC, Delhi. The manuscripts related to work accomplished at IUAC are under preparation.

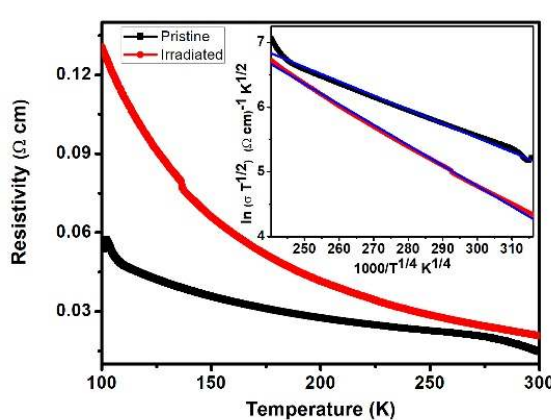


FIGURE 1 Temperature dependence of the resistivity for pristine and irradiated Zn-Sn-O thin films. Inset of figure shows the plots of  $\ln \sigma T^{1/2}$  against  $1000/T^{1/4}$  [2].

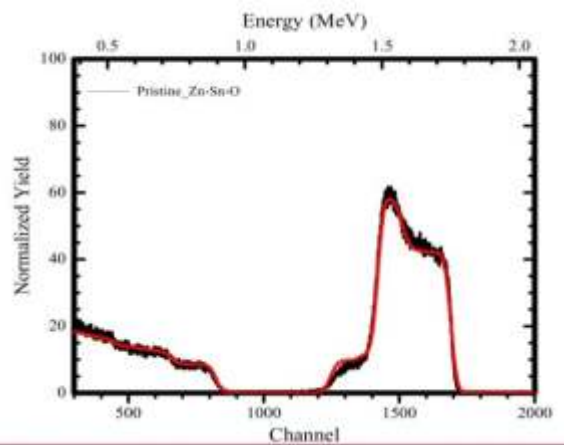


FIGURE 2 Representation of RBS spectrum (black color) and simulation of RBS data (red color) of pristine.

#### References

- [1] Y. Kumar, R. Kumar, R.J. Choudhary, A. Thakur, A.P. Singh. Reduction in the tilting of oxygen octahedron and its effect on bandgap with La doping in  $SrSnO_3$ . Accepted for publication in Ceramics International.
- [2] Y Kumar, R Kumar, K Asokan, and A P Singh. Effect of swift heavy ion irradiation on structural, electrical and optical properties of zinc-stannate thin films. AIP Conference Proceedings, 2142(1):080004, 2019. doi: 10.1063/1.5122432.

### 5.2.27 Effect of annealing on the magnetic properties of FeCo thin films

Garima Vashisht<sup>1</sup>, Indra Sulanja<sup>2</sup> and S. Annapoorni<sup>1</sup>

<sup>1</sup>Department of Physics and Astrophysics, University of Delhi, Delhi, India

<sup>2</sup>Inter-University Accelerator Centre, Aruna Asaf Ali Marg, New Delhi, India

FeCo thin films were deposited on Si <1 0 0> substrate by RF magnetron sputtering using equiatomic FeCo alloy target. Comparison study of two different thicknesses (80 nm and 800 nm) was performed in order to study the properties of bulk FeCo and its thin film form. The films were annealed at different temperatures (400 °C, 600 °C and 800 °C) in the presence of Ar (95%) + H<sub>2</sub> (5%) to reduce the possible oxides. No other impurity phases were observed for as prepared samples and for the samples annealed at 400 °C and 600 °C as per XRD analysis. On further annealing beyond 800 °C, formation of complex silicides due to the diffusion into the substrate was confirmed. The hysteresis measurements show that the magnetization of thinner samples (Fig 1(a)) increases on annealing while the thicker sample (Fig 2(a)) maintains the magnetisation. All the samples annealed at different temperatures of both the thinner and thicker series showed low coercivity ~ 100 Oe when the magnetic field is applied parallel to the film plane. Moreover, when the magnetic field is applied perpendicular to the film plane, the coercivity remains the same for as prepared FeCo of thickness ~ 80 nm and for the same annealed at 400 °C. However, the thinner films annealed at 600 °C shows a high coercivity of 1100 Oe in out-plane configuration due to large number of pinning centres created due to annealing.

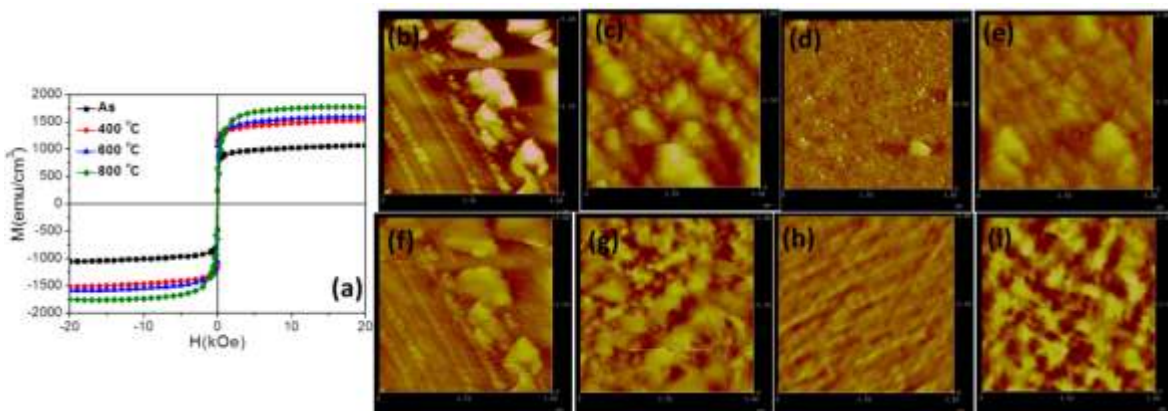


Figure 1. (a) Hysteresis loop of 80 nm FeCo and AFM images of FeCo films with 80 nm thickness (b) as prepared and annealed at (c) 400 °C (d) 600 °C (e) 800 °C and the corresponding MFM images of (f) as prepared and annealed at (g) 400 °C (h) 600 °C (i) 800 °C.

Atomic/Magnetic Force Microscopy (AFM/MFM) measurements were performed to further relate the grains with the domain structure of these films and explain the pinning effects. The topography images using AFM shows that the thicker films of 800 nm thickness are composed of smaller grains as compared to the thinner films of 80 nm. FeCo films of thickness 80 nm provided with no thermal treatment (fig. 1(b)) shows a continuous film with irregular lumps of FeCo distributed non-uniformly over the substrate. On annealing the film at 400 °C (fig. 1(c)), the granular structure was observed with grain size 105 nm. On further increasing the annealing temperature to 600 °C causes dewetting of the film resulting in its reduced roughness shown in fig. 1(d). The particles again agglomerate to form large grains of size 99 nm when the annealing temperature was further increased to 800 °C (fig. 1(e)). The magnetic mapping of these samples was performed using MFM in tapping mode with cantilever tip maintained at height 40 nm. The as prepared FeCo with 80 nm film thickness does not show a difference in the topography and phase images due to low magnetization in this film (fig. 1(f)). The thermal treatment at higher temperatures shows the magnetic contrast different from the topography. The oppositely oriented domains show a phase shift of 2° in the MFM images. Large domains with 400 nm width and several micrometres in length were observed for FeCo films with thickness 80 nm annealed at 400 °C (fig. 1(g)). The dewetting process occurred at annealing at 600 °C causes the formation of stripe-like domains shown in fig. 1(h). Further increasing the annealing temperature to 800 °C, results in the formation of domains with sizes ~300 nm, which is smaller than those obtained at lower annealing temperature (fig. 1(i)). This can be attributed to the formation of silicides which acts as pinning centres in the magnetization reversal process.

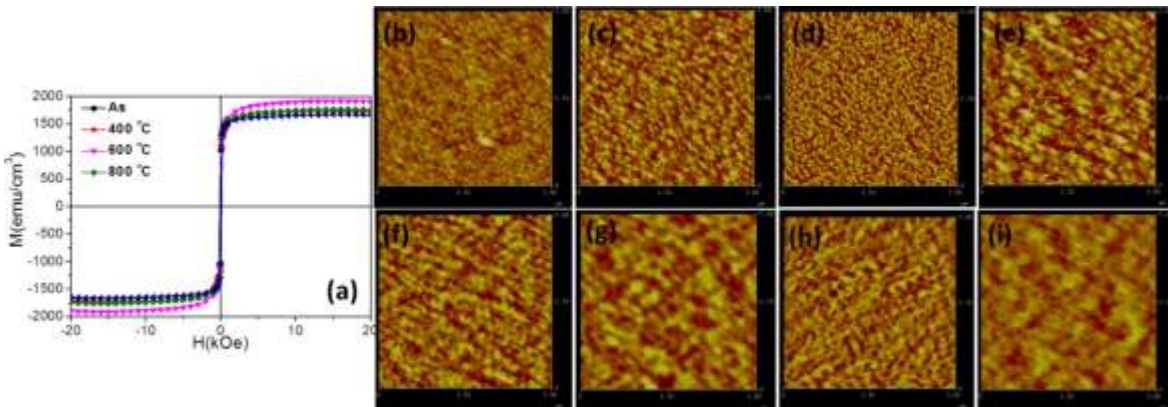


Figure 2. AFM images of FeCo films with 800 nm thickness (a) as prepared and annealed at (b) 400 °C (c) 600 °C (d) 800 °C and the corresponding MFM images of (e) as prepared and annealed at (f) 400 °C (g) 600 °C (h) 800 °C.

Similar trends are obtained in the thicker films of 800 nm thickness. The grain size of as prepared FeCo films with 800 nm thickness and those annealed at 400 °C, 600 °C and 800 °C is 67 nm, 97 nm, 120 nm and 130 nm respectively (fig. 2(a)-(d)). The domain sizes of the same also increases from 215 nm to 498 nm for as prepared to FeCo films annealed at 800 °C (fig. 2 (e)-(f)). It is worth mentioning that the domain size at 600 °C is found to be 160 nm (fig. 2 (g)). This is the temperature when dewetting occurs at film-substrate interface. However, due to the higher thickness of these films, complete dewetting does not takes place giving rise to the granular structure on the surface of the thicker films.

Hence, a comparative study was made to study the effects of annealing at different temperatures for FeCo thin films of 80 nm and 800 nm thickness. The magnetization and MFM studies reveal the presence of pinning centres after annealing. The effect of pinning centres created by ion beam irradiation would be further investigated (BTR Number: 64521) and the MFM's will be compared.

### 5.2.28 Development of Thin film Solar cells: Experimental and Theoretical Approach

Ramphal Sharmaetal

Department of Physics, Dr. Babasaheb Ambedkar Marathwada University, Aurangabad 413 004. Maharashtra, India.

**Development of organic/inorganic PANI/ZnO 1D nanostructured hybrid thin film solar cell by soft chemical route:** The ultrafast photo induced charge carrier transfer by 1D nanorods morphology of ZnO was obtained by soft chemical route providing high throughput and low-cost device production. The 1D ZnO nanorods thin films with c-axis oriented growth of ZnO showed decrease in length on annealing at 300 °C, which further changed the morphology and surface defects. The fabricated hybrid solar cell viz. PANI/pristine ZnO showed ~ 80% a higher efficiency than PANI/annealed ZnO due to the change in morphology as well as increased inter-particle junctions after annealing. Thus the study provides a possibility of further improvement in PANI/ZnO hybrid solar cell using 1D morphology.

**Theoretical and experimental study of bandgap modification of Mg-doped ZnS thin films:** ZnS and Mg-ZnS thin films were successfully grown by simple chemical bath deposition. The motivation for synthesis method is that it is economic, easy to handle, and low temperature. A sensible blue-shift in the band gap is achieved for Mg-ZnS. UV-Visible spectrophotometry confirms the blue-shift in the bandgap energy of Mg-ZnS as compared to intrinsic ZnS that can be used in many optoelectronic device applications. The computational results was performed by Medea VASP confirms the blue shift (increasing) bandgap which supports the experimentally determined results.

**Influence of annealing on chemically grown PbS thin films and its DFT study:** Through first-principles calculations, the structural and optoelectronic properties of FCC-PbS have been studied. These results have been correlated with the experimental results. The as-synthesized samples were annealed at 150 °C for 2 hr resulted in an increase in average crystallite size as well as x-ray peak intensity. These structural transformations further resulted in recrystallization of NC's which were confirmed by Raman analysis. FESEM micrograph confirms the random growth of NC's on the entire surface of the thin film. Also, PbS NC's thin-film revealed higher absorbance in the near-infrared (NIR) region and energy bandgap of ~1.59 and 1.61 eV for as-synthesized and annealed films respectively. The J-V graph shows a decrease in photocurrent when the solar simulator lamp light of 100 Watt intensity is incident on samples. Therefore, PbS NC's would be used for the development of the next-generation optoelectronic application and an efficient absorber layer for Solar cells.

#### Reference:

- [1] A. S. Dive *et al.*, Theoretical And Experimental Study of Bandgap Modification of Mg-Doped Zns Thin Films. *Review Of Research* Volume 1, (2019).
- [2] R. Sharma, A. Dive, S. H. Han, Influence of annealing on chemically grown PbS thin films and its DFT study. *AIP Conference Proceedings*, (2019).

## 5.3 RADIATION BIOLOGY

### 5.3.1 Study of DNA damage response pathway of A549 cells treated with carbon ion in presence of PARP-1 inhibitor

Payal Dey<sup>a</sup>, Sourav Ghosh<sup>a</sup>, Asitikantha Sarma<sup>b</sup> and Utpal Ghosh

<sup>a</sup>Department of Biochemistry & Biophysics, University of Kalyani, Kalyani, Nadia, West Bengal, PIN- 741235

<sup>b</sup>Inter-University Accelerator Center, New Delhi, Delhi -110067

Carbon ion radiotherapy is becoming very promising although detailed cellular response after 12C ion exposure is largely unknown. We have found that carbon ion beam is more lethal than gamma and radio-sensitivity was enhanced upon knocking down of PARP-1 gene. 12C produces double strand breaks which are more deleterious to the cells than single strand breaks if they remain unrepaired. In mammalian system, there are basically two pathways for DSB repair namely classical non-homologous end-joining (C-NHEJ) and homologous recombination (HR). Ku70/80 heterodimer plays a crucial role by binding to the site of DSBs and initiates repair process through NHEJ pathway. On the other hand, HR pathway is activated by MRN complex. The role of PARP-1 in cluster DNA damage is largely unknown. Our aim was to investigate role of PARP-1 in DNA repair after cluster DNA damage. We checked expression of various repair proteins in a time-dependent manner after treatment with C-ion and olaparib (PARP-1 inhibitor). With time the expression of repair proteins decreased. The data is shown in Fig 1.

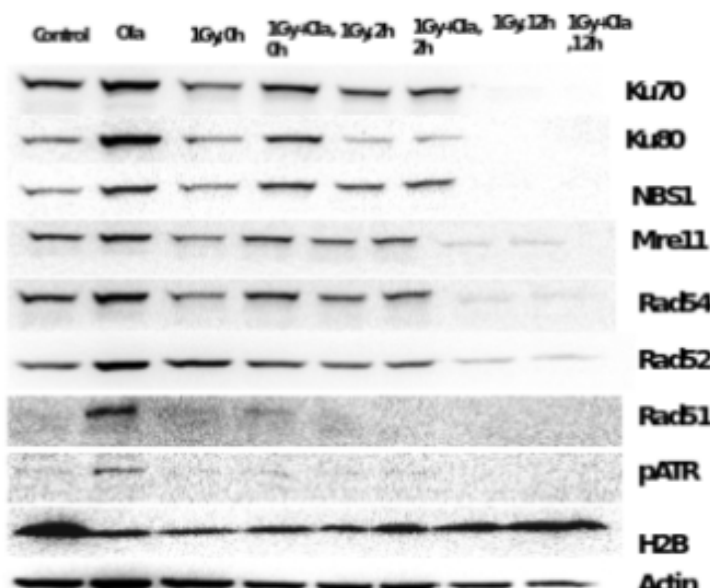


Fig 1. Expression of various repair proteins after 2 h and 12 h exposure with C12 in presence and absence of olaparib in A549 cells.

#### References:

- Ghorai, A., Bhattacharyya, N. P., Sarma, A. & Ghosh, U. Radiosensitivity and Induction of Apoptosis by High LET Carbon Ion Beam and Low LET Gamma Radiation: A Comparative Study. *Scientifica* (Cairo). **2014**, 1–10 (2014).

## 5.4 ACCELERATOR MASS SPECTROMETRY

### 5.4.1 Late Holocene Climate from the Central Ganga Plain, Sultanpur, Uttar Pradesh

Singh Atul K.<sup>1,2</sup>, Kumar Pankaj<sup>2</sup>, Sharma Rajveer<sup>2</sup> and Jaiswal Manoj K.<sup>1</sup>

<sup>1</sup>Indian Institute of Science Education and Research Kolkata, West Bengal, 741246, India,

<sup>2</sup>Inter University Accelerator Centre, New Delhi, 110067, India

The samples were collected from a lake in the Central Ganga Plain (CGP). Lake sediments are a good proxy for understanding the paleo-climate changes in the region because the source of sediments are from nearby places only. A total of 14 samples were collected for carbon dating using the Accelerator Mass Spectrometry (AMS) facility at IUAC, New Delhi. Samples were also collected for geochemical analysis, oxygen and carbon isotope measurements and grain size analysis. All of these proxies are helpful in estimating the palaeo-climatic conditions in which the deposition of the sediment took place. It was observed that the age of top-most sample was ~6,000 BP, this date should have been of recent times. The dates range from ~6,000-20,000 BP and are

difficult to correlate with the past climatic events of the region. The dates are significant because they pose a challenge to understand the geological phenomenon which are responsible for the deposition of the sediments and how the sedimentation rate control the depositional ages of the sample. A lot of work needs to be done in this direction.

#### **5.4.2 Reconstruction of the past climatic and sea level changes during the Late-Quaternary**

Sarswat Rajeev<sup>1</sup>, Singh Dharmendra Pratap<sup>1</sup>, Kumar Pankaj<sup>2</sup>

<sup>1</sup>National Institute of Oceanography, Goa,

<sup>2</sup>Inter University Accelerator Centre, New Delhi, 11067, India

A total 20 foraminifera samples were analysed for radiocarbon dating using the accelerator mass spectrometer (AMS) facility at IUAC New Delhi. The radiocarbon data was used to establish chronology of the sediments, collected from the southeastern Arabian Sea. The proxy data was then used to reconstruct past climatic changes during different time intervals. The radiocarbon based chronology helped in inferring

- Precise timing of the deglaciation in the northern Indian Ocean.
- Strong influence of the northern Indian Ocean in deglaciation by modulating high northern latitudinal processes.
- The upwelling regions of the tropical oceans contribute a significant amount of carbon-dioxide to the atmosphere.

This radiocarbon based chronology is utilized in the PhD thesis of Dharmendra Pratap Singh awarded by Goa University.

#### **5.4.3 AMS radiocarbon dating of core sediment samples from Rann of Kachchh, Gujarat, western India**

Ram Fulmati<sup>1</sup>, Sarkar Anindya<sup>1</sup>, Kumar Pankaj<sup>2</sup>

<sup>1</sup>Department of Geology & Geophysics, Indian Institute of Technology, Kharagpur-721302, India.

<sup>2</sup>Inter-University Accelerator Centre, New Delhi-110067, India.

The evolution of Rann of Kachchh through Holocene has always intrigued researchers to dig down its evolutionary history as it may hold clues to the rise and decline of the well-known Harappan Civilization in the Indian Subcontinent. Although the Rann looks apparently monotonous, its landscape is shaped as a combined effect of land, sea and tectonic interactions especially during the Holocene. Decline of such an advanced human settlement has often been alluded to past climate shift. In spite of several geological studies, not much information as yet exists on the spatial and temporal relationship between the continental and marine processes occurring in this region during the Holocene. Contradictory hypothesis exist varying from the Rann being a marine gulf [1] and the decline of the Harappan Civilization occurred due to the withdrawal of the sea [1,2], to the changing summer monsoon intensities those drove the rise and abandonment of human settlements [3]. This study attempts to understand the palaeo-climatic and palaeo-environmental conditions of this region by using organic matter proxies in the Rann sediments.

Four sediment cores were raised from different parts of the Great Rann and Little Rann of Kachchh. Establishing a clear chronology of these cores is essential, since it will allow to anchor the age of the sediments across which the environmental signals and climatic events can be reconstructed through the Holocene. Also it will provide an idea on the timing of Rann sedimentation. For radiocarbon dating, the sediment samples were first oven dried at 60°C and crushed using agate mortar. Visible plant parts were physically removed during crushing. ~2 grams of the sediment samples were then subjected to Acid-Base-Acid (ABA) pretreatment in the IUAC Graphitization laboratory. 0.5M hydrochloric (HCl) acid and 0.1N sodium hydroxide (NaOH) solution were used for the ABA treatment. Treated samples were then graphitized and further used for carbon-14 measurements at IUAC using AMS facility.

The data obtained from the carbon-14 measurements will be used to establish (1) the chronology and sedimentation rate in the Rann and (2) to study and reconstruct the temporal changes in palaeoclimatic and palaeoenvironmental conditions by using bulk and compound specific stable carbon isotope ratios. The combined AMS <sup>14</sup>C and carbon isotope data will be used to establish the link or otherwise with the major Indus valley civilization sites of Kachchh.

#### **References:**

1. Gaur, A.S., Vora, K.H., Murali, S.R.M. and Jayakumar, S., 2013. Was the Rann of Kachchh navigable during the Harappan times (Mid-Holocene)? An archaeological perspective. *Current science*, pp.1485-1491.

2. Tyagi, A.K., Shukla, A.D., Bhushan, R., Thakker, P.S., Thakkar, M.G. and Juyal, N., 2012. Mid-Holocene sedimentation and landscape evolution in the western Great Rann of Kachchh, India. *Geomorphology*, 151, pp.89-98.
3. Ngangom, M., Bhandari, S., Thakkar, M.G., Shukla, A.D. and Juyal, N., 2017. Mid-Holocene extreme hydrological events in the eastern Great Rann of Kachchh, western India. *Quaternary International*, 443, pp.188-199.

#### **5.4.4 Radiocarbon dating using AMS of samples collected from Salona Lake, Central Ganga Plain**

Amir Mohd<sup>1</sup>, Paul Debajyoti<sup>1</sup>, Malik Javed<sup>1</sup>, and Kumar Pankaj<sup>2</sup>

<sup>1</sup>Department of Earth Sciences, Indian Institute of Technology Kanpur, Kanpur-208016, India.

<sup>2</sup>Inter-University Accelerator Centre, New Delhi-110067, India.

The present work was carried out by the Department of Earth Sciences, Indian Institute of Technology Kanpur in collaboration with IUAC, New Delhi. The focus of this work was to reconstruct paleoclimate and paleovegetation using the geochemical proxies of sediments collected from the Salona Lake (**26°10'05"N, 83°22'00"E**) situated in the Central Ganga Plain (CGP). The Indian Summer Monsoon (ISM) is the key factor controlling the socio-economic conditions of the people living in the Ganga Plain. Multi-proxy approach for paleoclimatic reconstruction from CGP is still sparse despite its great potential for assessing the vegetational changes, ecological fluctuations related to climate i.e., ISM. In order to achieve the complete temporal extent of the records to be generated from the lake, chronological constraints are needed. To establish a robust chronology of the lacustrine records, samples were dated for the bulk sediment organic carbon.

The samples were subjected to pretreatment in IUAC Graphitization laboratory. All the samples were processed using the standard acid-base-acid (0.5 N HCl and 0.1 N NaOH) method for removal of carbonates and humic acids. The organic carbon present in the sample was combusted in an elemental analyzer and the evolved CO<sub>2</sub> was purified and converted to graphite using an automated graphitization equipment (AGE). The <sup>14</sup>C/<sup>12</sup>C ratio was measured using a 500 kV Pelletron accelerator at the IUAC. All the samples have been analyzed and are under data reduction, hence the actual results in terms of dates are awaited.

#### **5.4.5 Report on Asurgarh Excavation, Odisha 2019-20**

Garnayak Dibishada B.<sup>1</sup>, Chopra Sundeepr<sup>2</sup>, Kumar Pankaj<sup>2</sup> and Sharma Rajveer<sup>2</sup>

<sup>1</sup>Archaeological Survey of India

<sup>2</sup>Inter University Accelerator Center, New Delhi

The Asurgarh fort in Kalahandi district of Odisha located (20° 14' 54" N; 83° 21' 8" E, MSL- 226m) on the right bank of the river Sandul, a tributary of the river Tel which in turn falls on the river Mahanadi. It is about 6km west of Narla Road Railway Station and about 2km north-east of Rupra Road Railway Station on the Raipur-Vizag Railway line. The fort is almost rectilinear in plan and covers an area of more than half square kilometer. It has massive earthen ramparts having 47m to 63m in width, 8m to 17m in height with four entrances, one in each direction and made of rammed rubble casing, *kankars* and mud with occasional brick facing at the entrances as evidence in the western gateway. On the eastern side of the fort there is an extensive lake known as Udaya-sagar, water from which may be used to fill up the moat or used by the resident of the fort. There was a moat on three sides of the fort- northern, eastern and southern whereas river Sandul, a tributary of the Tel, flowing on the western side of the fort serves as a natural moat.

The fort has legends and traditions associated with local folk lore. Locally the site is variously known as Asoka Gada and Asurgad (Asurgarh). Many believe that Asurgarh is a corrupt pronunciation of Asokagarh, named after King Asoka of the Mauryan dynasty who ruled over North India in the 3<sup>rd</sup> century B.C. According to few historian the site was an important center of Atavika people during 4<sup>th</sup>-5<sup>th</sup> century BCE and in the 4<sup>th</sup> Century C.E. it was under the sway of Vyaghrraraja of Mahakantara whom Samudragupta claimed to have defeated in the course of his South Indian campaign.

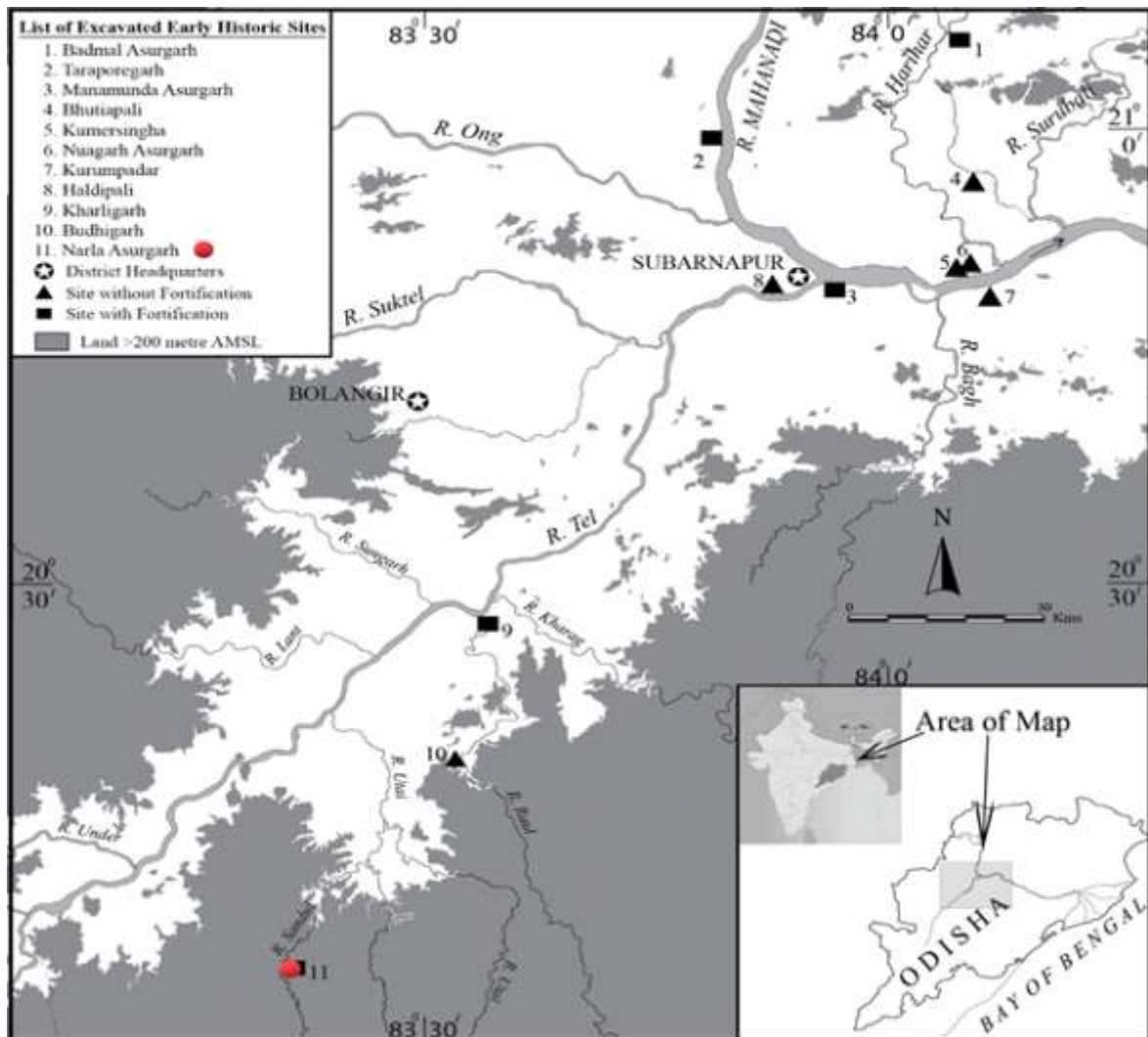
As per the licence granted by the Director General, Archaeological Survey of India, New Delhi, vide letter F.No. 17011/46/2018-EE, dated 9<sup>th</sup> October, 2018, the excavation Branch-IV, Bhubaneswar of the Archaeological Survey of India conducted excavation work at Asurgarh Fort in the field season 2018-19 under the direction of the first author.

The excavation yielded massive brick structures, stone paved roads, silver punch marked coins, silver and copper rings, large number of pottery and stone discs, beads of semiprecious stone; glass bangle pieces of different designs and colors, sling balls, pestle, iron equipment of both war and peace, ceramic assemblage in form of Black and Red ware, Black slipped ware, Red ware, Red slipped ware, and few painted sherds revealed in the lower strata during excavations. The material culture in the form beads and bangle in different shapes and color shows the artistic talent of the natives of that time. The findings of Coral beads and Imperial variety of

silver punch mark coins strongly indicates about long distant trade and association of hinterland people with seafaring people. The other significant discoveries of the site were terracotta sealings and terracotta ring well. The present season excavation shows that the site was inhabited by people since early Iron Age to early historic urban period which can be dated tentatively 600 BCE to 400 CE.

### Radiocarbon dating

The Charcoal samples have been collected from stratified layers and by taking proper procedure. Samples have been graphitized in the graphitization laboratory at IUAC, New Delhi. These samples will be measured using IUAC AMS facility. Results in terms of dates are awaited for further analysis of the historicity and antiquity of the site.



### 5.4.6 Radiocarbon dating using AMS of sediment samples from Kinnaur and Dehradun districts, Northwest Himalaya, India

Khan Firoz<sup>1,2</sup>, Meena N K<sup>2</sup>, Sundriyal Y.P.<sup>1</sup>, Sharma Rajveer<sup>3</sup>

<sup>1</sup>Department of Geology, HNB Garhwal University, Srinagar Garhwal, Uttarakhand -246174, India.

<sup>2</sup>Wadia Institute of Himalayan Geology, 33 GMS road Dehradun-248003, India.

<sup>3</sup>Inter-University Accelerator Centre, New Delhi-110067, India.

The present work was carried out by HNB Garhwal University, Srinagar Garhwal, Uttarakhand, India in collaboration with Wadia Institute of Himalayan Geology, Dehradun, Uttarakhand, India. The focus of this work was to establish Holocene climatic records using sediment samples from Himachal Pradesh and Uttarakhand then will correlate it with global climatic data. Samples have been collected from Kinnaur District, Himachal

Pradesh (31.3517°N, 78.4175°E & 31.3477°N, 78.4664°E) and Dehradun District, Uttarakhand (30.77°N, 77.83°E). Establishing a clear chronology of these sites is essential so that it will be helpful to reconstruct dry (cold) and wet (warm) climatic event of the Indian Summer Monsoon. Moreover, accurate dating of the site will also allow a clearer analysis of the environmental and climatic data available, allowing further reconstruction of Late Pleistocene environments during the Holocene in this country as well as globally. As per the literature, In the last millennium, the Indian Summer Monsoon (ISM) was strong during the Medieval Warm Period (MWP) now designated as Medieval Climate Anomaly (MCA) and Current Warm Period (CWP), punctuated by a weak phase during the Little Ice Age (LIA) and the Younger Dryas (YD). So we will correlate our  $^{14}\text{C}$  data (which was provided by IUAC after analysis of the samples) and proxies data with these events to know more accurately, which may be helpful to predict future climatic changes.

The sediment samples were pretreated using standard Acid-Base-Acid (ABA) pretreatment in IUAC Graphitization laboratory for  $^{14}\text{C}$  dating. Firstly, a batch of sediment samples was analysed to measure the percentage of organic carbon. After measurement of the organic carbon percentage, a known amount of sample was taken for the graphitization according to carbon present in the sample. Samples were graphitized using automated graphitization equipment (AGE) and produced graphites were measured using IUAC AMS facility by procedure described in following paper [1]. Measurement results were analysed using abc software and radiocarbon ages were calculated [1].

Currently, we are trying to calibrate and plot age-depth model of the  $^{14}\text{C}$  ages so that we compare these  $^{14}\text{C}$  ages with the TOC (Total organic carbon), Mineral magnetic, Isotopic data (carbon, nitrogen), diatoms and other proxies data to find out the correlation between past climatic phases and its variability.

#### References:

- Sharma, R., Umapathy, G.R., Kumar, P., Ojha, S., Gargari, S., Joshi, R., Chopra, S. and Kanjilal, D., 2019. AMS and upcoming geochronology facility at Inter University Accelerator Centre (IUAC), New Delhi, India. *Nuclear Instruments and Methods in Physics Research Section B: Beam Interactions with Materials and Atoms* 438 (2019) 124-130.

#### **5.4.7 Causes for the Decline of Indus Valley Civilization and Displacement in the period of 2350 BC – 1500 BC and those Impacts**

Esarapu Sai Krishna, P D Sabale, Shinde Vasant

*Department of Ancient Indian History, Culture and Archaeology, Deccan College Post Graduate and Research Institute, Deemed University, Pune.*

The present work is part of my PhD research work. For this different scholars based on the scientific research and data which they got and they are getting have postulated that the astronomical events such as asteroid or meteoritic or earth's magnetic field or sun's solar radiation have impacted or simultaneously of these events impacted the climate and played major role in the decline of Indus Valley and its contemporary Civilization during that time period.

So, according to archaeologists, historians, climatologists, geologists, geomorphologists, oceanographers, glaciologists, astronomers etc, too the above mentioned factors would have played major role in the decline of Indus Valley civilization. Therefore, one or two conditions would have triggered first and later other conditions would have followed in the fall of this great civilization and it also impacted the people as well as the society. Later, the Harappan's got displaced from the original locations and transformed from urban culture into rural culture with some urban aspects brought with them which they already know and used to some extent as per the available resources in the vicinity and intermixed peacefully with the other already present local people in those areas as they had good relations with them in the past.

Researcher would like to do C-14 dating in IUAC through AMS on the charcoal samples collected from the section of the Rakhigarhi site N 29°17', E 76° 06', situated in Hisar district of Haryana and Dholavira N 23° 53', E 70° 13' in Kachchh District of Gujarat which are Harappan sites. As I had analyzed some of the layers of the soil samples collected from those sections of the sites through geochemical for the presence of PGE (Platinum Group of Elements) and through petrography for the presence of well sorted spherules, as well as collected potsherds for studying the geomagnetism which falls under my selected time period for research in different scientific labs in India etc.

As the researcher also studying the displacement of the Indus valley civilization people especially to southern India if any that to in Telugu speaking states. Researcher had recently found new pre and proto historic sites in the forest area of Gundla Pochampally N 17°34' E 78°27', Medchal-Malkajigiri (earlier Ranga Reddy) District Telangana such as rock art sites and number of stone tools in which few rock art images are resembling with the Indus images which are present on Indus seals, also found burnt patch's on the surface of rock boulder near the

rock art site based on the observations the time period of that sites can be from 35000 BP to Early history and for that researcher would like to do C-14 dating on the collected samples from the burnt patch's on the rock boulder, pigments from the rock art site through AMS in IUAC and other scientific labs in India.

IUAC accepted the BTR-2 form for the Beam time for AMS dating of the seven samples and later the beam time scheduled, the research scholar had come and utilized the IUAC Lab and prepared the graphite of seven samples for the final stage of dating. The work is in progress and hence the actual results in terms of dates are awaited.

#### **5.4.8 Cosmogenic radionuclide dating using $^{10}\text{Be}$ from Thangu, Sikkim, eastern Himalaya, India**

Dubey Jyotsna<sup>\*1</sup>, Ali Nawaz S<sup>1</sup>, Kumar Pankaj<sup>2</sup>, Dhal Soumya<sup>2</sup>

<sup>1</sup>Birbal Sahni Institute of Palaeosciences, Lucknow-226007, India.

<sup>2</sup>Inter-University Accelerator Centre, New Delhi-110067, India.

The present work was carried out by Birbal Sahni Institute of Palaeosciences (BSIP), Lucknow in collaboration with Inter-University Accelerator Centre, New Delhi. The focus of this work was to establish the glacial chronology using CRN dating ( $^{10}\text{Be}$ ) in Thangu, north Sikkim, India. The samples have been collected from 27.892205 latitude and 88.536481 longitudes respectively. Defining the timing and extent of glaciation is important to understand the landscape evolution in glacial terrain. Moraines, an important glacial feature records the extent and timing of past glacial advances and retreat. Therefore, dating of such moraine sequences provides insights towards the sensitivity of glaciers to climate change. The Himalayas being the most dynamic, highest, youngest and tectonically active mountain belt exhibits an excellent record of glaciation. The timing and amplitude of paleoglaciations in Himalayan-Tibetan orogen is thus essential for understanding the past glacier dynamics and the forcing factors. Palaeoglaciations in the Himalayan region provide valuable information on the past climate variability and helps in understanding the glacier response to insolation driven Indian summer monsoon (ISM) and the mid-latitude westerlies driven moisture and low air temperature (Benn and Owen, 1998; Finkel et al., 2003; Yang et al., 2008).

The Sikkim Himalaya, an ISM dominated region, has preserved relict glacial landforms especially the moraines and provide an opportunity for understanding the response of glaciers to climate forcing and reconstructing the regional and global climatic changes during the late Quaternary. Hence, the present study aims at reconstructing the pattern of glaciation using moraine stratigraphy supported by Cosmogenic  $^{10}\text{Be}$  exposure dating to ascertain the glacial advance and retreat in Thangu, north Sikkim. The data thus generated would help in understanding the sensitivity of the valley glaciers of the north Himalaya, Sikkim and establish a relationship between glacier advance and its forcing factors which has wider implications for palaeoclimatic reconstructions.

16 samples were subjected to pretreatment in OSL lab of Birbal Sahni Institute of Palaeosciences, Lucknow and digestion of Quartz and removal of  $^{10}\text{Be}$  was done in AMS Chemistry lab, IUAC, New Delhi. Approximately 30 g pure quartz from each sample was taken in 250 ml PFA beaker. Doubled distilled HF and concentrated HNO<sub>3</sub> was used for complete digestion of Quartz. Each sample was picked up from beakers in diluted HCl and filtered using whatman No. 1 filter paper. Filtered samples were dried and then made up a volume up-to 10 ml using low normal HCl. 1 ml of the aliquot was kept for ICP-MS analysis for measurement of concentration of natural  $^9\text{Be}$  present in sample and appropriate carrier was added to rest 9 ml. Subsequently the sample was dried on hot plate and kept for column separation. Be was separated and purified using ion exchange chromatography. Be was precipitated as Be(OH)<sub>2</sub> using NH<sub>4</sub>OH at pH range 7-8. The precipitates were collected in quartz vials and heated in furnace. Temperature was increased gradually and finally fixed at 900° C. At this temperature Be(OH)<sub>2</sub> was converted to BeO which was further loaded to cathode with Nb powder in 1:3 ratios for AMS measurement. Total 12 samples were analyzed and ratio of  $^{10}\text{Be}/^9\text{Be}$  was obtained. Currently age calculation is in process and the results in terms of dates are awaited.

#### **References.**

1. Benn, D.I., Owen, L.A., 1998. The role of the Indian summer monsoon and the midlatitude westerlies in Himalayan glaciation: review and speculative discussion. *J. Geol. Soc.* 155, 353–363.
2. Finkel, R.C., Owen, L.A., Barnard, P.L., Caffee, M.W., 2003. Beryllium-10 dating of Mount Everest moraines indicates a strong monsoonal influence and glacial synchronicity throughout the Himalaya. *Geology* 31, 561–564.
3. Yang, B., Brauning, A., Dong, Z., Zhang, Z., Keqing, J., 2008. Late Holocene monsoonal temperate glacier fluctuations on the Tibetan Plateau. *Glob. Planet. Change* 60, 126–140.

#### **5.4.9 Radiocarbon dating using AMS of samples from Bundelkhand region of Central India.**

Singh Saurabh K<sup>1</sup>, Tripathi Jayant K<sup>1</sup> and Kumar Pankaj<sup>2</sup>

<sup>1</sup>School of environmental Sciences, Jawaharlal Nehru University, New Delhi-110067

<sup>2</sup>Inter-University Accelerator Center, New Delhi-110067

The present work was carried out by School of environmental Sciences, Jawaharlal Nehru University. The focus of this work was to establish a procedure to obtain reliable dates of different samples. Samples have been collected from depositional basins of Bundelkhand region, around the lat long - 25.00E, 79.00N. Establishing a clear chronology of this site is essential, since it will allow the finds to be put into a clear chronological context with respect to the appearance and disappearance of several key phenomenon. Moreover, accurate dating of the site will also allow a clearer analysis of the environmental and climatic data available, allowing further reconstruction of late Holocene in this country.

The samples were subjected to pretreatment in IUAC Graphitization laboratory. The samples were processed using the standard method as per protocol followed at IUAC for the radiocarbon age determination using deposited organic matter into basins. Samples were measured at IUAC using AMS facility.

#### **5.4.10 Appraisal of regional and local groundwater-surface water dynamics and residence time using ages determined by carbon-14 dating in parts of North-Western India**

Shekhar Shashank<sup>1</sup>, Sarkar Aditya<sup>2</sup>, Yadav Akhilesh Kumar<sup>1</sup>, Ali Shakir<sup>1</sup>, Kumar Pankaj<sup>3</sup>, Sharma Rajveer<sup>3</sup>

<sup>1</sup>Department of Geology, University of Delhi, Delhi-110007, India.

<sup>2</sup>Department of Geology, Presidency University, West Bengal-700073, India.

<sup>3</sup>Inter-University Accelerator Centre, New Delhi-110067, India.

This present work entitled “Appraisal of regional and local groundwater-surface water dynamics and residence time using ages determined by carbon-14 dating in parts of North-Western India” is being carried out by Department of Geology, University of Delhi in collaboration with IUAC, New Delhi. As of now samples have been processed and graphitization of each samples done. The samples were graphitized in IUAC Graphitization laboratory. Measurement of sample will be done at IUAC using AMS facility. C-14 dating of each sample is under process and the actual results in terms of dates are awaited.

Thirty groundwater samples collected during various fields and the calcareous nodules from various depths in Delhi were submitted for carbon-14 dating.

The samples were graphitized using carbonate handling system (CHS) in IUAC Graphitization laboratory. The groundwater samples were transferred into vials and flushed for nearly 10 minutes by inert gas He. Phosphoric acid was added in each vial using a syringe and heated at 85 - 90°C and produced CO<sub>2</sub> were transferred to the zeolite trap in automatic graphitization equipment (AGE). This CO<sub>2</sub> was reduced into graphite using hydrogen over iron powder in quartz tube at 580°C. For this purpose, in total 21 ml of each sample was required.

The calcareous nodules were first washed by deionized water until all dirt of the sample was removed. Afterwards, samples were given ultrasonic bath for complete removal of soils from the samples and then samples were dried completely in oven at 50°C. Next, the sample was crushed to a fine power and transferred into a vial and graphitized using AGE as described in case of ground water. These graphitized samples will be measured using 500 kV pelletron accelerator at IUAC. *The actual results in terms of dates are awaited.*

#### **5.4.11 Centennial and millennial scale climate and vegetation changes during Holocene in the Central-Western Himalaya**

Rawat Suman<sup>1</sup>, Sinha Anurag<sup>1</sup>, Kumar Pankaj<sup>2</sup>, Chopra Sundeep<sup>2</sup>

<sup>1</sup>Wadia Institute of Himalayan Geology, 33, G.M.S. Road, Dehradun – 248 001, India

<sup>2</sup>Inter-University Accelerator Centre, New Delhi-110067, India.

In the present study, multi proxy record (environmental magnetism, TOC % and grain size) has been generated from a 2.3 m long sedimentary profile from Chamoli Garhwal (named DSH) to understand the Indian summer monsoon variability during the Holocene. The sedimentary profile shows distinct seven charcoal layers at 5-8, 27-34, 39-42, 81-84, 91.5-92, 98.5-99, and 155-159 cm depth intervals. These dark black organic rich layers have been deposited due to rapid accumulation of organic matter in warm wet climatic conditions. The chronology of the sedimentary profile is established with 9 radiocarbon dates using the IUAC AMS facility. The

base sample of profile (at 230 cm depth) yields radiocarbon age of  $9761 \pm 110$  BP (~11,220 cal yr BP) indicating sediment record covers entire Indian summer monsoon history of Holocene period. The preliminary results based on the TOC %, environmental magnetism and grain size analysis indicate strengthened ISM during ~11220-8320 cal yr BP with maximum intensity during 8700-8320 cal yr BP. This strengthens ISM period corresponds to early Holocene monsoon maxima. Subsequently, from ~8320-5090 cal yr BP weakening of ISM strength is observed with intermittent warm-wet period between ~7060 and 6580 cal yr BP. From ~5090-2480 cal yr BP stable monsoon conditions were found and enhanced warm-wet conditions after ~2480 cal yr BP up to 1250 cal yr BP. The monsoon strengthen weakened from ~1250 to 520 cal yr BP. Modern improved monsoon conditions in the region was found after ~520 Cal yr BP. The detail climate interpretation for understanding the mechanism and causes for the change in ISM strength is in progress.

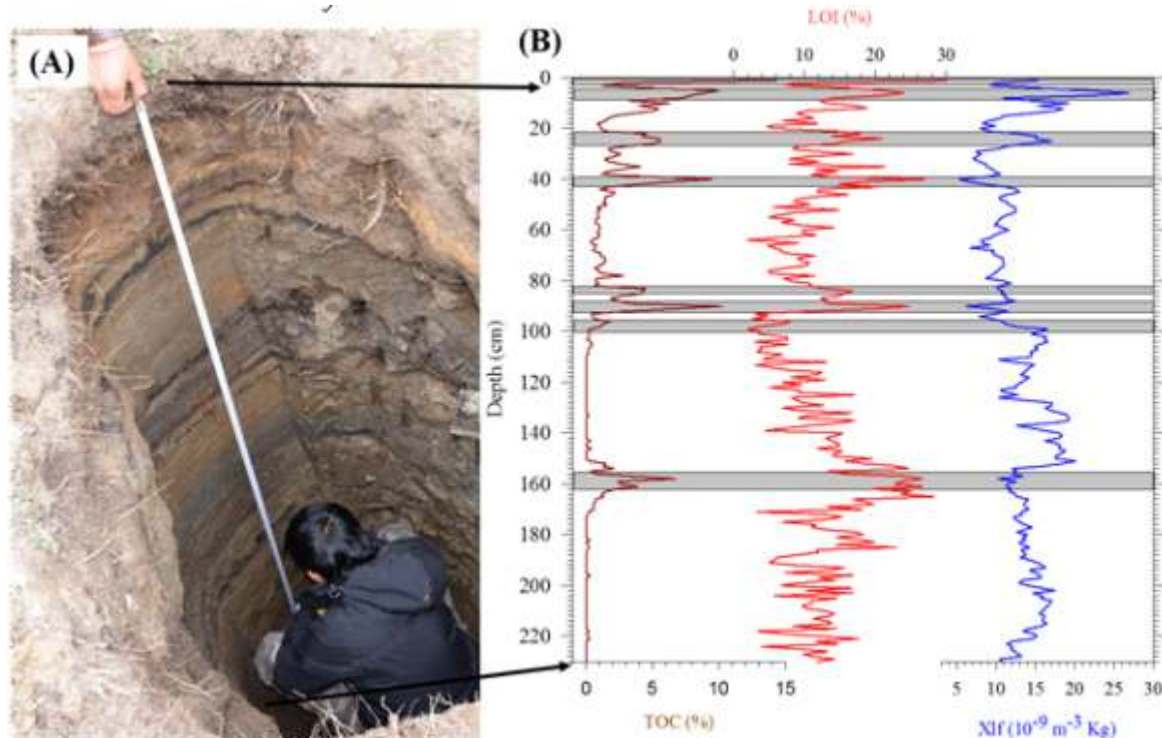


Figure 1. A) Field photograph of the DSH profile showing distinct lithological variations marked by charcoal and oxidised layers and B) Total organic Carbon, Loss on ignition and magnetic susceptibility results of the DSH profile.

#### 5.4.12 Radiocarbon dating using AMS, XRF and XRD of samples from River Yamuna

<sup>1</sup>Chopra Vivek, <sup>2</sup>Sharma Jai Gopal, <sup>3</sup>Singh Neelratan, <sup>4</sup>Kumar Pankaj, <sup>4</sup>Ojha Sunil, <sup>4</sup>Sharma Rajveer, <sup>4</sup>Khandelwal Deeksha

<sup>1</sup>PhD research scholar, Department of Biotechnology, Delhi-110007, Delhi Technological University, Delhi-110042 India.

<sup>2</sup>Professor & Head, Department of Biotechnology, Delhi Technological University, Delhi-110042 India.

<sup>4</sup>Inter University Accelerator Centre, New Delhi.

The present work was carried out by following institute in collaboration with another institute. The focus of this work was to establish a procedure to obtain reliable dates of different soil samples taken from river Yamuna bed. Samples have been collected from following location ( $28^{\circ}85'61.7''N$   $77^{\circ}20'80.2''E$  and  $28^{\circ}32'10.5''N$   $77^{\circ}19'29.6''E$ ) at river Yamuna in Delhi.

The samples were subjected to pretreatment in IUAC Graphitization laboratory. Samples were measured at IUAC using AMS facility. Soil samples compositions were also analyzed using XRF and XRD.

Aim of the study is to analyze the environmental conditions of river Yamuna in pre historic times by comparing the type of algal species found in soil samples compared to respective ages of the soil samples. The study helps in better understanding of our knowledge about river deposits and aquatic ecosystem hence it is significant in conservation studies.

#### References.

1. Ruwer, Daiane Trevisan, Marcelo Corrêa Bernardes, and Liliana Rodrigues. "Diatom Responses to Environmental Changes In the Upper Paraná River Floodplain (Brazil) During the Last ~1000 years." Journal of paleolimnology, v. 60, 4 pp. 543-551. doi: 10.1007/s10933-018-0039-7

#### **5.4.13 AMS $^{14}\text{C}$ Dating of samples from ocean and lake sediments for establishing chronology to see variability in the Indian monsoon system during the Holocene**

Gupta, Anil Kumar<sup>1,\*</sup>, Majumder, Jeet<sup>1</sup>, Kaushik, Arun<sup>1</sup>, Sengupta, Sreya<sup>1</sup>, Singh, Shweta<sup>2</sup>, Kumar, Pankaj<sup>3</sup>

<sup>1</sup>Department of Geology and Geophysics, Indian Institute of Technology Kharagpur, Kharagpur- 721302, India

<sup>2</sup>Wadia Institute of Himalayan Geology, 33 General Mahadeo Singh Road, Dehradun-248001, India

<sup>3</sup>Inter University Accelerator Center (IUAC), New Delhi.

The present work is being carried out by the research group of Prof. Anil K Gupta, IIT Kharagpur, in collaboration with IUAC, New Delhi. The primary objective is to establish a proper chronological order to the sediment samples collected from the eastern Arabian Sea and different lakes located in Uttar Pradesh, Uttrakhand and Haryana. Two sediment cores (SK-291/GC17 and SK-291/GC08) from the outer continental shelf of the eastern Arabian Sea, which were collected during the Sagar Kanya Cruise expedition in 2011, were chosen to study marine proxies. The latitude and longitude of the cores are N15°07.64' and E72°56.69', N12°34.0' and E74°11.47', respectively. The cores were sliced at an interval of 1cm in the top 100 cm of the cores and at an interval of 2 cm below 100 cm. On the other hand, sediment cores were collected from three northern Himalayan lakes Tadag Taal (Chaukhutia, Uttrakhand), Tikkar Taal (Panchkula, Haryana) and Sherla lake (Panchkula, Haryana) using a piston corer. The latitude and longitude of the lakes are N29°52.612' and E079°25.864', N30°39.488' and E077°04.722', N30°40.070' and E077°07.207', respectively. These cores were sliced at an interval of 0.5 to 1 cm for subsampling. Moreover, sediment samples were also collected from Lilour Lake, Uttar Pradesh in the Ganga basin (Latitude N28.44° and longitude E79.04°), which was sliced at an interval of 1 cm for further analysis.

A total of 60 samples were analyzed for radiocarbon dating at IUAC. These include 10 samples from marine sediment core SK-291/GC17, 10 samples from Sherla lake, 14 from Tadag taal lake, 18 from Tikkar taal lake, and 8 samples from Lilour lake. Pretreatment was applied to the samples in the IUAC Graphitization laboratory. Eventually, CO<sub>2</sub> is formed from each sample and is mixed with H<sub>2</sub> gas and passed through the Fe powder surface that acts as a catalyst and converts the gas into graphite. Radiocarbon ages are later calculated from this graphite [1]. The radiocarbon dates provide age validation to the samples. However, not all AMS  $^{14}\text{C}$  dates are significant, some results showing revers ages.

The radiocarbon dates of the core SK-291/GC17 provide a timeline that enables us to see the variation in abundances of benthic foraminifera and pteropods as well as the total organic carbon (TOC) of the sediment, during the Holocene. In the case of lake sediments, *the radiocarbon ages from Tikkar taal are compared with the grain size measurement values for providing better insight into the energy condition of the lake. Bulk carbonate samples from Tadag taal and Sherla lake were analyzed for stable carbon and oxygen isotopes, to infer the productivity and temperature at the time of deposition. However, some of the samples have given erroneous dates. Whether this can be related to the sudden influx of sand and gravel layers within clay layers or human errors*, we require to reanalyze and verify 6 dates from Tadag tall, 7 dates from Sherla lake, 10 dates from Tikkar taal. From the Lilour lake, stable isotope ratio ( $\delta^{13}\text{C}$ ), TOC and grain size were produced to see the small-scale changes in monsoon over the Indian subcontinent as well. The results of the study from marine and lake cores are being synthesized and will shortly be submitted for publications in journals of high repute.

*We propose to date samples from the core SK-291/GC08 and lake sediments from Uttar Pradesh, Odisha, West Bengal and Rajasthan lakes in future. This will enable us to have a broader insight into the variability of the Indian Monsoon system during the Holocene.*

##### **References:**

- Sharma, Rajveer, G. R. Umapathy, Pankaj Kumar, Sunil Ojha, Satinath Gargari, Rajan Joshi, Sundeep Chopra, and Dinakar Kanjilal. "AMS and upcoming geochronology facility at Inter University Accelerator Centre (IUAC), New Delhi, India." *Nuclear Instruments and Methods in Physics Research Section B: Beam Interactions with Materials and Atoms* 438 (2019) 124-130.

#### **5.4.14 Chronology of sediments from Ladakh: Implications to Palaeoclimate reconstruction**

Phartiyal Binita<sup>1</sup>, Joshi Priyanka<sup>1</sup>, Kumar Pankaj<sup>2</sup>

<sup>1</sup>Birbal Sahni Institute of Palaeosciences, 53 University Road, Lucknow, UP, India.

<sup>2</sup>Inter-University Accelerator Centre, New Delhi-110067, India.

With an objective of providing a chronology of past damming phases in the TanglangLa catchment and palaeoclimate reconstruction in east Ladakh work was conducted. Sections along the villages of Meru, Gya, Sasoma and Rumtse located along the Gya river were studied in details. These villages lie on the alluvial flat, as tributary streams open into Gya river. Moving upstream from Meru to Rumtse, several geomorphological and archeological features are encountered along the river on both the banks. Moving downstream from Rumtse,

sections were dated to  $21803 \pm 90$  cal years BP;  $13090 \pm 56$  cal years BP and  $4527 \pm 39$ . The Sasoma caves which lie beneath a thick capping of matrix supported unsorted angular to sub-angular sequence with interbedded clays (buff coloured facies) were dated to  $19953 \pm 98$  cal years BP. All these represent the damming phases. Further work of the intensity and reconstruction of these damming phases in the Late Quaternary is under progress.

The palaeolake section at Pashkyum, Kargil which was dated from ~43843 to 27000 yrs BP, multi-proxy analysis for Palaeoclimate reconstruction is under progress.

#### **5.4.15 Radiocarbon dating using AMS of samples from Vaigai River Civilization Site**

Mu. Ramkumar<sup>1\*</sup>, K. Kumarasamy<sup>2</sup>, K. Balasubramani<sup>3</sup>, R. Nagarajan<sup>5</sup>, M. Santosh<sup>5</sup>, Sharma Rajveer<sup>6</sup>

<sup>1</sup>Department of Geology, Periyar University, Salem-638011, India

<sup>2</sup>Department of Geography, Bharathidasan University, Tiruchirappalli-620024

<sup>3</sup>Department of Geography, Central University of Tamil Nadu, Thiruvaroor

<sup>4</sup>Department of Applied Geology, Curtin University Sarawak, Malaysia

<sup>5</sup>School of Earth Sciences and Resources, China University of Geosciences Beijing, China.

<sup>6</sup>Inter-University Accelerator Centre, New Delhi-110067, India.

The present work was carried out with collaborations between the institutes listed above with active support from the IUAC facility at New Delhi. Sediment samples were collected in excavated pit dug in a paleochannel-natural levee-point bar complex wherein human habitation surfaces were presumed to be located. A total of 30 sediment samples together with bone remains, artifacts, pottery were collected from the site. Establishing chronological relationship between the sediment samples in stratigraphy and the artifacts collected is crucial in interpreting of ancient civilizational development, timing of habitation and stages of cultural advancements. In addition, accurate dating of the site and samples will advance our understanding on the paleoclimatic extremes that led to occurrence, shifting and abandonment of civilizational surfaces during Neolithic in the Vaigai Basin.

The samples were subjected to pretreatment in IUAC Graphitization laboratory. The first batch of 4 sediment samples, one organic carbon layer and two bones and a pottery shard was processed using the standard methods. These have provided a chronological control partly over the excavated site and with which a manuscript entitled Neolithic civilization sites and extreme climate related channel avulsion: Evidence from the Vaigai River Basin, southern India has been prepared and submitted to the Archaeological Science: Reports and is under review.

#### **5.4.16 Paleoclimate study from southern Bay of Bengal using Forams as proxy**

Agarwal Nitin<sup>1</sup>, D. Senthil Nathan<sup>1</sup>, Sharma Rajveer<sup>2</sup>, Kumar Pankaj<sup>2</sup>, Chopra Sundeep<sup>2</sup>

<sup>1</sup>Department of Earth Sciences, Pondicherry University, Pondicherry-605014, India.

<sup>2</sup>Inter-University Accelerator Centre, New Delhi-110067, India.

Two Gravity core have been collected on board Sagar Kanya (SK344) from the off shore of Tamilnadu at a depth of 2000m from mean sea level (of core length 2.7m and 3.2m respectively). The first core sample (Sk344/GC01) is collected from  $11^{\circ}24.82300'N$ ,  $80^{\circ}28.66700'E$  whereas the second core (Sk344/GC02) is collected from  $10^{\circ}16.60600'N$ ,  $80^{\circ}50.36400'E$ . The cores have been micro sampled at 1cm interval throughout to get a high-resolution paleoclimatic reconstruction. Accurate dating of foraminifera will help us in establishing a clear chronology of this samples will help us to put the major oceanic and landform changes with respect to time. The study regarding the samples involves organic matter analysis of sediments, isotopic study of CNO for paleomonsoon, paleoecology, paleo-oceanography. Mg/Ca ratio will be used for paleosalinity and foraminiferal distribution.

The sediment samples from different lengths of the core were taken, washed and forams were separated from them. Then these were put on a sorting tray, separated under a microscope and 10mg weight was collected at Pondicherry University. Then they were taken to IUAC for analysis. Here the foram samples were again weighed and treatment for graphitization was done. A few sediment samples were also analysed in IUAC where pretreatment of samples was done. This involves Acid-Base-Acid treatment then freeze-drying of samples and finally C percentage was measured to check the carbon content before graphitizing the samples. Then the samples were graphitized using automated graphitization equipment (AGE) and measured using IUAC AMS facility.

There has been a success in processing both the forams and sediment samples. The dates obtained show a clearly chronology between them and are in sequential order. The dates obtained range from recent to Pleistocene. The Stable Isotope study is been carried on to further relate them and put in a chronological order and then the findings will be published in some reputed journals

**References.**

1. Saalim, S.M., Saraswat, R., 2018. Assessing the ecological preferences of agglutinated benthic foraminiferal morphogroups from the western Bay of Bengal. *Deep-Sea Research Part II: Topical Studies in Oceanography*.
2. Manasa, M., Saraswat, R., Nigam, R., 2016. Assessing the suitability of benthic foraminiferal morpho-groups to reconstruct past monsoon from the Bay of Bengal. *J. Earth Syst. Sci.* 125, 571–584.
3. Rao, N.R., Kamatchi, P., Ramesh, S., 2013. Deep-sea foraminifera in a short core from the Bay of Bengal: ecological comparisons with the South China and Sulu Seas. *Arab. J. Geosci.* 6, 3269–3280.
4. Hayward, B., Sabaa, Ashwaq t., 2010. Cenozoic record of elongate, cylindrical, deep-sea benthic foraminifera in the Indian Ocean. *Journal of Foraminiferal Research.* 40, 113–133
5. Katz, m., Cramer b., 2010. Traditional and emerging geochemical proxies in foraminifera. *Journal of foraminiferal research.* 40, 165–192

#### **5.4.17 <sup>14</sup>C dating of sediment core from Ponnaiyar River Basin- Implication to understanding the temporal variation in organic matter source**

Singh Pramod<sup>1</sup>, A. Venugopal<sup>1</sup>, Kumar Pankaj<sup>2</sup>, Sharma Rajveer<sup>2</sup>, Ojha Sunil<sup>2</sup>, Kusuma K.N<sup>1</sup>. and Chopra Sundeep<sup>2</sup>

<sup>1</sup>Department of Earth Sciences, Pondicherry University, Kalapet, Puducherry 605014, India

<sup>2</sup>Inter-University Accelerator Center, Aruna Asaf Ali Marg, New Delhi 110067, India

The organic particulate matter source particularly in the riverine sediments is significant as it has great importance in understanding the drainage and geo-morphological shifts in the inland region, and sea level and climate fluctuation in the marginal coastal region. The geochemistry of the sediments along with  $\delta^{13}\text{C}$ , organic carbon and C/N ratio of organic matter is important in such studies because it records the systematic shift in climate and the organic matter source between terrestrial and marine.

In above context work has been initiated on two sediment cores from the Ponnaiyar river basin, one retrieved from lake in the inland Dharmapuri region and another from the river estuary, both located in Tamil Nadu. It is intended to find the organic carbon source along with the variation in sediment chemistry and mineralogy to infer the record of past variation in NE monsoon strength and the temporal fluctuation of terrestrial and marine organic matter input in the sediments to understand the past fluctuation in sea level during the Holocene. For above purpose it becomes essential to find the chronology of the sediments for which <sup>14</sup>C measurements have been initiated at AMS facility at IUAC.

Field work was carried out to collect the sediments from the trenched section from inland lake and through core pipes in the estuary. 54 samples have been collected from the lake section at 5 cm interval from Dharmapuri and 1m core has been retrieved from estuary which has been sub-sampled. Alternate samples have been processed and geochemical analysis on 40 samples have been carried out for major and trace elements at the XRF facility in IUAC. C, N and  $\delta^{13}\text{C}$  measurements on these samples have been carried out at Pondicherry University. For obtaining the preliminary geochronology initially first batch of 12 samples were selected, 8 from lake section and 4 from estuary core and were sent to IUAC. Samples were pretreated using acid-base protocol in the graphitization laboratory in IUAC. After pretreatment samples were subjected to graphitization. Enough graphite could be obtained from 9 samples, whereas 3 sample could not be graphitized because of less carbon content in the sample. Subsequently the 9 samples were measured using AMS facility at IUAC for obtaining <sup>14</sup>C dates. Out of the above, 6 dates obtained have given promising results and 3 have shown reversal. Now we plan to analyze second batch of samples at AMS facility including few from the already collected core to check for the reversals obtained and improve the chronology. In addition, we shall retrieve one more core from the lake and include few samples from it. Two Research scholar/project staff visited IUAC for carrying out above work.

The interpretation of the data is in progress. After carrying out analysis on new set of samples to improve the geochronology constructed from first batch of analysis, we plan to submit a manuscript for publication.

#### **5.4.18 Benthic Foraminiferal Distribution and Oceanographic Changes in Krishna- Godavari Basin: Evidences from NGHP Hole 3B**

Chowdhury Sarmistha<sup>1</sup>, Bhaumik Ajay Kumar<sup>1</sup> and Kumar Pankaj<sup>2</sup>

<sup>1</sup>Department of Applied Geology, IIT (ISM), Dhanbad, Jharkhand-826004, India

<sup>2</sup>Inter-University Accelerator Centre, New Delhi-110067, India.

The present work is carried out by the Department of Applied Geology, IIT(ISM), Dhanbad and Inter-University Accelerator Centre, New Delhi. The main aim of this work to obtain <sup>14</sup>C dates of mixed foraminifera (Benthic and Planktic) to establish the paleomonsoonal and paleooceanographic event during the late pleistocene. The samples are collected from the offshore part of Krishna-Godavari basin, Bay of Bengal (Lat:15°53.8919'N,

Long:  $81^{\circ}53.9678'E$ ). Precise age estimation of the sediment column will help us to locate the exact timing of all paleoenvironments accurately. Moreover, accurate age calculation of this site will show a clear trend of sedimentation rates and global correlation of paleoclimatic events during the late pleistocene.

**Experimental Details:** We have analyzed foraminifera (both benthic and planktic  $> 125\mu m$ ) for the  $^{14}C$  dating using the foraminiferal calcitic test collected from the NGHP Hole 3B, Krishna-Gadavari offshore basin. Total 8-10  $\mu g$  carbonate sample was weighed for the analysis of each sample before the analysis.

Graphitization of the samples were done in the IUAC Graphitization laboratory and the samples are processed described in the following paper [1]. We are still working on the interpretation part and wait for isotope data so that we can correlate with other proxies data to understand the paleoclimatic oscillation. Supportive data analysis and documentation are in progress that will be summarized in the future publication.

#### References:

- Sharma, R., Umapathy, G.R., Kumar, P., Ojha, S., Gargari, S., Joshi, R., Chopra, S. and Kanjilal, D., 2019. AMS and upcoming geochronology facility at Inter University Accelerator Centre (IUAC), New Delhi, India. *Nuclear Instruments and Methods in Physics Research Section B: Beam Interactions with Materials and Atoms* 438 (2019) 124-130.

#### 5.4.19 Radiocarbon dating using AMS of samples from Gujarat Region

Prizomwala Siddharth<sup>\*1</sup>, Das Archana<sup>1</sup>, Vedpathak Chintan<sup>1,2</sup>, Sodhi Aashima<sup>1,2</sup>, Sharma Rajveer<sup>3</sup>, Kumar Pankaj<sup>3</sup> and Chopra Sundeep<sup>3</sup>

<sup>1</sup>Institute of Seismological Research, Gandhinagar, Gujarat- 382007, India.

<sup>2</sup>Research Scholars, Gujarat University, Ahmedabad-380009

<sup>3</sup>Inter-University Accelerator Centre, New Delhi-110067, India.

The present work was carried out by Institute of Seismological Research, Gandhinagar, Gujarat in collaboration with Inter-University Accelerator Centre, New Delhi. The aim of the present work was to establish a procedure to obtain reliable dates of different foraminifer samples. The samples have been collected from the Mainland Gujarat regions; Navagam ( $22^{\circ}51'0.00"N, 72^{\circ} 23'0.00"E$ ), Kamatalav ( $22^{\circ}19'N, 72^{\circ}16'E$ ) and from the periphery of the north of Morbi ( $23^{\circ}16'40.3"N 71^{\circ}26'22.8"E$ ). The collected samples were then selected and the selected samples were further used to; pick the, in-situ planktic foraminifers. The establishment of a clear chronology of these sites is of utmost importance, since it will allow us to procure a clear chronological context. Moreover, accurate dating of these sites will also allow a stronger analysis of the environmental and climatic data available, allowing further reconstruction of the Middle-Late Holocene environments; which is a hot topic of debate as it hosted the mighty Harappan civilization and its links with environmental change.

The carbonate samples are graphitized using the Carbonate Handling System (CHS) in IUAC Graphitization laboratory. The foraminifer samples were transferred into the vials and then these vials were flushed with helium gas. In next step, these foraminifers samples were hydrolyzed using phosphoric acid and produced  $CO_2$  was transferred to zeolite trap in automated graphitization equipment (AGE) (Sharma et al. 2019). The trapped  $CO_2$  was transferred into a tube filled with iron powder where it is reduced into graphite at  $580^{\circ}C$  with hydrogen gas.

For shell sample, surface was leached using 0.1M HCL and the obtained  $CO_2$  was flushed with an inert gas (Helium). The remaining sample was then hydrolyzed and graphitized as described above (Sharma et al. 2019).

The first batches of the samples were processed using the standard method explained above. Amidst the five samples measured, only one sample yielded the age of  $6389 \pm 27$  yr BP while the remaining samples did not yield measurable amounts of organic carbon.

The second batch of the Foraminifer samples is ready for analysis and waiting for the next available lab time slot at IUAC.

#### References:

- Sharma, R., Umapathy, G. R., Kumar, P., Ojha, S., Gargari, S., Joshi, R., Chopra, S., & Kanjilal, D., AMS and upcoming geochronology facility at Inter University Accelerator Centre (IUAC), New Delhi, India. *Nuclear Instruments and Methods in Physics Research Section B: Beam Interactions with Materials and Atoms* 438 (2019) 124-130.

#### 5.4.20 RADIOCARBON DATING USINGAMS OF SAMPLES

Nayan Sujet

Archaeological Survey of India, Aizawl Circle

The present work was carried out by Archaeological Survey of India, Aizawl Circle in collaboration with Inter-University Accelerator Centre, New Delhi. The site of Vangchhia has been selected for archaeological

excavation with the view to know the cultural sequence of the area as the region was not explored earlier scientifically. With this objective, different samples have been collected from the excavation site  $23^{\circ}12'11.94''N$  latitude and  $93^{\circ}19'58.64''E$  longitude. From the total samples collected, seven samples i.e., two bones, four charcoals and one burnt wood were submitted for the process of Radiocarbon dating at IUAC, New Delhi. These samples were collected in between February 2019 to April 2019 excavation. Establishing the clear chronology of this site is crucial. There was no archaeological excavation in Mizoram before. Vangchhia is the first excavation and the similar culture expands to an area of 10 sq km. Understanding of the chronological context will help to reconstruct the history of this region. The excavation and accurate dating of the site has been most promising, and is bound to have important bearings on the history of the Mizo.

Four charcoal samples and one burnt wood were processed on 14/10/2019 using the standard method in IUAC Graphitization laboratory. First extraneous materials were removed physically through scrapping by using tweezers. Through this method, dirt, any introduced secondary materials are removed from the surface. After that, the samples were treated with Acid-Base-Acid (ABA) protocol. Firstly, the samples were put on 0.5M HCl for three hours to remove impurities. For the second steps, the samples were treated with 0.1M NaOH for another 3 hours, and at the end the samples were again treated with 0.5M HCl for two more hours. After these treatments were over, the samples were freeze drying overnight. At the end of ABA protocol, the samples were collected and their weight was measured, it needs to be less than 2 mg. After that graphitization process started.

The bone samples, taken for analysis were first cleaned physically. For this it was washed thoroughly by using ultrasonic bath. Secondary deposits were removed through scrapping. The bone samples were then dried at  $45^{\circ}C$  and crushed into powder. To remove the carbonate impurities the samples were soaked overnight in 0.2M HCl. After that the samples were washed free of HCl by repeated centrifugation and decanting with distilled water, then vacuum-dried. The sample was ready for isotopic analysis. Due to the requirement of longer treatment of the samples and the limited time schedule, the samples along with substitute for each sample were handed over to the lab In-charge to process further.

Currently these samples pretreated and graphitized during the beam time 14/10/2019 to 19/10/2019 were loaded into the ion source of AMS system. As the work is still in progress, the actual results in terms of dates are awaited.

#### **5.4.21 AMS dating of the Archaeological sites of Digaru – Kolong River Valley**

Kumar Jitendra<sup>1</sup>, Sharma Sukanya<sup>1</sup> and Sharma Rajveer<sup>2</sup>

<sup>1</sup>Department of Humanities and Social Sciences, IIT Guwahati, Assam- 781039, India

<sup>2</sup>Inter University Accelerator Centre, New Delhi-110067, India.

The present work was carried out as a part of PhD work by Jitendra Kumar under the supervision of Prof. Sukanya Sharma of Indian Institute of Technology Guwahati in collaboration with Inter University Accelerator Centre, New Delhi. The primary objective of this work was to establish a procedure to obtain reliable dates of Charcoal samples from the archaeological sites of Digaru – Kolong River Valley. Samples have been collected from Bagibari village ( $26^{\circ}11'24.23''N$  latitudes and  $92^{\circ}3'33.18''E$  longitudes) and Marakdola village ( $26^{\circ}4'3.52''N$  latitudes and  $91^{\circ}53'33.92''E$  longitudes) at Kamrup district of Assam. Establishing a clear chronology of these sites is essential, since it will allow the finds to be put into clear chronological context with respect to the appearance and disappearance of several key phenomena. Moreover, accurate dating of the site will also allow a clearer analysis of the environmental and climatic data available, allowing further reconstruction of Late Pleistocene environments during the Holocene in the Northeast India.

The pretreatment of samples were done in IUAC Graphitization laboratory which were processed as per the recommendations of following paper [1], which recommends the physical pretreatment as removal of any visible contaminations and chemical pretreatment using (Acid-Base-Acid) ABA protocol. Samples were measured at IUAC using AMS facility.

There has been a success in processing the Charcoal samples using method described in paper [1] and we have graphitized samples. The work is in progress and hence the actual results in terms of dates are awaited.

#### **Reference:**

1. Rajveer Sharma, G.R. Umapathy, Pankaj Kumar, Sunil Ojha, Satintha Gargari, Rajan Joshi, Sundeep Chopra, Dinakar Kanjilal, AMS and upcoming geochronology facility at Inter University Accelerator Centre (IUAC), New Delhi, India, *Nuclear Inst. And Methods in Physics Research B* 438 (2019) 124-130

## 5.4.22 AMS Dating of bones from the Late Pleistocene fossiliferous horizon in the Manjra Valley, District Latur, Maharashtra.

Sathe Vijay<sup>1</sup>, Chakraborty Prateek<sup>1</sup>, Kumar Pankaj<sup>2</sup> and Sharma Rajveer<sup>2</sup>

<sup>1</sup>Department of AIHC & Archaeology, Deccan College Postgraduate & Research Institute, Deemed University, Pune 411006, India.

<sup>2</sup>Inter University Accelerator Centre, New Delhi-110067, India.

The present work was carried out by the Palaeontology Laboratory of the Department of AIHC & Archaeology, Deccan College Postgraduate & Research Institute Deemed University, Pune in conjunction with the AMS and Pelletron Group, IUAC in the months of March and April 2019. The focus of this work was to establish a procedure through which reliable AMS dating of fossil bone and teeth could be carried out, using the material from sites in the Manjra Valley (dist. Latur, Maharashtra) as a case study.

The Manjra River valley is one of the richest fossil site complexes in the Indian subcontinent, and has yielded almost complete evidence of a full food chain structure from apex predator to scavengers. Establishing a clear chronology of this site is essential, since it will allow the finds to be put into a clear chronological context with respect to the appearance and disappearance of several key fauna. Moreover, accurate dating of the site will also allow a clearer analysis of the environmental and climatic data available, allowing further reconstruction of Late Pleistocene environments during the Middle Palaeolithic in Peninsular India.

Due to the low organic content in fossilised tissue, AMS dating has generally been considered inaccurate or error-prone. However, not many efforts have been made using the dental collagen powder from fossilised teeth, which are generally much more resistant to breakdown and decomposition thanks to the protection of the tooth enamel. In the present study, collagen was obtained from the molar teeth of large vertebrates, by drilling into the enamel-dentine junction.

The samples were then subjected to two different processes of AMS dating. The first batch was processed using the standard method, and did not yield measurable amounts of organic carbon. Therefore, larger amounts of sample were taken for the second batch, which were processed as per the recommendations of Cherkinsky 2009, which recommends the treatment of fossil collagen powder using acetic acid for better preservation of organic carbon.

There has been a great success in processing the bone samples using method described by Alex Cherkinsky and we have graphitised samples. As per the method recommended by Cherkinsky (2009), on achieving collagen extraction finally it has become possible to date the samples whose results are given in Table 1.

The results assume great significance in providing a definite chronological frame to the Late Pleistocene fauna in Peninsular India. Though there are several C14 dates available for Acheulian and fossil vertebrate sites in Peninsular river valleys, mostly all have been based on molluscs which were found in association with the fossils. The dates were obtained so far using conventional radiocarbon dating procedures, and as said earlier, the samples used were freshwater bivalve shells instead of actual fossils. The 'hard water' reservoir effect, and diagenesis of the outer layers of the shell can affect the age produced from these samples, rendering them less reliable (Preece et al. 1983, Yates 2016, Wright 2017). In addition to this, owing to taphonomic bias involved in the depositional history of vertebrates, their precise association with fossils has always been contested. It is for the first time that fossilised bones have been dated directly and the values are in close congruity with biostratigraphical and skeletal and morphological parameters. The dates are a definite indication that the period to which the fauna belonged was closely approaching the Last Glacial Maximum (LGM). Hence the palaeoecological inferences drawn using isotope chemistry and histology of calcified tissues provide crucial link to the palaeoenvironmental conditions that prevailed in the Manjra valley in the terminal phase of the late Pleistocene.

A detailed discussion on the recently obtained AMS dates on three bone samples is under preparation which would culminate into a research publication jointly with the collaborators of the IUAC, New Delhi.

### References.

- Cherkinsky, Alexander 2009. Can we get a good radiocarbon age from "bad bone"? Determining the reliability of Radiocarbon Age from Bioapatite. Radiocarbon 51 (2), 647-655.
- Preece, R.C., Burleigh, R., Kerney, M.P., Jarzembski, E.A., 1983. Radiocarbon age determinations of fossil Margaritifera auricularia (Spengler) from the River Thames in West London. Journal of Archaeological Science 10, 249-257.
- Wright, D.K., 2017. Accuracy vs. precision: Understanding potential errors from radiocarbon dating on African landscapes. African Archaeological Review 34, 303-319.
- Yates, T., 2016. Studies of non-marine mollusks for the selection of shell samples for radiocarbon dating. Radiocarbon 28, 457-463

### 5.4.23 Cosmogenic Radionuclide dating of glacial deposits of Thajiwas valley of Kashmir Himalaya

Paul Omar<sup>1</sup>, Romshoo Shakil<sup>1</sup>, Dar Reyaz<sup>1</sup>, Kumar Pankaj<sup>2</sup>, Chopra Sundeep<sup>2</sup>, Pattanaik Jitendar<sup>3</sup>, Dal Soumaya Prakash<sup>2</sup>

<sup>1</sup>Department of Earth Sciences, University of Kashmir, 190006

<sup>2</sup>Inter University Accelerator center (IUAC) New-Delhi 110067

<sup>3</sup>Center for Geography and Geology, Central University Punjab 151001

In the present study, glacial-moraine boulder samples of the Thajiwas glacial valley were analyzed using cosmogenic radionuclide dating to assess the past glacial advances and retreat events of the Thajiwas glacier. The samples from the CRN dating were collected from the lateral and the terminal moraines of the already published glacial-geomorphic map by Dar et al 2017. The samples collected from the field were grinded to the preferable mesh size and the magnetic separation of the Quartz was carried out using Frantz isodynamic magnetic separator. The samples were subsequently processed for the <sup>10</sup>Be and <sup>26</sup>Al cosmogenic Radionuclide dating.

#### Sample preparation and processing:

The pure quartz separated using Frantz isodynamic magnetic separator were processed chemically to extract Be(OH)<sub>2</sub>. Be(OH)<sub>2</sub> was the thermally decomposed to the BeO, the process seems to be oxidation but it is not oxidation it is called calcination as there is no change in oxidation of both Beryllium and Oxygen. The BeO was then mixed with the Niobium (Nb) was pressed into the cathodes using the cathode press at the AMS lab in IUAC (Inter University Accelerator Center), New Delhi. The cathodes were inserted into the ion source of the AMS (Accelerator mass spectrometer) to get the <sup>10</sup>Be counts. The whole chemical analysis was carried out using standard procedures after Nishiizumi et al. (1989) and the calculation for the concentration of <sup>10</sup>Be per gram of quartz was carried out using the methodology of Balco, 2006.

#### Sampling Processing details

Glacial chronologies based on the moraine dating techniques have found central place in the reconstruction of paleoclimate. There are large number of studies on glacial landform dating in the Himalayas. However, no such studies have been carried in the intermontane Kashmir valley to date glacial landforms. The cosmogenic <sup>10</sup>Be dates from the well-preserved moraines of the Thajiwas glacial valley in this study suggest that the area has clearly responded to the global climatic shifts. The present study clearly supports the view that like other Himalayan glaciers, the Thajiwas glacier located in the Greater Himalayan range also shows advancement during the global last glacial maximum. In between gLGM and younger Darya stage, the Thajiwas glacier shows rapid deglaciation and then huge advancement during the younger Darya stage. The valley also preserves the records of the Little ice age effects but the effect of the LIA glaciation is not huge. The change in the glacier surface area shows that the glacier has receded from 47.4 km<sup>2</sup> during last glacial maximum to 3.60 km<sup>2</sup> at present.

#### References

1. Dar, R. A., Jaan, O., Murtaza, K. O., & Romshoo, S. A. (2017). Glacial-geomorphic study of the Thajwas glacier valley, Kashmir Himalayas, India. *Quaternary International*, 444, 157-171.
2. Nishiizumi, K., Winterer, E. L., Kohl, C. P., Klein, J., Middleton, R., Lal, D. and Arnold, J. R., 1989. Cosmic ray production rates of <sup>10</sup>Be and <sup>26</sup>Al in quartz from glacially polished rocks, *J. Geophys. Res.* 94 17907–17915.
3. Balco, G. (2006). Converting Al and Be isotope ratio measurements to nuclide concentrations in quartz. *Cosmogenic Nuclide Lab, University of Washington* <http://hess.ess.washington.edu>.

### 5.4.24 Report On SEM Facility Used At Inter-University Accelerator Centre

Sinha Sayan<sup>1</sup>, Sathe Vijay<sup>1</sup>, Ojha Sunil<sup>2</sup>, Kumar Pankaj<sup>2</sup>

<sup>1</sup>Deccan College Postgraduate and Research Institute, Deemed University, Pune

<sup>2</sup>Inter-University Accelerator Centre (IUAC), New Delhi.

The following is a brief report regarding the SEM facility used at Inter-University Accelerator Centre (IUAC), New Delhi. The work was conducted between the time duration 04.02.2020 to 07.02.2020.

A total of sixty samples were examined during this time. All the samples were that of human teeth – ancient and modern ones combined. The experiment was conducted as a part of an M.Phil research topic titled “From Diet to Tooth Enamel Microstructure: A Case Study in the Teeth of Present and Ancient Humans In Indian Context”.

The human teeth unique enamel microstructural features are a result of at least two million year of dietary evolution, combined with environmental imperatives. The present research focuses on the question, whether enamel microstructural distinctions can be made between people following a strictly vegetarian and those following a somewhat of a mixed diet inducting more non vegetarian food, over several generations

approximately a few hundred years. If the results yield as positive, the tooth enamel of archaeological human teeth samples from the site of Farmana, can be examined in juxtaposition with the modern samples to see if dietary inferences can be drawn. The hierarchical structural complexity in the tooth enamel of modern and ancient humans will also be documented. As already noted, more than a million year of evolution does lead to enamel microstructural changes, the research will try to examine whether a relatively shorter time-span of dietary specialization leads to any distinguishable change in enamel of humans.

The ground, polished and etched tooth samples were taken in to the SEM lab of IUAC for observation. Out of the total sixty samples, forty samples were modern ones and the rest twenty were archaeological samples. The archaeological samples had been embedded in epoxy resin earlier for sectioning. Thus, they had to be kept in a freeze drier at the graphitization laboratory at IUAC overnight. This was done in order to remove the excess moisture present in the epoxy blocks. The samples were then observed under the scanning electron microscope. The sample size and height were not always uniform. Some of modern human teeth were already fragile while acquiring, and even though carefully ground and polished, fragments broke off them. However due to the expertise of the lab assistants, no difficulty was faced in mounting them in the stub for observation. Out of sixty tooth samples, half were a part of the vertical section and the other half was that of horizontal section of the tooth. This was because the research aimed at studying the prism size diameter, prism width, prism density, Hunter Schreger Bands (HSBs) and prism decussations, along with dentinal tubules density. If one were to study the vertical section, one would observe HSBs and prism decussations while horizontal sections will yield observations of prism size diameter, prism compactness, prism width. All of these observations have been taken from each of enamelo-dentinal junction (EDJ) that is inner enamel, middle enamel and outer enamel. In case of horizontal sections, higher magnifications of 1500X, 2000X, 2500X and 3000X were used to observe the prism interlocking pattern. For measurements of the prism length, prism width and density, the help of the Smile software (exclusively available with the SEM operating computer) was used. Hunter Schreger bands were observed in vertical sections of the samples; taken at lower magnifications of 300X, 400X and 700X to get a broader picture of the band patterns and their movement away from EDJ and close to EDJ. Multiple images were taken for the same sample at varying magnifications, keeping in mind the tedious task of observing the minute details of microstructural differences between them.

All the images were collected from the SEM operator computer through a DVD. The comparative statistical analysis of the data collected will be prepared soon and produced in form of an M.Phil thesis.

#### **5.4.25 Estimation of denudation rates using $^{10}\text{Be}/^{9}\text{Be}$ ratio around Chilka Lake and Anshupa Lake, Odisha coast**

Chinmay Dash<sup>1</sup>, Soumya Prakash Dhal<sup>2</sup>, Pankaj Kumar<sup>2</sup>, Pitambar Pati<sup>2</sup>, Sundeep Chopra<sup>2</sup>

<sup>1</sup>Indian Institute of Technology Roorkee, Uttarakhand-247667

<sup>2</sup>Inter University Accelerator Centre, Aruna Asaf Ali Marg, near Vasant Kunj, New Delhi, Delhi-110067

#### **1. Introduction**

The present study is carried out to estimate the catchment average denudation rates from two lakes along the Mahanadi delta, i.e., the Chilka Lake and the Anshupa Lake (Fig.1). Although both these lakes are situated in the core monsoon zone of India, they represent different environmental settings. The Chilka Lake is a brackish water lake receiving its sediments from metamorphic rocks of the Eastern Ghats, and the Anshupa Lake is a freshwater lake with sediment source from the Athgarh sandstones. The present study aims to compare denudation rates of two lakes experiencing the same climatic condition in different environmental settings.



Figure 1 Location of Chilka Lake and Anshupa Lake along the Manananadi delta

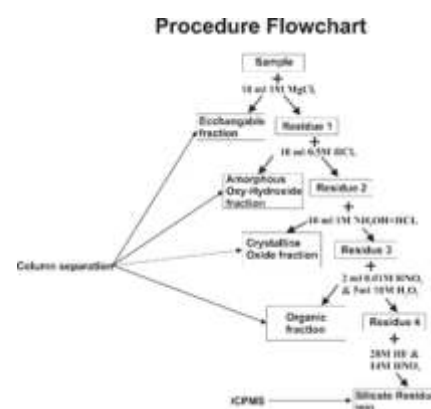


Figure 2. Flowchart showing details of chemical procedure undertaken before AMS measurements.

## 2. Materials and methods

AMS measurements for beryllium isotopic ratios were carried out from two sediment cores from both the lakes. A total number of 33 samples were analyzed from selected depths for AMS  $^{10}\text{Be}$  measurements. Details of chemical procedures undertaken are shown in fig.2.

## 3. Results and Discussion

$^{10}\text{Be}/^9\text{Be}$  ratios for Anshupa Lake vary from  $5.26 \times 10^{-10}$  to  $1.64 \times 10^{-10}$ . Denudation rates (D) calculated on samples from different depths using the equation of von Blanckenburg *et al.* (2012) show a variation from  $391.93 \pm 41.66$  to  $94.69 \pm 5.7$  T/km $^2$ /yr. For Chilka Lake  $^{10}\text{Be}/^9\text{Be}$  ratios vary from  $5.25 \times 10^{-10}$  to  $1.94 \times 10^{-10}$  and the denudation rate vary from  $272.9 \pm 1.12$  to  $68.4 \pm 2.18$  T/km $^2$ /yr. The above results indicate that the denudation rate in Anshupa Lake catchment is more compared to that of Chilka Lake catchment. The catchment rocks of Anshupa Lake being sedimentary are more prone to weathering and erosion compared to the metamorphic rocks of the Eastern Ghats. Detailed analysis of denudation rates and manuscript writing is in progress.

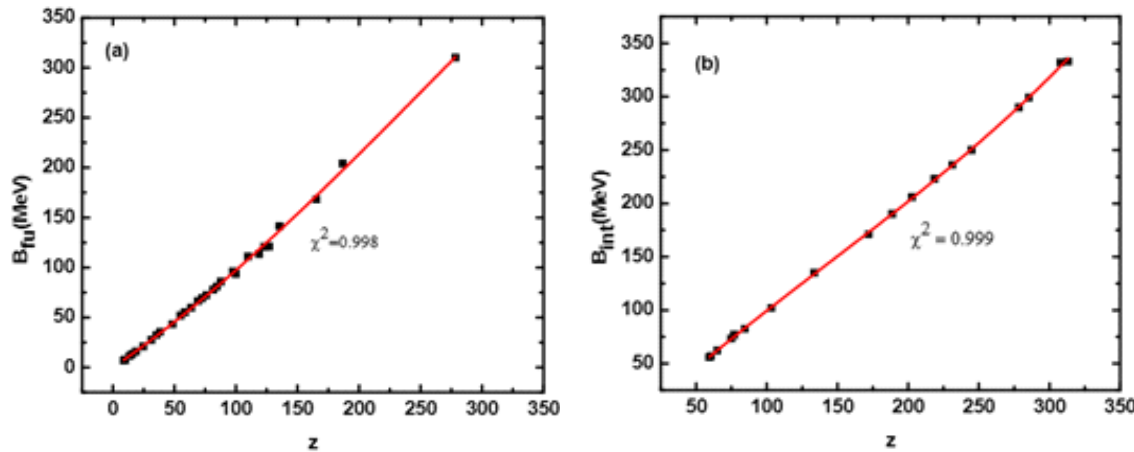
## 5.5 ATOMIC PHYSICS

### 5.5.1 In search of a good nucleus-nucleus potential

D.K. Swami, Yash kumar, S. Chakraborty and T. Nandi

Inter University Accelerator Centre, Aruna Asaf Ali Marg New Delhi-110067

We have constructed empirical formulae for fusion and interaction barrier heights using experimental values available in the literature. Fusion excitation function measurements are used for the former and back angle quasi-elastic excitation function for the latter case. The fusion barriers so obtained have been compared with various model predictions such as Bass potential [1], Christensen and Winther[2], Broglia and Winther [3], Aage Winther [4], Siwek-Wilczyński and J.Wilczyński [5], Skyrme energy density function model [6], and the São Paulo optical potential [7] along with experimental results. The comparison allows us to find the best model, which is found to be the Broglia and Winther model. Further, to examine its predictability, the Broglia and Winther model parameters for the Woods-Saxon potential are used in couple channel calculation using the code CCFULL in no couplings to obtain total fusion cross sections. Though the Broglia and Winther model radius parameter needs a little variation for some reactions, a good agreement is found between these calculated and experimental values for beam energies above the fusion barriers. Thus, this model can be useful for planning experiments, especially ones aiming for producing super heavy elements. Similarly, current interaction barrier heights have also been compared with the Bass potential model meant for the interaction barrier predictions and found a reasonable agreement. Nevertheless, the present model is chosen for further use as it is based on the experiments. We believe the current interaction barrier model prediction will be a good starting point for future quasi-elastic scattering experiments. Whereas both the Broglia and Winther model and our interaction barrier model will have practical implications in carrying out physics research near the Coulomb barrier energies.



Fusion and interaction barrier plots: (a) the fusion barrier,  $B_{\text{fu}}$  (MeV), as obtained from the fusion excitation function experiments and (b) the interaction barrier,  $B_{\text{int}}$  (MeV), from the quasi-elastic scattering experiments, are plotted against the dimensionless parameter  $z$  and the plots have been fitted with polynomial functions.

The polynomial function that fits the Bfu vs z data is as follows:

$$B_{fu} = -0.21549 + 0.84733z + 0.00146z^2 - 0.00000175z^3; 8 \leq z \leq 278$$

and the other function that fits the Bint vs z data is given below:

$$\int B_{int} = -13.47 + 1.26z - 0.002z^2 - 0.00000403z^3; 59 \leq z \leq 313$$

#### References:

1. R. Bass, Nucl. Phys. A231, 45 (1974).
2. P. R. Christensen and A. Winther, Phys. Lett. 65B, 19 (1976).
3. W. Reisdorf, J. Phys. G:Nucl.Part.Phys. 20, 1297 (1994).
4. A. Winther, Nucl. Phys. A 594, 203 (1995).
5. K. Siwek-Wilczynska, J. Wilczynski, Phys. Rev. C 69, 682 024611 (2004).
6. V. Zanganeh, M. Mirzaei and N. Wang, Commun. Theor. 684 Phys. 64, 177 (2015).
7. A. S. Freitas, L. Marques, X. X. Zhang, M. A. Luzio, 686 P. Guillaumon, R. Pampa Condori and R. Lichtenthaler, 687 Braz J Phys 46,120 (2016).

#### 5.5.2 Fabrication of thin targets for Atomic Physics experiment

R. Gupta<sup>1,2</sup>, C.V. Ahmad<sup>1,2</sup>, K. Chakraborty<sup>1,2</sup>, Abhilash S. R.<sup>3</sup>, D. Kabiraj<sup>3</sup> and P. Verma<sup>1\*</sup>

<sup>1</sup>Department of Physics, Kalindi College, University of Delhi, East Patel Nagar, New Delhi-110008.

<sup>2</sup>Department of Physics and Astrophysics, University of Delhi, New Delhi-110007.

<sup>3</sup>Inter University Accelerator Centre, Aruna Asaf Ali Marg, New Delhi-110067.

\*drpunitaverma.nature@gmail.com

Probing the inner shell electrons of a heavy atom (atomic number  $Z_2$ ) using accelerated heavy ions (atomic number  $Z_1$ ) forms an important aspect of studying Atomic Physics. For the case of close, adiabatic collisions with  $Z_1+Z_2 \geq 100$  superheavy elements displaying quasi-molecular phenomenon [1] with atomic numbers greater than that of any stable element known can be investigated. To study such phenomena, the fundamental requirement is that of a thin film of heavy  $Z_1$  target. Further, to understand the cross-section dependencies, various thicknesses of the target are required.

Recently, an experiment in atomic physics beamline in beam hall II was performed to investigate quasi-molecular phenomenon in collisions of heavy ions with heavy atoms. For the experiment, thin films with different thicknesses of targets  $73 \leq Z_2 \leq 83$  (where  $Z_2$  is target atomic number) were fabricated in Target laboratory of IUAC. The thicknesses varied from  $10 \mu\text{g}/\text{cm}^2$  to  $250 \mu\text{g}/\text{cm}^2$ . All the films were prepared with carbon backing of thickness  $\sim 15-20 \mu\text{g}/\text{cm}^2$ .

Targets of Pb and Bi thin films were prepared using thermal deposition method. For Ta, Au electron gun vaporization procedure was utilised. All the depositions were carried out in high vacuum  $\sim 10^{-6}$  torr pressure. Initially,  $38.6 \mu\text{g}/\text{cm}^2$  (or 100 nm) thin BaCl<sub>2</sub> was deposited on clean glass slides. This acted as the releasing agent. On the layer of BaCl<sub>2</sub>, carbon layer was deposited by gradually increasing the emission current. This ensured growth of a smooth film of carbon on releasing agent. The glass slides with carbon layer were, then, annealed at 250°C. The annealed slides with BaCl<sub>2</sub> and carbon layers were utilized for target deposition. In all cases, the rate of deposition was kept constant ( $\sim 1 \text{ \AA/s}$ ) to ensure uniform epitaxial deposition. Finally, the prepared target films were floated in warm distilled water and extracted on specially prepared steel target holders [2-4]. These holders were mounted on target ladder for the experiment with ion beam.

#### References

- [1] W. Lichten, J. Phys. Chem., 84, 17 (2002) 2102-2116.
- [2] Abhilash *et al.*, J Radioanal Nucl Chem 305 (2015) 749-753.
- [3] Abhilash *et al.*, J Radioanal Nucl Chem 299 (2014) 1137-1139.
- [4] Abhilash S R and D Kabiraj, Proceedings of the DAE-BRNS Symp. on Nucl. Phys. 61 (2016) 1062-1063.

## 5.6 RADIATION PHYSICS

### 5.6.1 Investigating the Thermoluminescent Properties of $\text{KCaBO}_3:\text{Dy}$ , $\text{KCaPO}_4:\text{Dy}$ and $\text{Ca}_3(\text{PO}_4)_2:\text{Dy}$

A.Pandey<sup>1</sup>, Chirag Malik<sup>1</sup>, Kanika Sharma<sup>1</sup>, Pratik Kumar<sup>2</sup>, D.Sen<sup>3</sup> and Birendra Singh<sup>3</sup>

<sup>1</sup> Department of Physics, Sri Venkateswara College, University of Delhi, Daula Kuan, New Delhi

<sup>2</sup> Medical Physics Unit, IRCH, AIIMS, New Delhi 110029, India.

<sup>3</sup> Inter-University Accelerator Centre, Aruna Asaf Ali Marg, New Delhi 110067, India.

The phosphor investigated for its thermoluminescence properties was potassium calcium borate doped with dysprosium ( $\text{KCaBO}_3:\text{Dy}$ ). It was synthesized by solid state diffusion method. Crystallite size calculated using Scherrer's formula was found to be around 117 nm. The bandgap of the material was determined using ultraviolet-visible diffuse reflectance spectroscopy (UV-VIS DRS). The phosphor was irradiated by photon beams (of 1.25 MeV gamma and 4.88 eV UV rays) and ion beams (of 65 MeV and 85 MeV of O<sub>6+</sub> and 75 MeV of C<sub>6+</sub>) with different doses in order to study its TL properties. The phosphor showed good TL sensitivity towards these ionizing radiations. A good linear dose response was also shown by the phosphor for photon beam exposure. However, in case of ion beams exposure, dose response of the phosphor was good only for low energy oxygen ion beam. The phosphor also showed good PL properties with sharp peaks present in the PL emission and excitation spectra corresponding to the characteristic peaks of the dopant Dy. The CIE was used to determine the chromaticity coordinates and colour temperature in order to examine the phosphor's application in white LEDs. And it gives overall emission almost in white region. All these good characteristics make this phosphor a suitable candidate for radiation dosimetry and solid state lighting. This work has been published in *Journal of Luminescence*, Volume 216 (2019) 116692 as a full length paper [1] <https://doi.org/10.1016/j.jlumin.2019.116692>

Potassium calcium phosphate doped with Dy ( $\text{KCaPO}_4:\text{Dy}$ ) was investigated for its TL properties. This phosphor was reported for the first time for their luminescence (both thermo and photoluminescence) properties. It was prepared via two methods, solid-state diffusion method and combustion method. The phosphor prepared by solid state diffusion method showed variation in their crystallite size on varying the concentration of the dopant Dy. The crystallite size varied from approximately 46 nm to 53 nm on varying the concentration of the dopant from 0.1 mol% to 0.4 mol%. Dopant concentration-dependent bandgap mechanics in the phosphor was used to explain the behaviour of TL glow curves obtained from gamma and ultraviolet irradiation along with the PL spectra of the phosphor. Further, this phosphor showed good TL sensitivity towards gamma rays (2.5 times more sensitive than standard TL material TLD-100) and UV rays (20 times more intense than TLD-100). Moreover, the given phosphor showed good linear dose response for gamma rays (with linearity ranging from 10 Gy to 2 kGy) and UV irradiation. Deconvolution was performed on the glow curves obtained for gamma (10 Gy) and UV irradiation (60 minutes) in order to calculate the kinetic parameters for the traps. Other characteristics of the TL material i.e. repeatability and fading were also studied for this phosphor. Decent PL properties with an overall emission lying very near to the white region were observed through the chromaticity index of CIE. All these characteristics make the phosphor (with 0.3 mol% Dy concentration) a potential candidate for radiation dosimetry and a UV convertible material for white-light-emitting diodes. On the other hand the phosphor  $\text{KCaPO}_4$  prepared through combustion method was found to optimize at 0.1 mol% dopant concentration for gamma irradiation. A simple and broad TL glow curve for the sample irradiated with gamma rays showed peak temperature at about 150 °C. The dose response of the phosphor showed linearity from 10 Gy to 2 kGy. Further this phosphor also exhibited good PL properties. The overall emission of phosphor either lied in the white region or in the region, which is close to the white region. The good TL and PL properties make this phosphor a good candidate for radiation dosimetry as well as in the field of solid state lighting. This work has been published in *Radiation Physics and Chemistry*, 168 Volume (2020) Page no. 108561 as a full length paper [2]. <https://doi.org/10.1016/j.radphyschem.2019.108561>

Tricalcium phosphate ( $\text{Ca}_3(\text{PO}_4)_2:\text{Dy}$ ) was another phosphate phosphor studied for their TL and PL properties. The given phosphor having an effective atomic number Zeff = 15.785, equivalent to that of bones, was studied for its TL and PL properties. Different samples with varied concentrations of the dopant Dy<sup>3+</sup> (0.1, 0.2, 0.3, 0.4, 0.5, and 0.6 mol %) were synthesized by the chemical co-precipitation technique. The crystallite size was calculated using Scherrer's formula which was found to range between 27 nm and 49 nm. Samples were further irradiated by gamma rays (emitted from Co-60) with dose varying from 10 Gy to 5 kGy in order to study their TL properties. Concentration optimization of the given phosphor was done in terms of its TL sensitivity and was found to be 0.5 mol %. The TL dose response of the phosphor was linear over a wide range of dose. Deconvolution was performed on the glow curve for 10 Gy dose, giving six peaks (at 127°, 153°, 185°, 218°, 313° and 335°C) suggesting the presence of six different types of traps. Other characteristics of the TL material i.e. repeatability and fading were also studied. Overall, the phosphor showed promising results for its utility in

TL dosimetry. In addition, PL further confirmed the presence of dopant in the phosphor. Moreover, the dopant concentration was optimized in terms of the nanophosphor's PL intensity. The CIE was used to calculate chromaticity coordinates, colour rendering index and colour temperature in order to investigate the phosphor's application in white LEDs. This investigation confirms that the given phosphor also gives luminescence in the white region. This work has been published in Applied Radiation and Isotopes, Volume 158 (2020) Page no. 109062 as a full length paper [3] <https://doi.org/10.1016/j.apradiso.2020.109062>

#### References

- [1] Malik, C., Rathi, P., Singh, B., & Pandey, A. (2019). An investigation of luminescence properties of gamma, ultraviolet and ionbeam irradiated phosphor KCaBO<sub>3</sub>:Dy Journal of Luminescence, 216, 116692.
- [2] Malik, C., Meena, R., Rathi, P., Singh, B., & Pandey, A. (2020). Effect of dopant concentration on luminescence properties of a phosphor KCaPO<sub>4</sub>:Dy Radiation Physics and Chemistry, 168, 108561.
- [3] Malik, C., Kaur, N., Singh, B., & Pandey, A. (2020). Luminescence properties of tricalcium phosphate doped with dysprosium Applied Radiation and Isotopes, 158, 109062.

#### 5.6.2 Thermoluminescence study of annealed alumina thin films for application in radiation dosimetry

S. Pal<sup>1</sup>, S. Bhowmick<sup>1</sup>, S. A. Khan<sup>2</sup>, D. Sen<sup>2</sup>, Birendra Singh<sup>2</sup>, D. Kanjilal<sup>2</sup>, A. Kanjilal<sup>1\*</sup>

<sup>1</sup>Department of Physics, School of natural sciences, Shiv Nadar University, Gautam Budhha Nagar, UP

<sup>2</sup>Inter University Accelerator Centre, Aruna Asaf Ali Marg, New Delhi

Thin film based radiation dosimeter is a present day need due to its advantages over single crystals and/or powder samples like easy handling, less usage of active material, device miniaturization, getting spatial dose distribution, online dosimetry especially for ion beam therapy, better homogeneity in a single batch, etc. [1, 2]. Here, we have chosen alumina as active material due to its high thermo-chemical stability, simple glow curve, good sensitivity at lower doses, and having ability for showing optically stimulated luminescence [3]. Alumina thin films (~300 nm) have been deposited on silicon by using radio frequency magnetron sputtering technique. The as-deposited films are found to be amorphous in nature. The films have also been annealed at two different temperatures (1100 °C and 1200 °C) for three hours to follow the changes in radiation sensitivity. All three samples have been exposed to gamma irradiation in a gamma irradiation chamber (source: Co-60; 3.4 kGy/hr) at Inter University Accelerator Centre (IUAC), New Delhi, India and thermoluminescence measurements have been carried out in a Harshaw 3500 Reader (Heating rate: 5 °C/s) at health physics lab, IUAC. Figure 1a shows the related glow curves taken after exposure of 2 kGy gamma irradiation. Significant enhancement in radiation sensitivity can be seen with annealing temperature, however it is non-monotonic in nature. On the other hand, the shape of the glow curves has been changed as a result of annealing. However, the glow curve obtained from 1200 °C annealed sample is better from the dosimetric point of view, as it has a single peak with substantial radiation sensitivity. Interestingly, the same thin film shows better linear radiation response in the range of 0.1-5 kGy [Fig. 1b]. To understand the reason behind such annealing induced variation in radiation sensitivity, several characterization like GIXRD, PL, SEM and TEM have been carried out and the results altogether indicate that the formation of nanocrystals that are embedded in amorphous matrix as well as drastic variation in the optically active defects centers play the key role in controlling the radiation sensitivity.

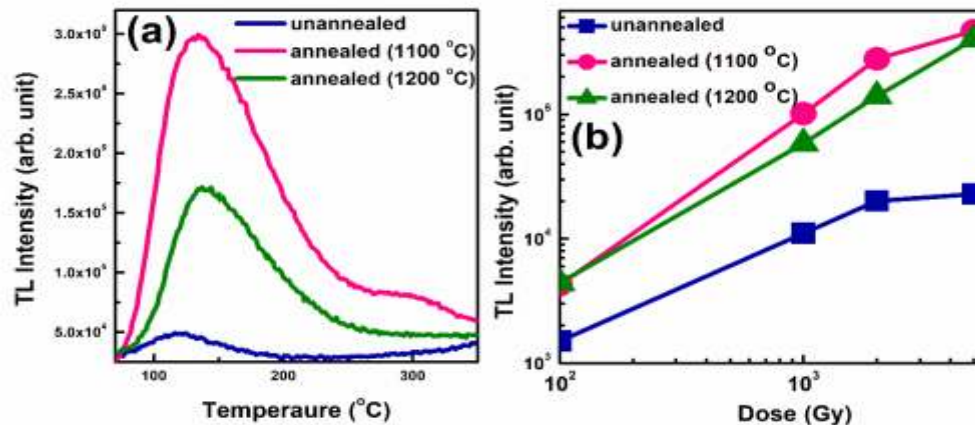


Figure (a) TL glow curves of unannealed, 1100 oC annealed and 1200 oC annealed samples;  
 (b) TL response curves of all three mentioned samples

#### References

- [1] C. P. Karger et al., Phys. Med. Biol. 55 (2010) R193
- [2] M. S. Akselrod et al., Rad. Prot. Dosim. 47 (1993) 159
- [3] L. Oster et al., J. Phys. D: Appl. Phys. 27 (1994) 1732
- [4] J. A. Bartz et al., Rad. Meas. 46 (2011) 1974

### 5.6.3 Effect of Fuel on the Defect Structure of MgAl<sub>2</sub>O<sub>4</sub> Nanostructures

Savita<sup>1,2</sup>, D. Sen<sup>3</sup>, Birendra Singh<sup>3</sup>, Ankush Vij<sup>4</sup> and Anup Thakur<sup>1</sup>

<sup>1</sup>Advanced Materials Research Lab, Dept of Basic and Applied Sciences, Punjabi University, Patiala

<sup>2</sup>Department of Physics, Punjabi University, Patiala-147 002, Punjab

<sup>3</sup>Health Physics Lab, Inter university Accelerator Center (IUAC), New Delhi

<sup>4</sup>Nanophosphors Lab, Department of Applied Physics, Amity University Haryana, Gurgaon

Presence of defects in the metal oxide materials affects the structural, electronic, optical, magnetic and dielectric properties of the material. Presently, defect induced photoluminescence is gaining much interest of the researchers [1-3]. MgAl<sub>2</sub>O<sub>4</sub>, a wide band gap (~7.8 eV) material, exhibits defect assisted photoluminescence due to the presence of various defect states within the band gap [4-5]. In the present work, the effect of fuel on the defect structure of MgAl<sub>2</sub>O<sub>4</sub>nanostructures is investigated. MgAl<sub>2</sub>O<sub>4</sub>nanostructures have been synthesized using three different fuels, monoethanolamine (MEA), glycine and urea. Samples were annealed at 700 °C to obtain the required spinel phase. X-ray diffraction patterns of the annealed samples indicated the formation of cubic single phase spinel structure with MEA and glycine fuels and an additional minor secondary phase of MgO in spinel phase with urea. Fourier transform infrared spectra revealed the formation of metal-oxygen bands in the spinel structure of MgAl<sub>2</sub>O<sub>4</sub>nanostructures. Thermoluminescence (TL) response of the nanostructures is studied by irradiating the samples with <sup>60</sup>Co  $\gamma$ -rays at varying radiation doses. A broad glow curve consisting of multiple traps is observed with all the three fuels. TL intensity is found to increase with the radiation dose upto 10 kGy and saturates at 12 kGy. Trap distribution and TL intensity varied with the fuel employed. Various shallow and deep traps are correlated to O– to F<sup>+</sup> centers.

#### References:

- [1] Jung, Y.K., Calbo, J., Park, J.S., Whalley, L.D., Kim, S. and Walsh, A., Journal of Materials Chemistry A, 7, 20254 (2019).
- [2] Ahmed, A., Siddique, M.N., Ali, T. and Tripathi, P., Applied Surface Science, 483, 463 (2019).
- [3] Hiller, D., López-Vidrier, J., Gutsch, S., Zacharias, M., Nomoto, K. and König, D., Scientific Reports, 7, 1 (2017).
- [4] Sawai, S. and Uchino, T., Journal of Applied Physics, 112, 103523 (2012).
- [5] Pathak, N., Ghosh, P. S., Gupta, S. K., Mukherjee, S., Kadam, R. M., & Arya, A., The Journal of Physical Chemistry C, 120, 4016 (2016).